Reversible phosphorylation of WOX5 protein controls the homeostasis of QC

Ling Chen[1*]

[1]State Key Laboratory of Hybrid Rice, Institute of Advanced Studies. Wuhan University, WuHan, China

[*]corresponding author: lingchen0206@whu.edu.cn

Highlights

The subfamily II of AtSKs stabilizes WOX5 protein by phosphorylating the GSK3 Motifs in the PEST domain

The subfamily II of the catalytic subunit of AtPP2A-Cs holoenzymes destabilizes WOX5 protein by dephosphorylating GSK3 Motifs

Reversible phosphorylation of WOX5 protein controls the homeostasis of the low proliferative activity of the QC cells and of the constant one-layer QC

In situ overexpressed WOX5 protein and phosphate-mimicked WOX5 protein are both sufficient for producing more quiescent cells

Summary

Fundamental questions of structural and functional homeostasis of the *Arabidopsis* QC in root stem cell niche remain elusive. WUSCHEL-RELATED HOMEOBOX 5 (WOX5) protein, which serves as a QC marker, yet the regulation of its homeostasis remains unknown. Here, we characterize a novel role of PEST domain in WOX5 protein, which stabilizes WOX5 protein by phosphorylating GSK3 Motifs (GMs). Next, we demonstrate that the subfamily II of *Arabidopsis* SHAGGY-like Kinases (AtSKs) stabilizes WOX5 protein by phosphorylating the GMs in the PEST domain and the subfamily II of the catalytic subunit of *Arabidopsis* PP2A (AtPP2A-Cs) holoenzymes destabilizes WOX5 protein by dephosphorylating the GMs. Moreover, we find both in situ overexpressed and phosphate-mimicked WOX5 protein can reduce the proliferative activity of the original stele initials (SI) and its daughter cells (SID), leading to the production of more quiescent cells. Taken together, our findings suggest that the homeostasis of WOX5 protein is modulated by reversible phosphorylation, which functionally controls the homeostasis of the QC cells' low proliferative activity. Furthermore, the subfamily II of AtPP2A-Cs structurally controls the homeostasis of one-layer QC by down-regulating WOX5 expression and destabilizing WOX5 protein in the SI and SID.

31 # Introduction

32 The quiescent centre (QC) was discovered and named by Frederick Albert Lionel Clowes through
33 observations of root tips of numerous plant species. Its existence was validated through the use of X-
34 irradiation and radioisotopes tracing in the 1950s (Barlow, 2015a, b; Barlow, 2015c; Dubrovsky and
35 Barlow, 2015). Clowes's subsequent work confirmed that the QC mainly consists of G1 cells, which
36 were not in a strictly quiescent state but in a resting state that can slowly participate in the cell cycle
37 when needed (Clowes, 1968). Until 1993, the QC of *Arabidopsis thaliana* was firstly described by
38 Dolan and his colleagues (Dolan et al., 1993). Thus, the definition of QC in *Arabidopsis* includes two
39 aspects: Structurally, the QC, which is one layer cells (average of four cells) reside at the center of the
40 "closed root apical meristem (RAM)", surrounded by initials (Clowes, 1981; Dolan et al., 1993);
41 Functionally, these one-layer QC cells with a very low rate of nuclear DNA synthesis or very low
42 proliferative activity serve as a reservoir of surrounding mitotically active stem cells and the organizer
43 of the stem cell niche (SCN) (Barlow, 2015c; Claudia et al., 1997; Dubrovsky and Barlow, 2015).

44 To date, great progress in molecular regulation of *Arabidopsis* QC's formation and function has been
45 made. Two GRAS family transcription factors SCARECROW (SCR) and SHORT-ROOT (SHR) play
46 a prominent role in positioning and specifying the QC. They form a ternary complex with
47 RETINOBLASTOMA-RELATED (RBR) to inhibit asymmetric stem cell division and reinforce
48 quiescence in the QC (Cruz-Ramírez et al., 2012; Cruz-Ramírez et al., 2013; Laurenzio et al., 1996;
49 Nakajima et al., 2001; Sabatini et al., 2003). Additionally, the C2H2 zinc finger family transcription
50 factor JACKDAW (JKD) (one of the BIRDs) contributes to QC specification and maintenance by
51 interacting with SCR and SHR (Clark et al., 2020; Long et al., 2015; Long et al., 2017). Similarly,
52 PLETHORA (PLT) family of AP2-domain transcription factors are required for the QC specification
53 and maintenance. These factors operate in a parallel pathway with SCR and SHR or in a convergence
54 path with SCR through forming a ternary complex with teosinte-branched cycloidea PCNA (TCP)
55 transcription factors (Aida et al., 2004; Shimotohno et al., 2018). However, why the QC cells always
56 occupy just one layer area or constantly exist just one layer at the centre of RAM in *Arabidopsis*
57 remains elusive.

58 Many factors modulate the proliferative activity of QC cells in *Arabidopsis*. One such factor is the
59 CELL CYCLE SWITCH 52 A (CCS52A), which mediates the repression of the QC's proliferative
60 activity in by activating the anaphase promoting complex/cyclosome (APC/C) (Vanstraelen et al.,
61 2009). Another factor, the ethylene response factor 115 (ERF115), is a target of the complex of
62 APC/$C^{CCS52A2}$ E3 ubiquitin ligase. ERF115 is naturally inhibited by proteolysis, and promotes QC
63 cells proliferation by activating the phytosulfokine 5 (PSK5) peptide in response to brassinosteroid or
64 damage to the root (Jefri et al., 2013). ASH1-RELATED3 (ASHR3), a histone 3 lysine

methyltransferase, is a direct target of E2Fa/b transcriptional factors and maintains the quiescence of QC cells (Kumpf et al., 2014). WUSCHEL-RELATED HOMEOBOX 5 (WOX5), a well-studied marker of QC, arises confinedly in the hypophysis of early globular embryo, slightly earlier than the period of QC birth. The WOX5 protein always keeps company with the QC development process from the embryonic stage to the postembryonic stage (Haecker et al., 2004). It is a well-known fact that the loss of WOX5 function causes partial loss of QC identity, premature differentiation of distal stem cells, and accelerated proliferative activity of QC cells (Burkart et al., 2019; Celine et al., 2014; Sarkar et al., 2007). Therefore, WOX5 not only plays a significant role in maintaining the quiescence of QC cells, but also acts as a central transcriptional factor of the SCN. However, how the QC permanently maintains the homeostasis of very low proliferative activity from the embryonic stage to the postembryonic stage remains unknown. WOX5 is a stereotypical transcriptional repressor with EAR motif. It targets several key downstream genes involved in the regulation of QC cell activity. For instance, WOX5 directly targets D-type cyclins and CDF4, the former promoting division of QC cells, and the latter facilitating differentiation of distal stem cells (Berckmans et al., 2020; Celine et al., 2014; Pi et al., 2015). Additionally, WOX5 indirectly regulates the expression of YUCCA1 (YUC1), SHR, CYCD6;1, which may be involved in regulating the mitotic activity of QC and initial cells (Clark et al., 2020; Savina et al., 2020; Tian et al., 2014). Several protein-protein interaction factors of WOX5, TOPLESS/TOPLESS-RELATED (TPL/TPR), HISTONE DEACETYLASE 19 (HDA19) and HAIRY MERISTEM (HAM), PLT, and BRASSINOSTEROIDS AT VASCULAR AND ORGANIZING CENTER (BRAVO) play important roles in the fate decision of distal stem cells and quiescence establishing of the QC (Burkart et al., 2019; Pi et al., 2015; Vilarrasablasi et al., 2014; Zhou et al., 2018). The direct upstream regulators of WOX5, REPRESSOR OF WUSCHEL1 (ROW1) grants the identity of QC by confining WOX5's expression to the QC cells, SEUSS (SEU) and SCR specify the QC by recruiting ASHR3 H3K36 methyltransferase SET DOMAIN GROUP 4 (SDG4) to activate WOX5's expression (Zhai et al., 2020; Zhang et al., 2015). The peptide CLAVATA3/ESR-RELATED 40 (CLE40) and its receptor *Arabidopsis* CRINKLY4 (ACR4), coreceptors CLAVATA1 (CLV1) and CLV3 INSENSITIVE KINASES (CIKs) mediate the non-direct upstream signals of WOX5, then regulate the activity of QC cells and distal stem cells (Berckmans et al., 2020; Stahl et al., 2013; Stahl et al., 2009; Zhu et al., 2021). However, the regulation of WOX5 protein homeostasis through post-translational modifications and its potential impact on the permanent maintenance of the low proliferative activity in quiescent center (QC) cells are still not understood.

Here, we identified a PEST domain in the WOX5 protein, which function remains undiscovered before in the WOX5 protein. Our investigation revealed that this PEST domain plays a crucial role in stabilizing the WOX5 protein, which in turn maintains the low proliferative activity of QC cells. Furthermore, we characterized that the PEST domain functions through the serine and/or threonine sites of GSK3 Motifs (GMs) in the PEST domain. Biochemical evidence demonstrated that the

101 subfamily II of AtSKs (the homologs of GSK3) interact with WOX5 by phosphorylating the GMs.
102 Genetic and chemical inhibition experiments demonstrated that the subfamily II AtSKs inhibit the
103 proliferative activity of QC cells from the embryonic stage to the post-embryonic stage by stabilizing
104 WOX5 protein. We further discovered that the subfamily II of catalytic subunit of *Arabidopsis* Protein
105 Phosphatase 2A (AtPP2A-Cs) interact with WOX5. In the subfamily II of AtPP2A-Cs (*c3c4*) loss of
106 function mutant, WOX5 protein has a significant increase in QC cells, stele initials (SI), and its
107 daughter cells (SID), which causes the appearance of more QC-like cells. Contrarily, overexpressed
108 the subfamily II of AtPP2A-Cs protein causes an increase of the proliferative activity of QC by
109 dephosphorylating the phosphorylated WOX5 protein. Furthermore, we observed that treatment with a
110 chemical inhibitor targeted against the subfamily II of AtSKs significantly reduces the elevated levels
111 of WOX5 protein in the *c3c4* mutant. This finding strongly suggests that the increased WOX5 protein
112 in *c3c4* is predominantly a phosphorylated form, specifically phosphorylated by the subfamily II of
113 AtSKs. In addition, the proliferative activity of SI and SID also decreases in *c3c4*, but this decrease
114 disappear in *c3c4wox5-1* triple mutant. Treatment with a specific chemical inhibitor targeted against
115 the subfamily II of AtSKs results in an opposing effect, causing an increase in the proliferative activity
116 of QC cells, as well as SI and SID cells in *c3c4*. These results reveal that increasing phosphorylated
117 WOX5 protein is required for reducing the proliferative activity of QC, SI, and SID in *c3c4*. Moreover,
118 in situ overexpressed WOX5 protein in QC cells, SI and SID recapitulated the phenotypes in *c3c4*.
119 Most importantly, the dynamic induction assay directly testify that accumulated WOX5 protein in QC
120 can reduce its proliferative activity, and accumulated WOX5 protein in SI and SID cells can reduce
121 their proliferative activity and convert these cells into QC-like cells at the postembryonic stage. These
122 data prove that increased WOX5 protein in QC cells and SI and SID is sufficient for reducing their
123 proliferative activity. The phosphate-mimicked WOX5 protein partially reproduces the phenotypic
124 characteristics observed in *c3c4*. However, treatment with a chemical inhibitor specifically targeting
125 the subfamily II of AtSKs does not lead to destabilization of the mimicked phosphorylated WOX5
126 protein, nor does it induce an increase in the proliferative activity. These results testify that phosphate-
127 mimicked WOX5 protein is also sufficient for reducing the proliferative activity.
128 In summary, our study uncovers that phosphorylation of WOX5 protein by the subfamily II of AtSKs
129 controls the low proliferative activity of QC. Oppositely, the subfamily II AtPP2A-Cs enhances the
130 proliferative activity of QC cells by dephosphorylating WOX5 protein. Additionally, the subfamily II
131 AtPP2A-Cs maintains just one-layer QC cells by downregulating the WOX5 expression and
132 destabilizing WOX5 protein in SI and SID. Taken together, reversible phosphorylation of WOX5
133 protein not only controls the homeostasis of the low proliferative activity in QC cells, but also controls
134 the homeostasis of one-layer QC from the embryonic stage to the postembryonic stage in *Arabidopsis*.

135 # Results:

136 ## The PEST domain stabilizes WOX5 protein and maintains low
137 ## proliferative activity of QC cells

138 Previous methods for identifying and imaging the QC, such as X-irradiation, β-rediation,
139 autoradiography, nucleoside analogs BrDU immunodetection, and EdU click reaction, have some
140 shortcomings (Clowes, 1961, 1963; Dolan et al., 1993; Kotogány et al., 2010). These methods can't
141 present the most natural proliferative activity because they may stimulate proliferation of QC cells.
142 Additionally, they are static. The 4D imaging method indicates that QC cells maintain low
143 proliferative activity (cell division intervals almost 110 hours) in Columbia-0 (Col-0) ecotype (Rahni
144 and Birnbaum, 2019). However, this dynamic method is not convenient to use in combining with
145 other genetic materials. The 3D quantitative analysis can visualize the number, volume, and division
146 pattern of QC cells, but this method is complicated (Lu et al., 2021). In order to describe the
147 phenotype of the proliferative activity of QC more easily and more directly, we firstly introduce the
148 index Proliferative Activity (PA) for defining the proliferative activity of QC. PA is the number of
149 dividing QC cells per root at the stage of mature embryo or 5 days after germination (DAG). Cell plate
150 on the longitudinal section is a natural marker showing the dividing cells. For getting the real PA of
151 QC as much as possible, we count the cell plates of dividing QC cells (marked as D_{cp} equals the sum
152 of the number of dividing QC cells of all the root tips) by viewing a mass of mature embryos (marked
153 as N_e equals the number of all the mature embryos) and root tips (marked as N_r equals the number of
154 all the root tips). So the PA equals D divided by N (the formulas are $PA_r = D_{cp} / N_r$ and $PA_e = D_{cp} / N_e$).
155 It is very difficult to investigate the regulation of WOX5 protein level since the very low WOX5
156 protein content exists in the root tips of *Arabidopsis*. Thus, we analyzed the protein sequence of
157 WOX5 and its homolog WUSCHEL (WUS) in silico through the ePESTfind prediction website of
158 http://embossgui.sourceforge.net/demo/manual/epestfind.html (Figure S1) (Rechsteiner and Rogers,
159 1996; Rogers et al., 1986). The output revealed a potential PEST domain with 18 amino acids between
160 position 152 and 171 of WOX5 protein sequence, which PEST score was +6.02 (greater than
161 threshold value +5.00 means a possible PEST domain with real interest). But the output showed no
162 potential PEST domain in the WUS protein sequence (Figure S1), the results are consistent with
163 previous report (Dolzblasz et al., 2016). However, the function of PEST domain remains unidentified.
164 Meanwhile, the low hydrophobicity index of 40.36 (Figure S1) indicated that the PEST domain might
165 be surface exposed and be accessible for the serine and/or threonine phosphorylation or protein-
166 protein interaction (Meyer et al., 2011). Since C-terminal green fluorescent protein (GFP) fused
167 WOX5 protein and N-terminal GFP fused WUS protein are the functional protein (Pi et al., 2015;
168 Rodriguez et al., 2016; Yadav et al., 2011). To explore the possible function of the PEST domain for
169 regulating the WOX5 protein, we thus introduced the WOX5-GFP, WOX5△PEST-GFP (full length

170 WOX5 protein deletes PEST domain) and GFP-WUS fusion protein into *wox5-1* driving by the full-
171 length promotor of WOX5 (Figure S2) for obtaining 10-15 rescued T_1 lines separately. We randomly
172 selected 4 homozygous lines (named as W5-1~W5-4, dP-1~dP-4, WU-1~WU-4 separately) (Figure
173 S3A) to perform semi-quantitative reverse transcription PCR (sqRT-PCR) and quantitative real time
174 PCR (qPCR) assays. We identified 6 rescued lines (W5-3, W5-4, dP-2, dP-3, WU-1, WU-2 separately)
175 with almost equal level of GFP expression (Figure S3), then we counted the PA_e at the mature
176 embryonic stage and the PA_r at 5 DAG of the 6 rescued lines and *wox5-1*. The PA_e (=0.028) and PA_r
177 (=0.129) of WOX5-GFP/*wox5-1* rescued lines was significantly lower than the PA_e (=0.640) and PA_r
178 (=0.694) of WOX5△PEST-GFP/*wox5-1* lines (Figure 1A,B,F,G,H,I), the PA_e (=0.640) and PA_r
179 (=0.694) of WOX5△PEST-GFP/*wox5-1* rescued lines markedly lower than the PA_e (=1.234) and PA_r
180 (=1.917) of GFP-WUS/*wox5-1* rescued lines (Figure 1B,C,F,G,I,J), the PA_e (=1.234) and PA_r (=1.917)
181 of GFP-WUS/*wox5-1* lines extremely lower than the PA_e (=1.976) and PA_r (=3.023) of *wox5-1*
182 (Figure 1C,D,F,G,J,K). The results indicated that WOX5-GFP protein with the PEST domain could
183 rescue the PA_e and PA_r of *wox5-1* up to almost equal to the wild type (WT) (Col-0 ecotype) (Figure
184 3A,H), however, WOX5△PEST-GFP protein and GFP-WUS protein, both are without the PEST
185 domain, could not completely rescue the PAe and PAr of *wox5-1*. At the same time, we quantified the
186 fluorescence of GFP fusion protein in the QC zone at 5 DAG of the 6 lines and *wox5-1* (the value of
187 blank background) (Figure 1D,E). The intensity of WOX5-GFP fusion protein was markedly higher
188 than the intensity of WOX5△PEST-GFP and GFP-WUS fusion protein (Figure 1A~C,E), revealed
189 that the PEST domain stabilizes WOX5 protein. Further analysis revealed that tandem three GMs
190 (S/T-X-X-X-S/T^{-P}) (named GM3, GM4 and GM5) (Fiol et al., 1990; Youn and Kim, 2015) exists in
191 the PEST domain, in addition, other two GMs (named GM1 and GM2) in the protein sequence of
192 WOX5 out of the PEST domain (Figure S4). Previous studies had shown that the S/T sites at the N
193 terminal of the GMs were the real phosphorylation sites being phosphorylated by GSK3s, but the S/T
194 sites at the C terminal of the GMs are the primed phosphorylation sites being phosphorylated by other
195 kinases (Ali et al., 2001; Patel and Woodgett, 2017). Thus, to investigate which GMs are involved in
196 regulating stability of WOX5 protein and the QC's proliferative activity. We constructed five
197 plasmids (WOX5mGM1-GFP, WOX5mGM2-GFP, WOX5mAll-GFP, WOX5m5A-GFP, and
198 WOX5m3A-GFP) using site-directed mutagenesis, these plasmids were also introduced into *wox5-1*.
199 We then randomly selected 4 homozygous lines (named mGM1-1~mGM1-4, mGM2-1~mGM2-4,
200 mAll-1~mAll-4, m5A-1~m5A-4, and m3A-1~m3A-4 separately) (Figure S5) from descendants of 10-
201 15 rescued T_1 lines to perform sqRT-PCR and qPCR assays, we identified 10 rescued lines (mGM1-1,
202 mGM1-4; mGM2-1, mGM2-2; mAll-2, mAll-3; m5A-1, m5A-2; m3A-2, m3A-3 separately) with
203 almost equal GFP expression (Figure S5). We next also counted the PA_e at the mature embryonic
204 stage and the PA_r at 5 DAG of the 10 rescued lines. The PA_e and PA_r of WOX5mGM1-GFP/*wox5-1*

205 rescued lines and WOX5mGM2-GFP/*wox5-1* rescued lines were similar to WOX5-GFP/*wox5-1*
206 rescued lines (Figure S6A,B,G,H,I,J). The PAe/ PAr of WOX5mAll-GFP/*wox5-1* , WOX5m5A-
207 GFP/*wox5-1* , and WOX5m3A-GFP/*wox5-1* rescued lines were significantly higher than the
208 WOX5mGM1-GFP/*wox5-1* and WOX5mGM2-GFP/*wox5-1* rescued lines (Figure S6A~C,G~M),
209 indicating that GM3,GM4 and GM5 in the PEST domain rather than GM1 and GM2 inother
210 domains of wox5 play a crucial role in maintaining the low proliferative activity of QC.. Meanwhile,
211 we quantified the fluorescence of GFP fusion protein in the QC zone at 5 DAG of the 10 rescued lines.
212 The intensity of WOX5mGM1-GFP and WOX5mGM2-GFP fusion protein were significantly higher
213 than the intensity of WOX5mAll-GFP, WOX5m5A-GFP, and WOX5m3A-GFP fusion protein
214 (Figure S6A~F), which revealed that GM3, GM4 and GM5， instead of GM1 and GM2, are critical
215 for stabilizing WOX5. Taken together, the GMs in the PEST domain stabilizes WOX5 protein and
216 maintains the low proliferative activity of QC cells.
217 In addition, we introduced the WOX5-GFP, WOX5△PEST-GFP, GFP-WUS, WOX5mGM1-GFP,
218 WOX5mGM2-GFP, WOX5mAll-GFP, WOX5m5A-GFP, and WOX5m3A-GFP fused protein into
219 QC184/*wox5-1* line for obtaining homozygous lines. The β-glucuronidase (GUS) staining for 48-72
220 hours showed WOX5-GFP/QC184/*wox5-1* (40/42), WOX5mGM1-GFP/QC184/*wox5-1* (40/43), and
221 WOX5mGM2-GFP/ QC184/*wox5-1* (36/38) lines completely rescued the GUS activity of
222 QC184/*wox5-1* (36/36) line almost be equal to QC184 (27/28) (Figure S7A~E). However, GFP-WUS/
223 QC184/ *wox5-1* (31/54), WOX5△PEST-GFP/ QC184 /*wox5-1* (29/54), WOX5mAll-GFP/ QC184/
224 *wox5-1* (31/55), WOX5m5A-GFP/ QC184/ *wox5-1* (25/42), and WOX5m3A-GFP/ QC184/ *wox5-1*
225 lines (28/47) partially rescued the GUS activity of QC184/*wox5-1* (Figure S7F~O). These results
226 indicate that increased QC proliferative activity causes a decrease of QC184 GUS activity.

227 The subfamily II of AtSKs interact with WOX5 in the QC cells

228 In mammals, glycogen synthase kinase-3 (GSK3s) are involved in almost all pathways including
229 Insulin signalling pathway (glycogen metabolism), Notch signalling pathway (tissue patterning and
230 cell polarity), Transforming Growth Factor β (TGFβ) signalling pathway (proliferation and
231 differentiation), and canonical Wnt/β-catenin pathway (stem cell pluripotency and self-renewal) (Patel
232 and Woodgett, 2017). In plants, GSK3s also are involved in many important pathways, such as
233 brassinosteroid (BR) signalling pathway, ABA signalling pathway, Auxin signalling pathway,
234 stomatal development and stress response (Houbaert et al., 2018; Li et al., 2020; Youn and Kim, 2015).
235 However, whether GSK3s regulate root stem cell pluripotency and self-renewal needs to be clarified.
236 There are 10 GSK3s in *Arabidopsis* (AtSKs), also known as SHAGGY-like kinases (Youn and Kim,
237 2015), since only mutated the GMs in the PEST domain of WOX5 could be almost equal to the role
238 of truncation of PEST domain in regulating the QC proliferative activity and the stability of WOX5
239 protein (Figure 1 and Figure S6). Hence, we want to figure out which GSK3s may be involved in

240 phosphorylating WOX5 protein. Firstly, we performed sqRT-PCR assay, the results showed that all
241 ten AtSKs express in the one centimeter root tips of Col-0 at 5 DAG (Figure S8). Next, we obtained
242 all transcriptional reporters of ten AtSKs (Figure S8) We found that only the subfamily I(AtSK11,
243 AtSK12,AtSK13), subfamily II (AtSK21, AtSK22, AtSK23) of AtSKs, and AtSK32 expressed in the
244 QC (Figure S9 and Figure 2A). Meanwhile, we used the yeast 2-hybrid (Y2H) assay to screen all
245 AtSK proteins for interactions with the WOX5 protein. The results revealed that only the subfamily II
246 of AtSKs (ATSK21, ATSK22 and ATSK23) have the weak interaction with WOX5 (Figure 2B). On
247 the whole, only the subfamily II of AtSKs may interact with WOX5 in root tips. To further testify that
248 the subfamily II of AtSKs interact with WOX5, we performed bimolecular fluorescent complimentary
249 (BiFC) in the *nicotiana tabacum*. The results showed that the positive control HAIRY MERISTEM
250 4(HAM4) interacts with WOX5 (Figure S10A) (Zhou et al., 2018), the members of subfamily II of
251 AtSKs (ATSK21, ATSK22, and ATSK23) interact with WOX5 (Figure 2C), the negative control
252 RGA not interacts with WOX5 (Figure S10B), and AtSK21 not interacts with WUS (Figure S10C).
253 Owing to the three proteins of the subfamily II of AtSKs share very high amino acid sequence
254 similarity (Figure S11), so we selected AtSK21 as a representative for the following assays. Pull-down
255 in vitro assays revealed MBP-WOX5 interacts with GST-AtSK21, but MBP-WOX5 not interacts with
256 GST, and MBP not interacts with GST and GST-AtSK21 (Figure 2D). Finally, we combined
257 p35S:Flag-AtSK21/Col-0 (He et al., 2019) with p35S:LhGR-pOp:WOX5-YFP/Col-0 (Pi et al., 2015)
258 for obtaining the double homozygous line, thereafter we performed co-immunoprecipitation (CoIP) in
259 vivo using GFP beads for enriching WOX5-YFP fusion protein, the input proteins and
260 immunoprecipitation protein detected by immunoblotting using anti-Flag and anti-GFP antibodies.
261 The data revealed that AtSK21 protein can interact with WOX5 protein in *Arabidopsis* (Figure 2E).
262 Taken together, the subfamily II of AtSKs interacts with WOX5 in vitro and in vivo.

263 WOX5 is epistatic to the subfamily II of AtSKs in inhibiting the
264 proliferative activity of QC cells

265 To figure out whether the subfamily II of AtSKs are involved in regulating proliferative activity of QC
266 cells, and to testify the genetic connection between WOX5 and the subfamily II of AtSKs, we
267 combined the *wox5-1* and *atsk21/22/23* (Yan et al., 2009) for obtaining the quadruple mutant
268 (*atsk21/22/23/wox5-1*). Thereafter, we counted the PAe and PAr of a lot of mature embryos and root
269 tips of WT, *wox5-1*, *atsk21/22/23* and *atsk21/22/23/wox5-1* by using the improved mPS-PI staining
270 technique (Truernit et al., 2008). The PAr and PAe of Col-0 are very low as 0.071 and 0.059, which is
271 remarkably lower than the value of *wox5-1* that equal to 2.803 and 2.203. (Figure 3A,B,F,G,H,I). This
272 result revealed that WOX5 maintains the low proliferative activity of QC cells, which is consistent
273 with previous reports (Burkart et al., 2019; Celine et al., 2014). The PAr and PAe of *Wassilewskija*
274 (Ws) (the WT of *atsk21/22/23*) are low as 0.273 and 0.073, which is remarkably lower than the PAr

275 and PAe of *atsk21/22/23* (equal to 1.396 and 0.731) (Figure 3C,D,F,G,J,K). This result revealed that
276 the subfamily of AtSKs also inhibit the proliferative activity of QC cells. The PAr and PAe of *wox5-*
277 *1/atsk21/22/23* are very high as 2.831 and 2.053, which is not different with the PAr and PAe of *wox5-*
278 *1* (Figure 3E,F,G,L). This result indicates that WOX5 is epistatic to the subfamily II of AtSKs in
279 inhibiting the proliferative activity of QC cells. A small molecule, Bikinin (Bik), acts as an ATP
280 competitor, which inhibits kinase activity of seven AtSKs (AtSK11, AtSK12, AtSK13, AtSK21,
281 AtSK22, AtSK23, AtSK31) (De Rybel et al., 2009). To determine the optimum concentration of Bik
282 for inhibiting the kinase activity of the subfamily II of AtSKs, we planted Col-0 and Ws on the ½ MS
283 medium (containing 1% agar and 1% sucrose) with 0 (DMSO, the Mock), 15 and 30 μM Bik. We
284 found that treating with the 30 μM Bik (Figure S12A,B,D,G), rather than the Mock and the 15 μM
285 Bik treatment (Figure S12C,E,F), could simulate the downward spiral root tips phenotypes of
286 *atsk21/22/23* root tips that like the instant noodles. Thus, we simultaneously planted Col-0, Ws and
287 *wox5-1* on the ½ MS medium containing 30 μM Bik or with DMSO (the Mock). Compared to the
288 Mock, treating with the 30 μM Bik, the value of PAr of Col-0 significantly increased from 0.245 to
289 1.712 ,while Ws increased from 0.245 to 1.547 (Figure S13A~D,G), which had almost no difference
290 with the PAr of *atsk21/22/23* (Figure S13H). These results also that 30 μM Bik treatment can mimic
291 the increased QC proliferative activity of *atsk21/22/23*, and it was only the subfamily II of ten AtSKs
292 that involved in inhibiting proliferative activity of QC cells. However, treating with the 30uM Bik, the
293 PAr of *wox5-1* almost had no difference with the Mock (from 2.771 to 2.875) (Figure S13E~G),
294 which also indicated that WOX5 is epistatic to the subfamily II of AtSKs in maintaining low
295 proliferative activity of QC cells.
296 In addition, we planted the QC184 line, QC184/*wox5-1* line and QC25 line, QC25/*wox5-1* line on the
297 ½ MS medium with 30 μM Bik or Mock. We took GUS staining using 5DAG root tips, the GUS
298 activity in the QC of QC184 line and QC25 line on the Mock are higher than on the 30 μM Bik
299 (Figure S14A,C,E,G), however, in the *wox5-1* backgroud, the QC cells' GUS activity of QC184 and
300 QC25 with 30 μM Bik treatment is not different from the Mock (Figure S14B,D,F,H). The results
301 indicated that increased QC proliferative activity causes a decrease of QC184/QC25 GUS activity and
302 WOX5 is epistatic to the subfamily II of AtSKs in maintaining the identity of QC.

303 The subfamily II of AtSKs inhibit the proliferative activity of QC cells by 304 phosphorylating and stabilizing the WOX5 protein

305 Since the subfamily II of AtSKs and WOX5 protein interact in inhibiting the proliferative activity of
306 QC cells, we want to figure out how these kinases regulate the WOX5 protein in the QC cells.
307 Therefore, we performed the sqRT-PCR and qPCR assays, in contrast to the Ws, the mRNA level of
308 WOX5 got no change in the *atsk21/22/23* (Figure S15A,B), suggesting that the subfamily II of AtSKs
309 does not affect the transcriptional level of WOX5 in *Arabidopsis*. We then combined stable

310 homozygous lines of pWOX5:nlsGFP/Col-0 and pWOX5:WOX5GFP/Col-0 (Pi et al., 2015) to Ws
311 and *atsk21/22/23*, quantification of GFP fluorescence in the QC at the 5DAG root tips showed that the
312 expression level of WOX5 in *atsk21/22/23* was not different to in Ws (Figure 4A,B,C), however, the
313 protein level of WOX5 in *atsk21/22/23* was markedly lower than in Ws (Figure 4D,E,F). Moreover,
314 we treated the pWOX5:nlsGFP/Col-0 and pWOX5:WOX5GFP/Col-0 lines with 30 μM Bik (the
315 DMSO as the Mock) for 5 days. The quantification of GFP fluorescence in the QC also revealed that
316 the WOX5's expression level of pWOX5:nlsGFP/Col-0 on the Mock was not different to on 30 μM
317 Bik (Figure S16A,B,E), but the WOX5's protein level of pWOX5:WOX5GFP/Col-0 on the Mock
318 was markedly higher than on 30 μM Bik (Figure S16C,D,F). These data indicate that the subfamily II
319 of AtSKs stabilizes WOX5 protein in the QC cells, and the reducing WOX5 protein causes the
320 increase of the proliferative activity of QC cells (Figure S13E,F,G) and the decrease of QC184/QC25
321 GUS activity (Figure S14A,C,E,G).
322 According to the Figure S6 and the Figure 4A~F, we concluded that the GMs in the PEST domain
323 stabilizes WOX5 protein and the subfamily II of AtSKs stabilizes WOX5 protein. Thus, we speculate
324 that the subfamily II of AtSKs stabilizes WOX5 protein by phosphorylating the GMs in the PEST
325 domain. To testify this speculation, on one hand, we constructed three plasmids (WOX5-GFP,
326 WOX5m5D-GFP, WOX5m3D-GFP) (Figure S17A) by using site-directed mutagenesis, they were
327 introduced into *atsk21/22/23*, we selected 4 homozygous lines (named W5-1~W5-4, 5D-1~5D-4, 3D-
328 1~3D-4 separately) randomly from descendants of 10-15 T_1 phosphate-mimicked lines to perform
329 sqRT-PCR and qPCR assays, we identified 6 lines (W5-1, W5-2; 5D-1, 5D-2; 3D-1, 3D-2 separately)
330 with almost equal GFP expression (Figure S17B,C,D). We next counted the PA_e at the mature
331 embryonic stage and the PA_r at 5 DAG of these 6 phosphate-mimicked lines. The PA_e and PA_r of the
332 WOX5m3D-GFP/*atsk21/22/23* lines and WOX5m5D-GFP/*atsk21/22/23* lines were similar to the Ws
333 (Figure S18) and were significantly lower than the WOX5-GFP/*atsk21/22/23* lines (Figure 4G~J,
334 L~O), which indicated that these phosphate-mimicked lines could rescue the phenotype of
335 *atsk21/22/23*. Meanwhile, we quantified the fluorescence of GFP fusion protein in the QC zone at 5
336 DAG of the 6 lines. The intensity of WOX5m5D-GFP and WOX5m3D-GFP fusion protein were
337 markedly higher than WOX5-GFP fusion protein (Figure 4G~I, K), which revealed that these
338 phosphate-mimicked WOX5 protein could rescue the stability of WOX5 protein in the *atsk21/22/23*,
339 suggesting that the subfamily II of AtSKs stabilizes WOX5 protein by phosphorylating the GMs in the
340 PEST domain, and indicating that increased WOX5 protein can reduce the PA of QC. On the other
341 hand, we constructed prokaryotic expression vectors of GST-AtSK21, GST-AtSK21(K69R) (the
342 kinase dead type), MBP-WOX5, MBP-WOX5△PEST, MBP-WOX5mAll, MBP-WOX5m5A, MBP-
343 WOX5m3A and MBP-BZR1 (the positive control) (He et al., 2002), we purified these tagged protein
344 using MBP beads and GST beads, the images of CBB staining showed that we obtained the purified

345 MBP-BZR1, MBP, MBPWOX5, MBPWOX5△PEST, MBP-WOX5mAll, MBP-WOX5m5A, MBP-
346 WOX5m3A substrate proteins and GST-AtSK21, GST-AtSK21(K69R) kinase proteins (Figure S19A).
347 Thereafter, we performed kinase assay in vitro, and then running proteins in the Mn^{2+} Phos-tag SDS-
348 PAGE after terminating kinase reaction, the experiment group showed that GST-AtSK21 could
349 phosphorylate MBP-WOX5 (Figure S19C), but could not phosphorylate MBP-WOX5△PEST, MBP-
350 WOX5mAll, MBP-WOX5m5A, MBP-WOX5m3A (Figure S19C), GST-AtSK21(K69R) also could
351 not phosphorylate MBP-WOX5 (Figure S19C). In conclusion, the subfamily II of AtSKs stabilizes
352 WOX5 protein by phosphorylating the GMs in the PEST domain. Taken together, (the subfamily II of
353 AtSKs-) phosphorylated WOX5 protein inhibits proliferative activity of QC cells and maintains
354 identity of QC.

355 The subfamily II of AtPP2A-Cs interact with WOX5 in the QC cells

356 Since AtSKs stabilize WOX5 protein by phosphorylating the GMs, we speculate that phosphatases
357 may antagonize phosphorylation of AtSKs by dephosphorylating the GMs, therefore maintain the
358 homeostasis of WOX5 protein in the QC. In mammals, the Wnt/β-catenin signalling pathway plays a
359 crucial role in regulating pluripotency and proliferative activity of stem cell (Clevers et al., 2014;
360 Sokol, 2011). β-catenin serves as a central component of the Wnt/β-catenin signalling pathway, which
361 homeostasis is phosphorylated by GSK3 and dephosphorylated by PP2A holoenzyme, regulates the
362 activity of downstream central transcriptional factors (TFs) (MacDonald et al., 2009; Su et al., 2008).
363 In *Arabidopsis*, the QC is required for maintaining the homeostasis of SCN and is the source of stem
364 cells. WOX5, which serves as the central TF for maintaining the activity of QC, whether its
365 homeostasis is regulated by the pair of antagonists (GSK3s and PP2As) remains unknown. Thus, we
366 focus on five members of AtPP2A-Cs family owing to the catalytic subunit of PP2A holoenzyme is
367 required for dephosphorylation (Shi, 2009). We want to figure out which AtPP2A-Cs in the
368 *Arabidopsis* may be involved in dephosphorylating WOX5 protein. Firstly, we performed sqRT-PCR
369 assay, the results showed that all five AtPP2A-Cs expressed in the one centimeter root tips of Col-0 at
370 5 DAG (Figure S20). Next, we obtained all transcriptional reporters of five AtPP2A-Cs in Col-0
371 ecotype including subfamily I (pC1:nlsGFP, pC2:nlsGFP, pC5:nlsGFP); subfamily II (pC3:nls3×GFP,
372 pC4: nls3×GFP). We found that only AtPP2A-C3, AtPP2A-C4, AtPP2A-C5 expressed in the QC
373 (Figure 5A). Meanwhile, we constructed WOX5 on the BD and five AtPP2A-Cs on the AD for Y2H
374 assays, the results revealed that AtPP2A-C1, AtPP2A-C2, AtPP2A-C3 and AtPP2A-C4 have strong
375 interaction with WOX5 just like the positive control of WOX5 and TPR1 (Figure 5B) (Pi et al., 2015),
376 and the AtPP2A-C5 have no interaction with WOX5, and the negative control RGA have no
377 interaction with WOX5 (Figure 5B). On the whole, only the subfamily II of AtPP2A-Cs (AtPP2A-C3
378 and AtPP2A-C4) may interact with WOX5 in root tips. To further testify that subfamily II of AtPP2A-
379 Cs (AtPP2A-C3 and AtPP2A-C4) interact with WOX5, we performed BiFC in the *nicotiana tabacum*,

380 the results indicated that the positive control HAM4 interacts with WOX5 (Zhou et al., 2018) (Figure
381 S10A), the subfamily II of AtPP2A-Cs (AtPP2A-C3 and AtPP2A-C4) interacts with WOX5 (Figure
382 5C), the negative control RGA not interacts with WOX5 (Figure S10B) and AtPP2A-C3 not interacts
383 with WUS (Figure S10D). Thereafter, MBP pull-down in vitro assays revealed MBP-WOX5 interacts
384 with GST-C3 and GST-C4 (Figure 5D). Finally, we generated the transgenetic homozygous lines of
385 35S : Flag-C3/Col-0 and 35S : Flag-C4/Col-0, then we combined them with 35S : LhGR-pOp :
386 WOX5-YFP/Col-0 (Pi et al., 2015) line for obtaining the double homozygous lines of 35S : Flag-
387 C3/Col-0 × 35S : LhGR-pOp : WOX5-YFP/Col-0 and 35S : Flag-C4/Col-0 × 35S : LhGR-pOp :
388 WOX5-YFP/Col-0 separately. Thereafter we performed CoIP in vivo. The results revealed that
389 AtPP2A-C3 and AtPP2A-C4 proteins can interact with WOX5 protein in *Arabidopsis* (Figure 5E).
390 Taken together, the subfamily II of AtPP2A-Cs interacts with WOX5 in vitro and in vivo.

391 The subfamily II of AtPP2A-Cs increased the proliferative activity of QC 392 cells by dephosphorylating and destabilizing the WOX5 protein

393 Given that the subfamily II of AtSKs inhibit the proliferative activity of QC cells by phosphorylating
394 and stabilizing the WOX5 protein (Figure 4, Figure S19), and the subfamily II of AtPP2A-Cs interacts
395 with WOX5 protein (Figure 5). So we want to figure out whether the subfamily II of AtPP2A-Cs can
396 increase the proliferative activity of QC cells by dephosphorylating and destabilizing the WOX5
397 protein. Therefore, performed sqRT-PCR and qPCR using the cDNA from the mutant of loss function
398 of the subfamily II of AtPP2A-Cs (*c3c4*) (Spinner et al., 2013) or Col-0. In contrast to the Col-0, the
399 WOX5 expression level increased almost 1.5 times in the *c3c4* (Figure S21A). We then combined
400 pWOX5:nlsGFP/Col-0 and pWOX5:WOX5GFP/Col-0 (Pi et al., 2015) with *c3c4*. Quantification of
401 GFP fluorescence in the QC at the 5DAG root tips demonstrated that the expression level of WOX5 in
402 the QC of *c3c4* was comparable to that in Col-0 (Figure 6A~D,I). However, quantification of GFP
403 fluorescence in the SI and SID at the 5DAG root tips showed that the expression level of WOX5 in the
404 SI and SID of *c3c4* was markedly higher than Col-0 (Figure 6A~D,I). These data indicate that the
405 increased abundance of WOX5 mRNA is derived from the SI and SID, rather than from the QC cells
406 in *c3c4* mutants. We then quantified the protein levels of WOX5 in Col-0 and *c3c4* plants by
407 measuring the GFP fluorescence in the QC, SI and SID at the 5DAG root tips. The results showed that
408 the GFP fluorescence in the QC and SI of *c3c4* was significantly higher than that in Col-0 (Figure
409 6E~H,J). These results suggest that loss of function of the subfamily II of AtPP2A-Cs increased the
410 content of WOX5 protein in the QC by enhancing the stability of WOX5 protein, and increased the
411 content of WOX5 protein in the SI and SID by increasing the mRNA content of WOX5 and/or by
412 enhancing the stability of WOX5 protein. Thus, the subfamily II of AtPP2A-Cs destabilizes WOX5
413 protein.

414 WOX5 protein reduced in QC cells of *atsk21/22/23* (Figure 4D~F), but WOX5 protein increased in
415 QC cells of *c3c4* (Figure 6E~H,J). Consequently, we speculate that the subfamily II of AtPP2A-Cs
416 may promote the proliferative activity of QC cells by dephosphorylating the GMs being
417 phosphorylated by the subfamily II of AtSKs. To testify this speculation, firstly, we generated the
418 transgenetic homozygous lines of 35S : AtPP2A-C3-GFP/Col-0 and 35S : AtPP2A-C4-GFP/Col-0, we
419 extracted the total proteins of 2 centimeters root tips of 35S : AtPP2A-C3-GFP/Col-0 line and 35S :
420 AtPP2A-C4-GFP/Col-0 line at 5 DAG, we next used GFP beads to purify the holoenzymes of
421 AtPP2A-C3-GFP and AtPP2A-C4-GFP. The result of immunoprecipitation of anti-GFP showed that
422 we obtained the holoenzymes of AtPP2A-C3-GFP and AtPP2A-C4-GFP (Figure 6Q). Subsequently,
423 we conducted in vitro dephosphorylation assays and utilized Phos-tag-Mn^{2+}-SDS-PAGE to separate
424 phosphorylated proteins. Similarly to lambda protein phosphatases (Lambda PP), the holoenzymes of
425 AtPP2A-C3-GFP and AtPP2A-C4-GFP were also able to dephosphorylate the (GST-AtSK21-)
426 phosphorylated MBP-WOX5 protein (Figure 6W). In addition, we observed and quantified the PAr of
427 35S:AtPP2A-C3-GFP/Col-0 and 35S:AtPP2A-C4-GFP/Col-0 overexpressed lines, in comparison to
428 Col-0, all of these lines exhibited significantly increased PAr (Figure 6K,M,N). Furthermore, we
429 overexpressed AtPP2A-C3-GFP and AtPP2A-C4-GFP protein by using GAL4-VP16 transcriptional
430 activator driving by the full-length promotor of WOX5 genomic sequence, followed 6 multiple
431 upstream activation sequence (6×UAS) (pWOX5:GAL4-VP16-6×UAS: CDS-GFP, abbreviated as
432 GVUAS:CDS-GFP here after) (Figure S22). Compared to Col-0, all the specific overexpressed lines
433 also showed a significant increase in PAr (Figure 6L,O,P). These findings suggest that overexpression
434 of subfamily II of AtPP2A-Cs proteins can enhance the proliferative activity of QC. In summary, the
435 subfamily II of AtPP2A-Cs plays a role in reducing the WOX5 protein in QC, SI, and SID, thereby
436 increasing the proliferative activity of QC cells through the dephosphorylation of (the subfamily II of
437 AtSKs-) phosphorylated WOX5 protein.

438 WOX5 is necessary for producing more quiescent cells when loss of 439 function the subfamily II of AtPP2A-Cs

440 Since loss of function of the subfamily II of AtPP2A-Cs increased WOX5 protein in QC, SI, and SID
441 (Figure 6F~H,J), we reason that the phenotypes of *c3c4* mutant might appear more quiescent cells. To
442 testify this reasoning, firstly, we noticed that the 5 DAG seedling of *c3c4* in the ½ MS medium present
443 several different phenotypes including short root (22.60%), shorter root (37.57%), shortest root
444 (33.05%) and three cotyledons (6.78%) (Figure S23). Thus, we viewed the root tips and mature
445 embryos of *c3c4* carefully, the root tips at 5 DAG also have several phenotypes including (here we
446 firstly named as) two layers QC-like cells (41.11%) (Figure 7B), more and wider QC-like cells
447 (33.33%) (Figure 7C), one layer QC cells (25.56%) (Figure 7D), the mature embryos also have several
448 phenotypes including two layers QC-like cells (36.36%) (Figure 7H), more and wider QC-like cells

449 (35.06%) (Figure 7I), one layer QC (28.57%) (Figure 7J). Compared to Col-0 (Figure 7A,G), the
450 significantly increased abnormal phenotypes in two layers of QC-like cells and the presence of more
451 and wider QC-like cells suggest that in the *c3c4* , the proliferative activity of QC cells doesn't change,
452 but instead produces more QC-like cells originating from SI and SID. Then, we view the root tips of
453 *c3c4* by using another method of EdU (5-ethynyl-2'-deoxyuridine)-based S-phase assay (Kotogány et
454 al., 2010) because the cell plates of SI and SID are not convenient to counting. We transplanted the
455 4DAG seedling of *c3c4* to ½ MS with 2.5 μM EdU for 12 hours. After EdU staining, compare with
456 the images of one layer nondividing cells without EdU incorporation signal (95.59%) of WT (Figure
457 7M), the images of *c3c4* mutant can also be classified into three types including (here we firstly
458 named as) two layers nondividing cells without EdU incorporation signal (33.58%) (Figure 7N), more
459 and wider nondividing cells (38.06%) without EdU incorporation signal (Figure 7O), and one layer
460 nondividing cells (28.36%) without EdU incorporation signal (Figure 7P). These results showed that
461 the QC proliferative activity of the *c3c4* is similar to that of the WT, but the proliferative activity of SI
462 and SID of *c3c4* is significantly lower than that of the WT. These data demonstrate that increased
463 WOX5 protein in QC (Figure 6F~H,J) still maintains quiescence of QC cells, but increased WOX5
464 protein in SI and SID (Figure 6F~H,J) reduces the PA of SI and SID, therefore produced more
465 quiescent cells.
466 Since the reduced WOX5 protein in *atsk21/22/23* cause a decline of GUS activity QC184 and QC25
467 (Figure 4D~F, Figure S14A,C,E,G), we speculate that increased WOX5 protein in *c3c4* can lead to an
468 increase in GUS activity of QC184 and QC25. Thus, we combined QC25 and QC184 with *c3c4* for
469 obtaining QC25/*c3c4* and QC184/*c3c4* homozygous lines. After GUS staining assay, compare with
470 just one layer blue cells of QC184 (100%) (Figure 7S), the phenotypes of QC184/*c3c4* can be divided
471 into three types including (here we firstly named as) two layers blue cells (37.04%) (Figure 7T), more
472 and wider blue cells (30.25%) (Figure 7U) and one layer blue cells (31.48%) (Figure 7V), and the
473 GUS activity in QC of almost all QC184/*c3c4* is markedly higher than QC184. Likewise, compare
474 with just one layer blue cells of QC25 (95.56%) (Figure S24A), the phenotypes of QC25/*c3c4* can
475 also be divided into three types as above, including two layers blue cells (33.77%) (Figure S24B),
476 more and wider blue cells (34.42%) (Figure S24C) and one layer blue cells (31.82%) (Figure S24D),
477 and the GUS activity in QC of almost all QC25/*c3c4* is markedly higher than QC25. The results
478 suggest that increased WOX5 protein in QC of *c3c4* (Figure 6F~H,J) can increase GUS activity of
479 QC184 and QC25, and increased WOX5 protein in SI and SID (Figure 6F~H,J) of *c3c4* can also
480 enhance GUS activity of QC184 and QC25.
481 To further testify that WOX5 is necessary for producing more quiesent cells and increasing GUS
482 activity of QC184 and QC25. We further combined *wox5-1* with *c3c4* and QC25/*c3c4* and
483 QC184/*c3c4* for obtaining homozygous lines of *c3c4wox5-1*, QC25/*c3c4wox5-1*, QC184/*c3c4wox5-1*.
484 After mPS-PI viewing and EdU staining, the results show that the phenotypes of high PA cells and

485 one layer dividing cells of almost all *c3c4wox5-1* (Figure 7F,L) do not exhibit any significant
486 deviations from that of the *wox5-1* (Figure 7E,K) from the embryonic stage to the post-embryonic
487 stage. After GUS staining, the lack of GUS activity (here we named as one layer not blue cells) of
488 QC184/*c3c4wox5-1* (Figure 7X) is not different from that in QC184/*wox5-1* (Figure 7W), and the low
489 QC GUS activity (here we named as one layer light blue cells) of QC25/*c3c4wox5-1* (Figure S24E) is
490 not different from that in QC25/*wox5-1* (Figure S24F). These data suggest that WOX5 is necessary for
491 producing more quiescent cells and for increasing GUS activity of QC184 and QC25 in *c3c4*
492 background.
493 To demonstrate the requirement of phosphorylated WOX5 protein in producing additional quiescent
494 cells and elevating GUS activity of QC184 and QC25 in the absence of subfamily II of AtPP2A-Cs.
495 We used 30 μM Bik to processing genetic materials of pWOX5:nlsGFP/*c3c4* and
496 pWOX5:WOX5GFP/*c3c4*. Compared to the Mock, the GFP intensity in QC, SI, and SID regions of
497 transcriptional reporter exposed to the 30 μM Bik are not changed (Figure S25A~F,N). However, the
498 GFP intensity in the same regions of the protein reporter markedly decreased (Figure S25G~M,O),
499 indicating that increased WOX5 protein in *c3c4* mainly is the phosphorylated WOX5 protein.
500 Additionally, these phosphorylated WOX5 protein gradually degraded when the kinase activity of
501 subfamily II of AtSKs is continuously inhibited using 30 μM Bik. Therefore, we next used 30 μM Bik
502 to processing genetic material of *c3c4* mutant and viewed the root tips by using the mPS-PI method,
503 compared with the Mock, the proliferative activity of QC cells (Figure S26A~F) and QC-like cells
504 (Figure S26A,B,D,F) in the 30 μM Bik are markedly increased (Figure S26A~F). EdU staining assays
505 further demonstrated that the proliferative activity of QC cells (nondividing cells) and QC-like cells
506 (more and wider nondividing cells) in the 30 μM Bik are markedly enhanced (Figure S26G~L). These
507 findings suggest that a reduction in phosphorylated WOX5 protein levels can enhance the proliferative
508 activity of cells. Finally, we processing genetic materials of QC25/*c3c4* and QC184/*c3c4* using 30 μM
509 Bik and viewed root tips by GUS staining assays. Compared to the Mock, we observed a significant
510 reduction in GUS activity of QC25 and QC184 in QC, SI, and SID when treated with 30 μM Bik
511 (Figure S26M~X), suggesting that reduced phosphorylated WOX5 protein would lead to decreased
512 GUS activity in these cells. All these results suggest that increased phosphorylated WOX5 protein is
513 required for producing more quiescent cells and for increasing GUS activity of QC184 and QC25.
514 Cantharidin (CT), a potent inhibitor of the catalytic subunit (C subunit) of PP2A holoenzymes (Li and
515 Casida, 1992), is utilized to further confirm that the essential role of WOX5 in promoting the
516 production of quiescent cells and enhancing GUS activity in QC184 and QC25, by inhibiting the
517 subfamily II of AtPP2A-Cs. Firstly, to determine the optimum concentration of CT and time for
518 processing root tips, we transplant 4 DAG Col-0 seedlings to the ½ MS medium with 0 (DMSO, the
519 Mock), 15 and 30 μM CT for 24 hours, and 48 hours (Bian et al., 2020). We found that only the 30
520 μM CT for 48 hours could appear the phenotypes of short root and more root hairs which are similar

521 to the root phenotypes of *c3c4* mutant (Figure S27), rather than the Mock and 15 μM CT (Figure S27).
522 Furthermore, 30 μM CT effectively impedes the dephosphorylation activity of both AtPP2A-C3-GFP
523 and AtPP2A-C4-GFP in the reaction buffer. However, Lambda PP's dephosphorylation activity
524 remains unaffected by the presence of CT (Figure 6W). So we next transplanted 4 DAG seedlings of
525 Col-0 and *wox5-1* to the ½ MS medium with the Mock and 30 μM CT for 48 hours, then we viewed
526 the SCN of root tips using improved mPS-PI staining. We noticed that the starch grains of all root tips
527 of 30 μM CT for 48 hours disappeared or partly disappeared, also indicated that 30 μM CT for 48
528 hours could interface other pathways (like auxin distribution and/or gravitropism) by inhibiting the
529 dephosphorylation activity of the AtPP2A-Cs (Ballesteros et al., 2013; Bian et al., 2020; Rahman et al.,
530 2010). We observed that compare to the 100% one layer QC cells of the Mock (Figure S28A),
531 43.18% root tips of Col-0 in the 30 μM CT exhibited two layers QC-like cells (Figure S28B), 36.36%
532 showed more and wider QC-like cells (Figure S28C), 20.45% displayed one layer QC cells (Figure
533 S28D). However, the phenotype of *wox5-1* in 30 μM CT (90.24%), characterized by one layer high
534 PA cells (Figure S28F), showed almost no difference from that in the Mock (93.75%) (Figure S28E).
535 The EdU staining assays showed that compared with 95.24% one layer nondividing cells of the Mock
536 (Figure S28G), 44.83% root tips of Col-0 in the 30 μM CT were two layers nondividing cells (Figure
537 S28H), 34.48% were more and wider nondividing cells (Figure S28I), 20.69% were one layer
538 nondividing cells (Figure S28J). However, the phenotype (one layer dividing cells) of *wox5-1* in 30
539 μM CT (85.71%) (Figure S28L) was almost not different with in Mock (89.47%) (Figure S28K). The
540 results indicate that inhibiting the function of the subfamily II of AtPP2A-Cs by CT can also produce
541 more quiescent cells and WOX5 is required for it. Finally, we transplant 4 DAG seedlings of QC25,
542 QC25/*wox5-1* and QC184 QC184/*wox5-1* to the ½ MS medium with the Mock and 30 μM CT for 48
543 hours. The GUS staining assay showed a significant increase GUS activity in the QC cells of QC25
544 treated with 30 μM CT compared to Mock (Figure S29A~D,G~J), and GUS activity of QC25 and
545 QC184 appeared in the SI and SID (two layers blue cells and more and wider blue cells) in the 30 μM
546 CT, not in the Mock (Figure S29A~D,G~J). However, there was no significant difference in GUS
547 activity of QC25/*wox5-1* and QC184/*wox5-1* in 30 μM CT compared to the Mock (FigureS29E,F,K,L).
548 These data suggest that WOX5 is necessary for increasing GUS activity of QC184 and QC25 when
549 inhibiting the subfamily II of AtPP2A-Cs.
550 Taken together, all these results demonstrate that the subfamily II of AtPP2A-Cs regulates the
551 homeostasis of QC, and WOX5 protein is required for it.

552 In situ overexpressed WOX5 protein recapitulated more quiescent cells

553 The results of Figure 7, Figure S24, Figure S28 and Figure S29 proved that WOX5 protein was
554 required for producing more quiescent cells when loss of function of the subfamily II of AtPP2A-Cs,
555 however, it is yet to be determined whether WOX5 protein simultaneously upregulated in QC, SI, and

556 SID in WT causes production of more quiescent cells. Previous studies (Burkart et al., 2019; Pi et al.,
557 2015) and our WOX5 transcriptional reporters (Figure S30A,B) have all showed that WOX5 mainly
558 expressed in the QC cells and slightly expressed in the SI and SID. Thus, in order to obtain genetic
559 material of WOX5 protein simultaneously upregulated in QC, SI, and SID (here we called in situ
560 overexpressed WOX5 protein), we introduced the GVUAS:WOX5GFP plasmid into Col-0 and *wox5-*
561 *1*, obtained transgenetic homozygous lines of GVUAS:WOX5GFP/Col-0 and
562 GVUAS:WOX5GFP/*wox5-1*. Quantification of GFP intensity show that the WOX5GFP protein in QC,
563 SI, and SID of GVUAS:WOX5GFP/Col-0 line is significantly higher than the
564 pWOX5:WOX5GFP/Col-0 line (Figures S31A-E), and GVUAS:WOX5GFP/*wox5-1* line is also
565 markedly higher than pWOX5:WOX5GFP/*wox5-1* line (Figure S31F-J), suggesting that WOX5
566 protein in situ overexpressed successfully.
567 Firstly, we viewed pWOX5:WOX5GFP lines and in situ overexpressed WOX5 protein lines by
568 improved mPS-PI. Compared with the 100% one layer QC cells of root tips and mature embryos of
569 pWOX5:WOX5GFP/Col-0 line, 58.93% root tips and 52.63% mature embryos of
570 GVUAS:WOX5GFP/Col-0 line presented two layers QC-like cells (Figure S32B and S32F), 26.79%
571 root tips and 26.32% mature embryos of GVUAS:WOX5GFP/Col-0 line appeared more and wider
572 QC-like cells (Figure S32C and S32G), only 14.29% root tips and 21.05% mature embryos of
573 GVUAS:WOX5GFP/Col-0 line kept one layer QC cells (Figure S32D and S32H). These data
574 indicated that in situ overexpressed WOX5 protein in Col-0 could recapitulate the phenotypes of more
575 QC-like cells in *c3c4* from the embryonic stage to the postembryonic stage. Likewise, compared with
576 the 100% one layer QC cells of root tips and mature embryos of pWOX5:WOX5GFP/*wox5-1* line,
577 60.00% root tips and 54.00% mature embryos of GVUAS:WOX5GFP/*wox5-1* line presented two
578 layers QC-like cells (Figure S33C and S33H), 30.00% root tips and 36.00% mature embryos of
579 GVUAS:WOX5GFP/*wox5-1* line appeared more and wider QC-like cells (Figure S33D and S33I),
580 and 10.00% root tips and 10.00% mature embryos of GVUAS:WOX5GFP/*wox5-1* line kept one layer
581 QC cells (Figure S33E and S33J). These data indicated that in situ overexpressed WOX5 protein in
582 *wox5-1* not only rescued the phenotypes of *wox5-1* (Figure S33A and S33F), but also recapitulated the
583 phenotypes of more QC-like cells in *c3c4* from the embryonic stage to the postembryonic stage.
584 Secondly, EdU staining assays showed that compared with almost 91.67% one layer nondividing cells
585 of root tips of pWOX5:WOX5GFP/Col-0 line, 54.17% root tips of GVUAS:WOX5GFP/Col-0 line
586 presented two layers nondividing cells (Figure S32J), 30.56% appeared more and wider nondividing
587 cells (Figure S32K), 15.28% kept one layer nondividing cells (Figure S32L). The data indicated that
588 in situ overexpressed WOX5 protein in Col-0 could recapitulate the phenotypes of more nondividing
589 cells in *c3c4*. Likewise, compared with almost 90.48% one layer nondividing cells of root tips of
590 pWOX5:WOX5GFP/*wox5-1* line, 50.85% root tips of GVUAS:WOX5GFP/*wox5-1* line presented two
591 layers nondividing cells (Figure S33M), 32.20% appeared more and wider nondividing cells (Figure

592 S33N), 16.95% kept one layer nondividing cells (Figure S33O). The results suggest that in situ
593 overexpressed WOX5 protein in *wox5-1* not only rescued the phenotypes of 100% one layer dividing
594 cells of *wox5-1* (Figure S33K), but also recapitulated more nondividing cells in *c3c4*.
595 Thirdly, in order to further testify whether in situ overexpressed WOX5 protein can increase GUS
596 activity of QC25 and QC184 in QC, SI, and SID. We combined QC markers (QC184 and QC25) with
597 GVUAS:WOX5GFP/Col-0 line and GVUAS:WOX5GFP/*wox5-1* line for obtaining
598 QC184/GVUAS:WOX5GFP/Col-0, QC184/GVUAS:WOX5GFP/*wox5-1* homozygous lines and
599 QC25/GVUAS:WOX5GFP/Col-0, QC25/WOX5GFP/*wox5-1* homozygous lines. Then we processed
600 the 5 DAG root tips of these materials by GUS staining, compared with 100% one layer blue cells of
601 QC184 (Figure S32M) and QC25 (Figure S32Q), 40.82% root tips of
602 QC184/GVUAS:WOX5GFP/Col-0 line (Figure S32N) and 62.20% QC25/GVUAS:WOX5GFP/Col-0
603 line (Figure S32R) presented two layers blue cells, 44.90% root tips of
604 QC184/GVUAS:WOX5GFP/Col-0 line (Figure S32O) and 17.78% QC25/GVUAS:WOX5GFP/Col-0
605 line (Figure S32S) appeared more and wider blue cells, only 14.29% root tips of
606 QC184/GVUAS:WOX5GFP/Col-0 line (Figure S32P) and 20.00% QC25/GVUAS:WOX5GFP/Col-0
607 line (Figure S32T) kept one layer blue cells. The result show that the GUS activity in QC of all these
608 materials are markedly higher than QC184 (Figure S32M-P) and QC25 (Figure S32Q-T), and the
609 GUS activity in SI and SID appeared in most of these materials (Figure S32N-P and S32R-T), but not
610 in QC184 (Figure S32M) and QC25 (Figure S32Q). Likewise, compared with 100% one layer blue
611 cells of QC184 (Figure S33Q) and QC25 (Figure S33V), 37.04% root tips of
612 QC184/GVUAS:WOX5GFP/*wox5-1* line (Figure S33R) and 51.43% QC25/GVUAS:WOX5GFP/
613 *wox5-1* line (Figure S33W) presented two layers blue cells, 48.15% root tips of
614 QC184/GVUAS:WOX5GFP/*wox5-1* line (Figure S33S) and 31.43%
615 QC25/GVUAS:WOX5GFP/*wox5-1* line (Figure S33X) appeared more and wider blue cells, only
616 14.81% root tips of QC184/GVUAS:WOX5GFP/*wox5-1* line (Figure S33T) and 17.14%
617 QC25/GVUAS:WOX5GFP/*wox5-1* line (Figure S33Y) kept one layer blue cells. The results showed
618 in situ overexpressed WOX5 protein not only rescue the phenotypes of one layer not blue cells of
619 QC184/*wox5-1* (Figure S33P) and one layer light blue cells of QC25/*wox5-1* (Figure S33U), but also
620 increased GUS activity in QC, SI, and SID (Figure S33Q-T and Figure S33V-Y). All these data
621 indicated that increased WOX5 protein in SI and SID is sufficient for reducing the proliferative
622 activity of QC and enhancing GUS activity of QC184/QC25, and increased WOX5 protein in QC is
623 also sufficient for reducing the proliferative activity of QC and increasing GUS activity of
624 QC184/QC25.
625 Finally, in order to view directly increased WOX5 protein in QC cause its PA reduction and increased
626 WOX5 protein in SI and SID lead to these cells convert to QC-like cells. We introduced the
627 GVUAS:GR-WOX5GFP plasmid into *wox5-1*, obtained transgenetic homozygous lines of

628 GVUAS:GR-WOX5GFP/*wox5-1*. For observing the process of dynamic accumulation of WOX5GFP
629 protein, we plant seeds of lines of GVUAS:GR-WOX5GFP/*wox5-1* into ½ MS medium with 20 μM
630 Dexamethasone (Dex) and the Mock with DMSO. We viewed lots of root tips at selected 5 time nodes
631 (3.0 days, 3.5 days, 4.0 days, 4.5 days, 5.0 days) separately. Through the GFP imaging and PI staining
632 assays and EdU staining assays, we found that in the Mock (no induction), the GR-WOX5GFP protein
633 could not rescue the phenotypes of one layer high PA cells of *wox5-1* (100.00%) (Figure S34A and
634 S34G) and one layer dividing cells (100.00%) (Figure S34M). But the dynamic accumulation of
635 WOX5GFP protein in QC at 3.0 DAG after induction (20 μM Dex) causes one layer QC cells with
636 WOX5GFP protein (90.91%) (Figure S34B and S34H) and one layer nondividing cells (91.67%)
637 (Figure S34N). The dynamic accumulation of WOX5GFP protein in SI from 3.0 DAG to 4.5 DAG
638 after induction leads to the dividing SI cells (91.67%, 81.48%) (Figure S34N and S34O) with low
639 content WOX5GFP protein (90.91%, 91.30%) (Figure S34B,C,H,I) gradually convert to nondividing
640 one layer QC-like cells (65.51%, 50.00%) (Figure S34P,Q) with high content WOX5GFP protein
641 (88.88%, 62.50%) (Figure S34D,E,J,K). The dynamic accumulation of WOX5GFP protein in SID
642 from 4.5 DAG to 5.0 DAG after induction leads to dividing SID cells (50.00%) (Figure S34Q) with
643 low content WOX5GFP protein (62.50%) (Figure S34E,K) convert to nondividing one layer QC-like
644 cells (50.00%) (Figure S34R) with high content WOX5GFP protein (50.00%) (Figure S34F,L). These
645 data suggest that increased WOX5 protein in QC causes its PA reduction and increased WOX5 protein
646 in SI and SID lead to PA reduction of these cells.
647 Taken together, in situ overexpressed WOX5 protein is sufficient for producing more quiescent cells.

648 Phosphate-mimicked WOX5 protein partially recapitulated more 649 quiescent cells

650 To confirm the critical role of phosphorylated WOX5 protein in its stability and reduction of PA of SI
651 and SID. Firstly, we noticed that some phosphate-mimicked homozygous lines (WOX5m3D-
652 GFP/*atsk21/22/23* line #2 and WOX5m5D-GFP/*atsk21/22/23* line #1, line #22) recapitulated the
653 phenotype of two layers QC-like cells in *c3c4* from the embryonic stage to the postembryonic stage
654 (Figure S35B~D and S35G~I), but WOX5GFP/*atsk21/22/23* lines not appeared the phenotype of two
655 layers QC-like cells (Figure S35A and S35F). Meanwhile, compare with WOX5 protein, phosphate-
656 mimicked WOX5 protein not only increased in QC (Figure 4G~J), but also increased in SI and SID
657 (Figure S35E). The results indicate that although without kinase activity of the subfamily II of AtSKs,
658 phosphate-mimicked WOX5 protein can't be dephosphorylated by AtPP2A-Cs holoenzymes,
659 therefore, the WOX5 protein remains continuously phosphorylated and stabilized, leading to the
660 conversion of SI and SID cells into QC-like cells. Secondly, we introduced WOX5m3D-GFP and
661 WOX5m5D-GFP driving by the full-length promotor plus 5' untranslated region (UTR) and 3'UTR of
662 WOX5 genomic sequence (Figure S2) into Col-0, obtained WOX5m3D-GFP/Col-0 and WOX5m5D-

663 GFP/Col-0 homozygous lines. We found that phosphate-mimicked WOX5 protein of WOX5m3D-
664 GFP/Col-0 line #2 and WOX5m5D-GFP/Col-0 line #1 markedly increased in QC, SI, and SID (Figure
665 S36B-D) when compared with WOX5 protein of WOX5GFP/Col-0 line (Figure S36A and S36D),
666 suggesting that phosphate-mimicked WOX5 protein is more stable than WOX5 protein. Thus, we
667 speculate that the more stable phosphate-mimicked WOX5 protein will cause the PA reduction of SI
668 and SID. The improved mPS-PI staining showed that 38.30% root tips (Figure S37B) and 37.84%
669 mature embryos (Figure S37E) of WOX5m3D-GFP/Col-0 line #2, 41.67% root tips (Figure S37C)
670 and 39.47% mature embryos (Figure S37F) of WOX5m5D-GFP/Col-0 line #1 presented two layers
671 QC-like cells, but 100% root tips (Figure S37A) and 100% mature embryos (Figure S37D) of
672 WOX5GFP/Col-0 line were one layer QC cells. The EdU staining assays showed that 41.18% root
673 tips (Figure S37H) of WOX5m3D-GFP/Col-0 line #2 and 45.45% root tips (Figure S37I) of
674 WOX5m5D-GFP/Col-0 line #1 appeared two layers nondividing cells, but 88.00% root tips (Figure
675 S37G) of WOX5GFP/Col-0 line were one layer nondividing cells. These data suggest that phosphate-
676 mimicked WOX5 protein stabilizes itself and reduces PA of SI and SID, thus produces more quiescent
677 cells. To further confirm that whether stabilized phosphorylated WOX5 protein can enhance GUS
678 activity of QC184 in QC, SI, and SID. We introduced WOX5m3D-GFP driving by the full-length
679 promotor plus 5' untranslated region (UTR) and 3'UTR of WOX5 genomic sequence (Figure S2) into
680 QC184/*wox5-1*, then obtaining WOX5m3D-GFP/QC184/*wox5-1* homozygous lines. The GUS
681 staining assays showed that 44.44% root tips of WOX5m3D-GFP/QC184/*wox5-1* line appeared two
682 blue cells (Figure S37L), not only rescued the phenotypes of not blue cells of QC184/*wox5-1* (Figure
683 S37J), but also simultaneously enhanced the GUS activity in QC and SI when compared with the GUS
684 activity of WOX5GFP/QC184/*wox5-1* rescued line (Figure S37K). The results demonstrated that
685 stabilized phosphorylated WOX5 protein can enhance GUS activity of QC184 in QC and SI. Owing to
686 the subfamily II of AtSKs stabilizes WOX5 protein by phosphorylating the GMs (Figure S19), and the
687 30 μM Bik can destabilize WOX5-GFP protein by inhibiting the activity of the subfamily II of AtSKs
688 (Figure S16C~D and S16F). Thus, we want to figure out whether the 30 μM Bik can destabilize the
689 phosphate-mimicked WOX5 protein. Finally, we planted the WOX5m3D-GFP/Col-0 line and
690 WOX5m5D-GFP/Col-0 line in the 30 μM Bik and the Mock for 5 days. We observed root tips and
691 counted the PA of QC and quantified the fluorescence of GFP intensity in QC, SI, and SID. The
692 results showed that there were no significant differences in QC, SI and SID between 30 μM Bik and
693 the Mock (Figure S38A-I), meanwhile, the PAr of QC in 30 μM Bik was not different with the Mock
694 (Figure S38J), suggesting that inhibiting the kinase activity of the subfamily II of AtSKs by using 30
695 μM Bik, phosphate-mimicked WOX5 protein still stabilize itself in QC, SI, and SID, and chemical
696 inhibiting the activity of the subfamily II of AtSKs can't either destabilize the continuous
697 phosphorylated phosphate-mimicked WOX5 protein (WOX5m3D-GFP and WOX5m5D-GFP), nor
698 increase the PAr of QC. We further viewed root tips using EdU staining, the percentage of one layer

699 nondividing cells at 30 μM Bik was not significantly different between the WOX5m3D-GFP/Col-0
700 line (48.48%) and the WOX5m5D-GFP/Col-0 line (53.13%), compared to the Mock (50.00% and
701 51.61% respectively) (Figure S38K-L and S38O-P). Similarly, the percentage of two layers
702 nondividing cells at 30 μM Bik was also not significantly different between the WOX5m3D-GFP/Col-
703 0 line (42.42%) and the WOX5m5D-GFP/Col-0 line (40.63%), compared to the Mock (40.63% and
704 45.15% respectively) (Figure S38M-N and S38Q-R), suggesting that chemical inhibiting the activity
705 of the subfamily II of AtSKs could not increase the proliferative activity of the more quiescent cells
706 which produced by stabilized phosphate-mimicked WOX5 protein in SI and SID, too. In addition, we
707 planted the WOX5m3D-GFP/QC184/*wox5-1* line in the 30 μM Bik and the Mock for 5 days. The
708 GUS staining assays showed that the one layer blue cells of 30 μM Bik (45.76%) was not different
709 with the Mock (46.81%) (Figure S38S-T), and the two layers nondividing cells of 30 μM Bik (54.24%)
710 was also not different with the Mock (53.19%) (Figure S38U-V), suggesting that inhibiting the kinase
711 activity of the subfamily II of AtSKs by using 30 μM Bik, WOX5 protein can't maintain the activity
712 of QC184 GUS activity in QC (Figure S14A and S14E), but phosphate-mimicked WOX5 protein still
713 enhanced the activity of QC184 GUS activity not only in QC but also in SI and SID. Taken together,
714 phosphate-mimicked WOX5 protein is sufficient for producing more quiescent cells.

715 Conclusion

716 WOX5 protein is phosphorylated by the subfamily II of AtSKs and dephosphorylated by the
717 subfamily II of AtPP2A-Cs holoenzymes, the homeostasis of WOX5 protein is regulated by reversible
718 phosphorylation, which make sure the homeostasis of low proliferative activity of QC cells. In
719 addition, the subfamily II of AtPP2A-Cs increase the proliferative activity of SI and SID by down-
720 regulating WOX5 expression and reducing stability of WOX5 protein, which determine the
721 homeostasis of one layer QC cells.

722 Discussion

723 It is widely known that the WOX5 protein expresses in the QC cells and maintains their quiescence
724 from the embryonic stage to the postembryonic stage (Celine et al., 2014; Haecker et al., 2004).
725 However, QC cells are not in a strictly quiescent state (G0 stage) but in a resting state (G1 stage) with
726 very low proliferative activity, these resting QC cells can re-enter the cell cycle when needed (Clowes,
727 1968; Matosevich and Efroni, 2021; Ubogoeva et al., 2021). How accurately define the low
728 proliferative activity of QC is unclear. Here, we define the phenotype of QC proliferative activity by a
729 novel Proliferative Activity (PA) index, and we find that the dynamic balance of phosphorylated
730 WOX5 protein maintains the dynamic balance of low PA of QC. On one hand, the subfamily II of
731 AtSKs phosphorylate WOX5 protein and stabilize WOX5 protein, thereby inhibiting the proliferative
732 activity of QC cells and establishing quiescence. Consequently, no phosphorylation sites of WOX5
733 protein (truncation of PEST domain and all types of serine/threonine (S/T) to alanine (A) site-directed
734 mutagenesis) and no kinase activity (loss of function mutant of the subfamily II of AtSKs and
735 treatment with 30 μM Bik) will reduce WOX5 protein and increase PA of QC (Figure S39C,F). On

736 the other hand, the subfamily II of AtPP2A-Cs holoenzymes (may act as a molecular switch)
737 dephosphorylate the phosphorylated WOX5 protein and promote its degradation. This mechanism
738 facilitates proliferation in QC cells when required, as demonstrated by the increased PA of QC cells
739 upon overexpression of the subfamily II of AtPP2A-Cs holoenzymes (Figure S39F). In addition, why
740 constantly exist just one layer QC with low proliferative activity at the centre of RAM in *Arabidopsis*
741 from the embryonic stage to the postembryonic stage remains elusive. Our solid genetic proofs
742 including no phosphotase activity (loss-of-function mutations in the subfamily II of AtPP2A-Cs and
743 treatment with 30 μM CT), phosphate-mimicked WOX5 protein (all types of serine/threonine (S/T) to
744 asparticacid (D) site-directed mutagenesis), and in situ overexpressed WOX5 protein will increase
745 WOX5 protein in QC, SI, and SID and reduce PA of QC, SI, and SID. Consequently, this causes the
746 emergence of two layers QC-like cells and more and wider QC-like cells (Figure S39E,H). Moreover,
747 dynamic accumulation of WOX5 protein directly converts the SI and SID into QC-like cells. This is
748 the first discovery reveals that active stem cells can convert into quiescent stem cells in plants (Li and
749 Clevers, 2010). As a result, the subfamily II of AtPP2A-Cs enhance the proliferative activity of SI and
750 SID by down-regulating WOX5 expression and reducing stability of WOX5 protein, thus maintaining
751 the balance of one layer QC (Figure S39B).

752 To clarify the relationship between QC PA and QC identity, we use two promotor trapping lines of
753 QC25 and QC184 as QC identity markers (Brand and Perrimon, 1993). No phosphorylation sites of
754 WOX5 protein can't completely rescue the GUS activity of QC184, and no kinase activity
755 downregulates the GUS activity of QC184 and QC25 (Figure S7). Our findings suggest a reciprocal
756 relationship between WOX5 protein level, the PA of QC cells, and QC identity. Specifically, a
757 reduction in WOX5 protein levels enhances the PA of QC cells, while an increase in WOX5 protein
758 levels reduces QC PA and strengthens QC identity. Contrarily, no phosphotase activity, phosphate-
759 mimicked WOX5 protein, and in situ overexpressed WOX5 protein not only upregulate the GUS
760 activity of QC184 and QC25 in QC, but also increase the GUS activity of QC184 and QC25 in SI and
761 SID (Figure S29). This suggests that increased WOX5 protein levels in QC can reduce QC PA and
762 enhance QC identity. In contrast, increased WOX5 protein levels in SI and SID can reduce PA of SI
763 and SID cells leading to a reduction in their PA, resulting in their conversion to QC-like cells and
764 acquisition of QC identity. In a word, our results highlight that a decrease in QC PA enhances QC
765 identity, whereas the increased QC PA will weaken QC identity.

766 Reversible phosphorylation is one of the most common and crucial mode of post-translational
767 modifications for regulating protein stability and/or activity, thus mediating various cell signal
768 transduction pathways (Ardito et al., 2017). Phosphorylated by protein kinases and dephosphorylated
769 by protein phosphatases, these pairs of phosphate group antagonists are widely widespread in animals
770 and plants (Tan et al., 2021; Worby and Dixon, 2019). In mammals, a well-known pair of antagonist,
771 glycogen synthase kinase 3 (GSK3) and protein phosphatase 2A (PP2A), was involved in regulating
772 the homeostasis of β-catenin transcriptional coactivator in Wnt signaling pathway, thereby modulates
773 cell fate determination and stem cell pluripotency maintenance (MacDonald et al., 2009). Likewise, in
774 *Arabidopsis*, BR-INSENSITIVE 2 (BIN2) (a homolog of GSK3) and PP2A oppositely regulate the
775 key transcriptional factor BZR1 of brassinosteroid signalling (Di Rubbo et al., 2011; He et al., 2002;
776 Tang et al., 2011) and critical transcriptional factors AKSs (ABA-responsive kinase substrates) of
777 ABA signalling (Bu et al., 2017), thereby modulateing root growth and development, stem cell self-
778 renewal and stress adaption (Chen et al., 2020; Planas-Riverola et al., 2019). However, whether the
779 antagonist pair (GSK3 and PP2A) directly regulates the central transcriptional factor WOX5 in the
780 root stem cell niche remains unknown. In this study, we firstly find that WOX5 protein is modified by

781 reversible phosphorylation, which controls the homeostasis of QC. The subfamily II of AtSKs (the
782 homologs of GSK3 in *Arabidopsis*) stabilize WOX5 protein by phosphorylating the GSK3 motifs
783 (GMs) in PEST domain, and the subfamily II of AtPP2A-Cs holoenzymes destabilize WOX5 protein
784 by dephosphorylating the phosphorylated GMs (Figure S39A). Remarkably, the regulatory
785 mechanism of WOX5's stability is contrary to the β-catenin protein and BZR1 protein mediating by
786 GSK3 and PP2A (Di Rubbo et al., 2011; MacDonald et al., 2009), but is consistent with other proteins
787 and comports with the dual roles of phosphorylation of GSK3 (Hu and Yu, 2014; Yamamoto et al.,
788 1999; Ye et al., 2012). In order to investigate whether the WOX5 protein homeostasis is regulated by
789 post-translational modifications, we analyzed the WOX5 protein sequence and uncovered a signal
790 peptide, called PEST domain, that contributes to protein degradation (Belizario et al., 2008;
791 Rechsteiner and Rogers, 1996; Rogers et al., 1986). However, our solid genetic and biochemical
792 proofs testify that the PEST domain is accessible for phosphorylation and dephosphorylation, thus
793 controlling the homeostasis of WOX5 protein. These results suggest that the conformational flexible
794 PEST domain may play multiple roles in regulating protein homeostasis (Sandhu and Dash, 2006).

795 In conclusion, our findings answered two fundamental questions of why *Arabidopsis* always exists
796 just one-layer QC cells and how these one-layer QC cells always maintain low proliferative activity
797 (Figure S39B,D,G). In addition, the subfamily II of AtPP2A-Cs increase the proliferative activity of
798 SI and SID by down-regulating WOX5's expression and reducing stability of WOX5 protein, which
799 determine the homeostasis of one layer QC cells (Figure S39B,D,G).

800 EXPERIMENTAL MODEL AND SUBJECT DETAILS

801 Plant growth conditions

802 *Arabidopsis thaliana* plants were grown in nutrient soil and vermiculite (2:1) inside growth cabinets
803 held at 22℃ and 55% humidity with a 16/8 hours photoperiod (130 μmol.m^{-2}.s^{-1}). *Nicotiana*
804 *benthamiana* plants were grown in nutrient soil and vermiculite (2:1) inside chambers held at 25℃
805 and 65% with a 14/10 hours photoperiod (130 mmol.m^{-2}.s^{-1}).

806 In this study, seeds were stratified for 48-72 hours at 4°C in darkness to break dormancy before
807 planted onto the ½ MS medium. ½ MS medium refers to Murashige and Skoog medium with the
808 following recipe: 0.5× Murashige & Skoog MEDIUM including Vitamins (Duchefa Biochemie) and
809 0.5% (w/v) MES (Sangon Biotech (shanghai) Co.,Ltd.) at a pH of 5.7 supplemented with 1% agar
810 (SERVA high gel strength) and 1% sucrose (Sigma-Aldrich).

811 Transgenic plant lines

812 Transgenic plant lines were generated by *Agrobacterium tumefaciens*-mediated (GV3101 strain with a
813 Tetracyclin-resistant pSoup plasmid) floral dip transformation. Transgenic seedlings (T_1) were
814 selected in ½ MS medium with 1 μM Norflurazon (Norf) (Sigma-Aldrich) and 0.8% agar (SERVA
815 high gel strength) and without sucrose, all T_1 seedlings were transplanted on ½ MS medium with 50
816 μg/mL Ampicillin (Amp) and 1% agar (SERVA high gel strength) and without sucrose. Seeds of each
817 T_2 line that were harvested from each T_1 line was planted onto ½ MS medium with 1 μM Norflurazon
818 (Norf), homozygote T_3 lines (the seeds of Norf-resistant T_2 lines) were then identified by verifying
819 that all T_3 seedlings were Norf-resistant.

820 ## *Arabidopsis* mutant

821 In this study, the T-DNA mutant lines of *wox5-1*, *atsk21/22/23* and *c3c4* were obtained from Limin Pi
822 lab (Pi et al., 2015; Sarkar et al., 2007), Xuelu Wang lab (Yan et al., 2009), and Martine Pastuglia lab
823 (Spinner et al., 2013) under the background of Col-0, Wassilewskija (Ws), and Col-0 ecotype
824 respectively.

825 # METHOD DETAILS

826 ## Plasmid construction for *Arabidopsis* experiments

827 All plasmids (Table S1) for transformating *Arabidopsis* were generated from the NK43 vector, all
828 promotor sequences were amplified with primers (Table S1) by Phanta Max Super-Fidelity DNA
829 Polymerase (Nanjing Vazyme Biotech Co.,Ltd.) PCR from Col-0 DNA extracted by CTAB method,
830 all coding sequences were amplified by Phanta Max Super-Fidelity DNA Polymerase (Nanjing
831 Vazyme Biotech Co.,Ltd.) PCR from cDNA (see sqRT-PCR and qPCR assays), all these fragments
832 were cloned into NK43 vector by using In Fusion Cloning (ClonExpress® II One Step Cloning Kit,
833 Nanjing Vazyme Biotech Co.,Ltd.) and/or Restriction Cloning (FastDigest Restriction enzymes and
834 T4 DNA ligase kit, Thermo Fisher Scientific).

835 ## Site-directed mutagenesis

836 In order to change and/or delete some specific amino acids sites of proteins, site-directed mutagenesis
837 of CDS sequences of WOX5 and AtSK21 using In Fusion Cloning with special primers (Table S2).
838 Successful mutagenesis of CDS sequences of WOX5mGM1, WOX5mGM2, WOX5ΔPEST,
839 WOX5mAll, WOX5m5A, WOX5m3A, WOX5m3D, WOX5m5D, and AtSK21(K69R) were
840 convinced by DNA sequencing (Tsingke Biotechnology Co., Ltd.).

841 ## sqRT-PCR and qPCR assays

842 According to manufacturer's instructions, DNA-free total RNA was extracted from 50-100 mg root
843 tips (almost 1 cm length) of 5DAG seedlings by using FastPure® Plant Total RNA Isolation Kit
844 (Nanjing Vazyme Biotech Co.,Ltd.), cDNA was synthesized from extracted RNA (measured by
845 Thermo Fisher Scientific Nanodrop One^{C}) by using HiScript® III 1st Strand cDNA Synthesis Kit
846 (+gDNA wiper) (Nanjing Vazyme Biotech Co.,Ltd.), sqRT-PCR was performed by using Green Taq
847 Mix (Nanjing Vazyme Biotech Co.,Ltd.), qPCR was performed by using ChamQ SYBR Color qPCR
848 Master Mix (Nanjing Vazyme Biotech Co.,Ltd.). A sqRT-PCR primer pair GFPlinkF and GFPtaaR
849 were used to quantify expression level of GFP-fused protein (Table S3), sqRT-PCR primer pairs gene-
850 RT-Fs and gene-RT-Rs were used to quantify expression level of genes (Table S3), a primer pair
851 ACT2-RT-F and ACT2-RT-R were used to quantify expression level of ACT2 (AT3G18780, the
852 reference gene) (Table S3). A qPCR primer pair GFP111aaF and GFP162aaR were used to quantify
853 expression level of GFP-fused protein, WOX5-RT-F and WOX5-RT-R were used to quantify
854 expression level of WOX5 protein (Table S3), the reference gene was used to normalize gene
855 expression levels, reactions of qPCR were run on the CFX Touch 96-well Real-Time PCR Detection
856 Systems and were repeated three times.

857 ## GFP imaging and PI staining

858 Root tips of GFP fused protein transformed *Arabidopsis* were transferred onto slides and covered with
859 a drop of 100 times diluted Propidium Iodide (PI) solution (1.0 mg/mL) (Sigma-Aldrich) for one

860 minute, a coverslip was placed on top before the observation. All samples were imaged on the LEICA
861 TCS SP8 laser scanning confocal microscope with the HCX PL APO 40×/0.85 DRY objective, GFP
862 and PI fluorescence signals were detected by exciting with laser at 488nm and 552 nm, and by
863 collecting emission from 500-520 nm and 600-650 nm on a HyD detector and a PMT detector at the
864 sequential scan mode. All images were acquired by using the Leica Application Suite X software
865 3.5.2.18963. All pWOX5:WOX5GFP fluorescence and pWOX5:nlsGFP samples that were compared
866 in the publication were imaged with the same laser intensity 35.0 of 488 nm (accumulation twice) and
867 10.0 of 488nm (not accumulation), respectively.

868 Improved mPS-PI staining

869 We improved the mPS-PI staining method (Truernit et al., 2008), as described below. Root tips and
870 mature embryos of *Arabidopsis* were fixed in solution I (50% methanol and 10% acetic acid) at 4°C
871 for at least 12 h. Next, samples were rinsed with water twice and incubated in solution II [1% (w/v)
872 periodic acid] at room temperature for 1 hour. Samples were rinsed again with water twice, then,
873 incubated in solution III (Schiff reagent, 100 mM sodium metabisulphite and 0.15 N HCl) with
874 propidium iodide (a final concentration of 10 μg/mL) freshly added for 5 min. The samples were
875 transferred onto slides and covered with a drop of chloral hydrate solution (4 g chloral hydrate, 1 mL
876 glycerol, and 2 mL water), a coverslip was placed on top before observation. All samples were imaged
877 by the LEICA TCS SP8 laser scanning confocal microscope with the HCX PL APO 40×/0.85 DRY
878 objective, propidium iodide fluorescence signal were detected by exciting with a laser at 552 nm, and
879 by collecting emission from 600-650 nm on the PMT detectors. All images were acquired by using the
880 Leica Application Suite X software 3.5.2.18963.

881 BiFC in *Tobacco*

882 For BiFC assays, full-length CDS of *Arabidopsis* WOX5, AtSK21, AtSK22, AtSK23, AtPP2A-C3,
883 AtPP2A-C4, HAM4, RGA were amplified with primers (Table S3) by Phanta Max Super-Fidelity
884 DNA Polymerase (Nanjing Vazyme Biotech Co.,Ltd.) PCR from cDNA (see sqRT-PCR and qPCR
885 assays), and recombined into vectors containing each half of YFP (N or C terminus) (Walter et al.,
886 2004) to generate all needed plasmids (Table S4) with primers (Table S4) by using restriction cloning.
887 *Agrobacterium tumefaciens* cultures (GV3101 strain) carrying the plasmid pairs for testing the
888 specific interactions (p35S:WOX5-YFPN and p35S:CDS-YFPC) together with the p35S:nlsCFP (as a
889 nuclear marker) plasmid (Table S4) were grown overnight at 28°C in liquid LB broth containing 50
890 μg/mL kanamycin (Sigma-Aldrich), 25 μg/mL gentamicin (Sigma-Aldrich), and 10 μg/mL rifampicin
891 (Sigma-Aldrich). Cultures were centrifugated and the sediments were mixed with infiltration buffer
892 (10 mM $MgCl_2$ (Sigma-Aldrich), 10 mM MES (Sangon Biotech (shanghai) Co.,Ltd.), and 150 μM
893 acetosyringone (Sigma-Aldrich) at a pH of 5.6 and diluted to reach an OD600 of 1.0. Equal amount of
894 each diluted culture was pre-mixed, fully expanded 3rd or 4th leaves from 4/5-week-old *Nicotiana*
895 *benthamiana* plants were infiltrated with these pre-mixed cultures. The infiltrated *Nicotiana*
896 *benthamiana* plants were moved into darkroom at 22°C and 55% humidity for 12 hours, then were
897 moved into lightroom of 14/10 hours photoperiod (130 $mmol.m^{-2}.s^{-1}$) for 2 or 3 days. The infiltrated
898 tobacco leaves were imaged using a LEICA TCS SP8 laser scanning confocal microscope with the
899 HCX PL APO 40×/0.85 DRY objective. CFP, YFP fluorescence signals and bright field (BF) were
900 detected by exciting with laser at 448nm and 514 nm, and by collecting emission from 465-485 nm
901 and 525-540 nm on two PMT detector and a TLD detector (514 nm PMT trans) at the sequential scan
902 mode. All images were acquired by using the Leica Application Suite X software 3.5.2.18963.

903 ## Yeast Two Hybrid (Y2H)

904 For Y2H assays, full-length CDS of *Arabidopsis* WOX5, TPR1, AtSK11, AtSK12, AtSK13, AtSK21,
905 AtSK22, AtSK23, AtSK31, AtSK32, AtSK41, AtSK42, AtPP2A-C1, AtPP2A-C2, AtPP2A-C3,
906 AtPP2A-C4, AtPP2A-C5 were amplified by Phanta Max Super-Fidelity DNA Polymerase (Nanjing
907 Vazyme Biotech Co.,Ltd.) PCR from cDNA (see sqRT-PCR and qPCR assays), and recombined into
908 the vector pGADT7 and/or the vector pGBKT7 to generate all needed plasmids (Table S5) with
909 primers (Table S5) by using Restriction cloning and In Fusion cloning. Plasmid pairs for testing the
910 specific interactions were co-transformed into the yeast strain AH109. The yeast transformants were
911 grown on nutrient-restricted (without Trp, Leu, His, Ade) mediums (Clontech) 3-5 days to assess
912 interactions between various protein combinations.

913 ## Recombinant protein expression and purification

914 All plasmids (Table S6) for recombinant protein expression were generated from the vector pGEX-
915 4T-1 and modified vector pGEX(MBP)-4T-1, recombinant protein expression using E. coli (BL21
916 strain) were performed according to the GST Gene Fusion System Handbook (GE healthcare Life
917 Sciences). Recombinant GST-tagged proteins purification were performed according to the
918 manufacturer's instructions of Pierce™ Glutathione Superflow Agarose (Thermo Fisher Scientific),
919 and recombinant MBP-tagged proteins purification were performed according to the manufacturer's
920 instructions of Amylose Resin (NEB).

921 ## Pull-down in vitro Assays

922 For the pull-down in vitro assays, equal amount GST/GST-tagged input proteins, and MBP/MBP-
923 tagged input proteins, and 30 μL MBP beads (Amylose Resin) were incubated in the 1 mL PL buffer
924 [50 mM HEPES (pH=7.5), 150 mM NaCl, 1.5 mM MgCl2, 1 mM EGTA (pH=7.5), 1% Triton X-100,
925 5% Glycerol, 1 mM PMSF (Sigma Aldrich), 1× Protease Inhibitor Cocktail (EDTA-Free, 100X in
926 DMSO) (bimake.cn)] for 1-2 hours at 4°C with gentle shaking. Then, the MBP beads were collected
927 and washed with the PL buffer three times to eliminate nonspecific bindings. The beads of the pull-
928 down proteins were analyzed by Western Blot with the Mouse anti GST-tag mAb (1:2500, Abclonal).
929 Inputs were analyzed by Western Blot with Anti-MBP Tag (2A9) Monoclonal Antibody (1:5000)
930 Produce in Mouse (GNI) and Mouse anti GST-tag mAb (1:2500, Abclonal).

931 ## Co-Immunoprecipitation (Co-IP) assays

932 For the Co-IP assays, 0.5-1.0 g root tips of 5 DAG seedlings of homozygous lines (p35S:LhGR-
933 pOp:WOX5-YFP/Col-0, p35S:Flag-AtSK21/Col-0, p35S:Flag-C3/Col-0, p35S:Flag-C4/Col-0) and
934 double homozygous lines (p35S:LhGR-pOp:WOX5-YFP×p35S:FlagAtSK21, p35S:LhGR-
935 pOp:WOX5-YFP×p35S:FlagC3, p35S:LhGR-pOp:WOX5-YFP×p35S:FlagC4) were ground into
936 powder in liquid nitrogen and homogenized in 0.5-1.0 mL cold IP buffer [50 mM Tris-HCl (pH =7.4),
937 150 mM NaCl, 1 mM $MgCl_2$, 20% Glycerol, 0.2% NP40, 1× Protease Inhibitor Cocktail] by gentle
938 shaking or pipetting. Supernatants were incubated with anti-GFP beads for 4 h at 4°C with gentle
939 shaking and washed 4 times with the IP buffer. Proteins of the Co-IP were analyzed by Western Blot
940 with the Monoclonal ANTI-FALG® M2 antibody produced in mouse (Sigma Aldrich), proteins of
941 inputs were analyzed by Western Blot with the Anti-GFP from mouse (Roche) and Monoclonal
942 ANTI-FALG® M2 antibody produced in mouse (Sigma Aldrich).

943 ## Kinase assays

944 For kinase assays, kinase protein (GST-AtSK21), kinase-dead protein (GST-AtSK21K69R) and
945 substrate proteins (MBP, MBPWOX5, MBPWOX5ΔPEST, MBPWOX5mAll, MBPWOX5m5A,
946 MBPWOX5m3A) were generated by recombinant protein expression and purification. The kinase
947 reaction (the amount of substrate was 2-5 times of kinase) was performed in 50 μL kinase buffer [25
948 mM Tris-HCl (pH=7.5), 10 mM $MgCl_2$, 1 mM ATP (Sigma Aldrich), 2 mM DTT] containing or not
949 containing 30 μM Bik (Sigma Aldrich) at 30°C for 30-120 min, and then were incubated with 16 μL
950 4x loading buffer at 95°C for 10 minutes. The samples were sepereated by 8% SDS-PAGE gel
951 containing 50 μM Mn^{2+}- Phos-tag™ (see Mn^{2+}-Phos-tag™ SDS-PAGE assays) and were analyzed by
952 Western Blot with with the Anti-MBP Tag (2A9) Monoclonal Antibody (1:5000) Produce in Mouse
953 (GNI).

954 ## Dephosphorylation assays

955 For dephosphorylation assays, the Protein Phosphatase 2A holoenzymes of C3GFP and C4GFP were
956 extracted using lysis buffer [200 mM NaCl, 0.5% NP-40, 20 mM Tris-HCl (pH 8.0), 1x 1× Protease
957 Inhibitor Cocktail and 1 mM PMSF (Sigma Aldrich)] and puried using anti-GFP beads from the total
958 protein of root tips of homozygote p35S:C3GFP/Col-0 and p35S:C4GFP/Col-0 lines, and Lambda
959 Protein Phosphatase (Lambda PP) was purchased from NEB. After kinase reaction in kinase buffer, 30
960 μM Bik was added in the kinase buffer for 1 h, and then added 3 μL 10×Cutsmart and overdose of
961 phosphatase for 60-120 min, 30 μM CT was the negative control, and then were incubated with 4x
962 loading buffer at 95°C for 10 minutes. The samples were separated by 8% SDS-PAGE gel containing
963 50 μM Mn^{2+}- Phos-tag™ (see Mn^{2+}-Phos-tag™ SDS-PAGE assays) and were analyzed by Western
964 Blot with with the Anti-MBP Tag (2A9) Monoclonal Antibody (1:5000) Produce in Mouse (GNI).

965 ## Mn^{2+}-Phos-tag™ SDS-PAGE

966 According to the Phos-tag™ SDS-PAGE guidebook (Wako), we selected the optium concentration of
967 Mn^{2+}-Phos-tag™ (50 μM) and acrylamide (8%) for the separation of phosphorylated MBP-tagged
968 substrates. After migrating with a constant voltage of 100 V in cold Tris-glycine-SDS (TGS) running
969 buffer [25 mM Tris, 192 mM glycine, 0.1% SDS (w/v), pH 8.3] for 4 hours, and then transferred to
970 Immobilon®-P^{SQ} Transfer Membrane (0.2 μm, Merck Millipore Ltd.) in 1x transfer buffer [25 mM
971 Tris-HCl (pH 8.3), 192 mM glycine, 20% methanol (v/v)] containing 0.1% SDS (w/v) using a Bio-
972 Rad transfer apparatus, and then were analyzed by Western Blot.

973 ## Western blot

974 For immunoblotting, samples were lysed in cold PL buffer (see pull-down assays) or IP buffer (see
975 CoIP assays) or lysis buffer (see Dephosphorylation assays) mixed with 4x loading buffer [8% SDS
976 (w/v), 40% glycerol, 4% β-mercaptoethanol, 0.008% bromophenol blue, 0.25 M Tris-HCl (pH=6.8)],
977 and then boiled for 10 min. Subsequently, the samples were loaded in SDS-PAGE and transferred to
978 Immobilon®-P^{SQ} Transfer Membrane (0.2 μm, Merck Millipore Ltd.) in 1x transfer buffer using a
979 Bio-Rad transfer apparatus. The membrane was blocked with 5% non-fat milk in TBST [TBS buffer
980 (50 mM Tris-Cl, pH 7.6; 150 mM NaCl) containing 0.1% (v/v) Tween-20] at room temperature for 30
981 min while shaking, followed by incubation with primary antibody overnight at 4°C while shaking.
982 After three 10 min washes with TBST, membranes were incubated with species-specific secondary
983 antibodies at room temperature for 1 h while shaking. Following three 10 min washes in TBST, the
984 membrane was detected by enhanced chemiluminescent (ECL) substrate (ECL Substrate A, Peroxide

985 Solution B, Vazyme Code: E412-01) and imaged with ChemDoc™ XRS+ with Image Lab™
986 Software (Bio-rad).

987 Chemical inhibitors assays

988 For the kinase inhibitor assays in vivo, seeds were planted in the ½ MS medium containing 30 μM Bik
989 (Sigma Aldrich) for 6 days, for the kinase inhibitor assays in vitro, 30 μM Bik were added in the
990 kinase buffer. For the Protein Phosphatase 2A holoenzymes inhibitor assays in vivo, seeds were
991 planted in the ½ MS medium for 4 days and were transferred to the ½ MS medium containing 30 μM
992 CT (Sigma Aldrich) for 48 hours, for the Protein Phosphatase 2A holoenzymes inhibitor assays in
993 vitro, 30 μM CT were added in the kinase buffer.

994 GUS staining

995 The excised root tips of "QC25 marker line and its relevant genetic materials" and "QC184 marker
996 line and its relevant genetic materials" were incubated in GUS staining solution (0.2% Triton X-100,
997 2 mM 5-bromo-4-chloro-3-indolyl glucuronide, 2 mM $K_3Fe(CN)_6$, 2 mM $K_4Fe(CN)_6$, 50 mM $NaPO_4$,
998 pH 7.2) at 37°C for 2-4 hours and 48-72 hours, respectively. After destained with absolute ethanol at
999 room temperature for 2 hours, the samples were immersed in Lugol's solution (Sigma Aldrich) for 10
1000 s, and fixed and mounted with clearing solution [chloral hydrate:water:glycerol = 8:3:1, w/v/v).
1001 Images were captured by a differential interference contrast (DIC) microscopy (Leica DMC4500),
1002 with HC PL FLUOTAR 40×/0.80 objective.

1003 EdU staining

1004 EdU staining was performed following the modified protocol of the YF® 555 Click-iT EdU imaging
1005 kit (US EVERBRIGHT), as described below. Seedlings (4.0-4.5 DAG) grown on ½ MS medium were
1006 transferred to the ½ MS medium with 2.5 μM EdU for 12 hours, then excised root tips and immersed
1007 into 3.7% formaldehyde in PBS buffer (pH=7.3) for fixing 30 minutes at 4°C, then washed the
1008 samples with PBS buffer (pH=7.3). Added 0.5% Triton X-100 in PBS buffer (pH=7.3), incubated at
1009 room temperature for 20 minutes. After washing with PBS buffer (pH=7.3), samples were immersed
1010 in Click-iT working solution [1× Click-iT EdU reaction buffer (860 μL/mL), $CuSO_4$ (40 μL/mL), YF®
1011 555 Azide (2 μL/mL), 1× Click-iT EdU buffer additives (100 μL/mL)] for 30 minutes in darkness.
1012 Then washed the samples with PBS buffer (pH=7.3), and transferred onto slides and covered with a
1013 drop of water, a coverslip was placed on top before observation. Images were captured by the Leica
1014 TCS SP8 multiphoton (MP) system with the HC PL APO 20×/0.75 CS2 objective, EdU fluorescence
1015 signals were detected by exciting with laser at 552 nm, and by collecting emission from 600-650 nm
1016 on a PMT detector and a TLD detector (552 nm PMT trans). All images were acquired by using the
1017 Leica Application Suite X software 3.5.2.18963.

1018 QUANTIFICATION AND STATISTICAL ANALYSIS

1019 Quantification of GFP intensity in QC area and SI/SID area were analyzed using software of Leica
1020 LAS AF lite (quantify, sort in ROIs, mean value). All values were analyzed using GraphPad Prism
1021 (version 8.3.0) and Excel, significance of difference was examined by Student's t test, results were
1022 considered significant when $p < 0.05$. All data were presented with mean ± SD. Statistical tests, p
1023 values, number of biological and technical replicates, and number of independent experiments are
1024 indicated in the figure and figure legends.

1025

References

Aida, M., Beis, D., Heidstra, R., Willemsen, V., Blilou, I., Galinha, C., Nussaume, L., Noh, Y.-S., Amasino, R., and Scheres, B. (2004). The PLETHORA genes mediate patterning of the *Arabidopsis* root stem cell niche. Cell *119*, 109-120.

Ali, A., Hoeflich, K.P., and Woodgett, J.R. (2001). Glycogen synthase kinase-3: properties, functions, and regulation. Chemical reviews *101*, 2527-2540.

Ardito, F., Giuliani, M., Perrone, D., Troiano, G., and Lo Muzio, L. (2017). The crucial role of protein phosphorylation in cell signaling and its use as targeted therapy (Review). Int J Mol Med *40*, 271-280.

Ballesteros, I., Dominguez, T., Sauer, M., Paredes, P., Duprat, A., Rojo, E., Sanmartin, M., and Sanchez-Serrano, J.J. (2013). Specialized functions of the PP2A subfamily II catalytic subunits PP2A-C3 and PP2A-C4 in the distribution of auxin fluxes and development in *Arabidopsis*. The Plant journal : for cell and molecular biology *73*, 862-872.

Barlow, P.W. (2015a). The concept of the quiescent centre and how it found support from work with X-rays. I. Historical perspectives. Plant Root *9*, 43-55.

Barlow, P.W. (2015b). The concept of the quiescent centre and how it found support from work with X-rays. II. The molecular aftermath. Plant Root *9*, 56-67.

Barlow, P.W. (2015c). Origin of the concept of the quiescent centre of plant roots. Protoplasma *253*, 1-15.

Belizario, J.E., Alves, J., Garay-Malpartida, M., and Occhiucci, J.M. (2008). Coupling caspase cleavage and proteasomal degradation of proteins carrying PEST motif. Current protein & peptide science *9*, 210-220.

Berckmans, B., Kirschner, G., Gerlitz, N., Stadler, R., and Simon, R. (2020). CLE40 signalling regulates the fate of root stem cells in *Arabidopsis*. Plant Physiology, pp.00914.02019.

Bian, C., Guo, X., Zhang, Y., Wang, L., Xu, T., DeLong, A., and Dong, J. (2020). Protein phosphatase 2A promotes stomatal development by stabilizing SPEECHLESS in *Arabidopsis*. Proc Natl Acad Sci U S A *117*, 13127-13137.

Brand, A.H., and Perrimon, N. (1993). Targeted gene expression as a means of altering cell fates and generating dominant phenotypes. Development *118*, 401-415.

Bu, S.L., Liu, C., Liu, N., Zhao, J.L., Ai, L.F., Chi, H., Li, K.L., Chien, C.W., Burlingame, A.L., Zhang, S.W.*, et al.* (2017). Immunopurification and Mass Spectrometry Identifies Protein Phosphatase 2A (PP2A) and BIN2/GSK3 as Regulators of AKS Transcription Factors in *Arabidopsis*. Mol Plant *10*, 345-348.

Burkart, R.C., Strotmann, V.I., Kirschner, G.K., Akinci, A., Czempik, L., Maizel, A., Weidtkamp-Peters, S., and Stahl, Y. (2019). PLETHORA and WOX5 interaction and subnuclear localisation regulates *Arabidopsis* root stem cell maintenance. bioRxiv, 818187.

Celine, F., Ernst, A., Emily, S., Viola, W., Thomas, L., Walter, D., and Murray, J.A.H. (2014). WOX5 suppresses CYCLIN D activity to establish quiescence at the center of the root stem cell niche. Current Biology *24*, 1939-1944.

Chen, K., Li, G.J., Bressan, R.A., Song, C.P., Zhu, J.K., and Zhao, Y. (2020). Abscisic acid dynamics, signaling, and functions in plants. J Integr Plant Biol *62*, 25-54.

Clark, N.M., Fisher, A.P., Berckmans, B., Van den Broeck, L., Nelson, E.C., Nguyen, T.T., Bustillo-Avendano, E., Zebell, S.G., Moreno-Risueno, M.A., Simon, R.*, et al.* (2020). Protein complex stoichiometry and expression dynamics of transcription factors modulate stem cell division. Proc Natl Acad Sci U S A *117*, 15332-15342.

Claudia, V.D.B., Willemsen, V., Hendriks, G., Weisbeek, P., and Scheres, B. (1997). Short-range control of cell differentiation in the *Arabidopsis* root meristem. *Nature 390*, 287-289.

Clevers, H., Loh, K.M., and Nusse, R. (2014). An integral program for tissue renewal and regeneration: Wnt signaling and stem cell control. Science *346*, 1248012.

Clowes, F.A.L. (1961). Effects of β-radiation on meristems. Experimental Cell Research *25*, 529-534.

Clowes, F.A.L. (1963). X-Irradiation of Root Meristems. Annals of Botany *27*, 343-352.

Clowes, F.A.L. (1968). THE DNA CONTENT OF THE CELLS OF THE QUIESCENT CENTRE AND ROOT CAP OF ZEA MAYS. New Phytol *67*, 631-639.

Clowes, F.A.L. (1981). The Difference between Open and Closed Meristems. Annals of Botany *48*, 761-767.

Cruz-Ramírez, A., Díaz-Triviño, S., Blilou, I., Grieneisen, V.A., Sozzani, R., Zamioudis, C., Miskolczi, P., Nieuwland, J., Benjamins, R., and Dhonukshe, P. (2012). A bistable circuit involving SCARECROW-RETINOBLASTOMA integrates cues to inform asymmetric stem cell division. Cell *150*, 1002-1015.

Cruz-Ramírez, A., Díaz-Triviño, S., Wachsman, G., Du, Y., Arteága-Vázquez, M., Zhang, H., Benjamins, R., Blilou, I., Neef, A.B., and Chandler, V. (2013). A SCARECROW-RETINOBLASTOMA protein network controls protective quiescence in the *Arabidopsis* root stem cell organizer. PLoS biology *11*.

De Rybel, B., Audenaert, D., Vert, G., Rozhon, W., Mayerhofer, J., Peelman, F., Coutuer, S., Denayer, T., Jansen, L., Nguyen, L.*, et al.* (2009). Chemical Inhibition of a Subset of *Arabidopsis* thaliana GSK3-like Kinases Activates Brassinosteroid Signaling. Chemistry & Biology *16*, 594-604.

Di Rubbo, S., Irani, N.G., and Russinova, E. (2011). PP2A Phosphatases: The "On-Off" Regulatory Switches of Brassinosteroid Signaling. Science Signaling *4*, pe25-pe25.

Dolan, L., Janmaat, K., Willemsen, V., Linstead, P., Poethig, S., Roberts, K., and Scheres, B. (1993). Cellular organisation of the *Arabidopsis* thaliana root. Development *119*, 71-84.

Dolzblasz, A., Nardmann, J., Clerici, E., Causier, B., van der Graaff, E., Chen, J., Davies, B., Werr, W., and Laux, T. (2016). Stem Cell Regulation by *Arabidopsis* WOX Genes. Mol Plant *9*, 1028-1039.

Dubrovsky, J.G., and Barlow, P.W. (2015). The origins of the quiescent centre concept. New Phytol *206*.

Fiol, C.J., Wang, A., Roeske, R.W., and Roach, P.J. (1990). Ordered multisite protein phosphorylation. Analysis of glycogen synthase kinase 3 action using model peptide substrates. The Journal of biological chemistry *265*, 6061-6065.

Haecker, A., Groß-Hardt, R., Geiges, B., Sarkar, A., Breuninger, H., Herrmann, M., and Laux, T. (2004). Expression dynamics of WOXgenes mark cell fate decisions during early embryonic patterning in *Arabidopsis* thaliana. Development *131*, 657-668.

He, G., Liu, J., Dong, H., and Sun, J. (2019). The Blue-Light Receptor CRY1 Interacts with BZR1 and BIN2 to Modulate the Phosphorylation and Nuclear Function of BZR1 in Repressing BR Signaling in *Arabidopsis*. Mol Plant *12*, 689-703.

He, J.-X., Gendron, J.M., Yang, Y., Li, J., and Wang, Z.-Y. (2002). The GSK3-like kinase BIN2 phosphorylates and destabilizes BZR1, a positive regulator of the brassinosteroid signaling pathway in *Arabidopsis*. Proceedings of the National Academy of Sciences *99*, 10185-10190.

Houbaert, A., Zhang, C., Tiwari, M., Wang, K., de Marcos Serrano, A., Savatin, D.V., Urs, M.J., Zhiponova, M.K., Gudesblat, G.E., Vanhoutte, I.*, et al.* (2018). POLAR-guided signalling complex assembly and localization drive asymmetric cell division. Nature *563*, 574-578.

Hu, Y., and Yu, D. (2014). BRASSINOSTEROID INSENSITIVE2 interacts with ABSCISIC ACID INSENSITIVE5 to mediate the antagonism of brassinosteroids to abscisic acid during seed germination in *Arabidopsis*. Plant Cell *26*, 4394-4408.

Jefri, H., Toon, C., Filip, V., Heyndrickx, K.S., Jelle, V.L., Ilse, V., Sandy, V., Klaas, V., Geert, D.J., and Dominique, V.D.S. (2013). ERF115 controls root quiescent center cell division and stem cell replenishment. Science *342*, 860-863.

Kotogány, E., Dudits, D., Horváth, G.V., and Ayaydin, F. (2010). A rapid and robust assay for detection of S-phase cell cycle progression in plant cells and tissues by using ethynyl deoxyuridine. Plant methods *6*, 5-5.

Kumpf, R., Thorstensen, T., Rahman, M.A., Heyman, J., Nenseth, H.Z., Lammens, T., Herrmann, U., Swarup, R., Veiseth, S.V., Emberland, G.*, et al.* (2014). The ASH1-RELATED3 SET-domain protein controls cell division competence of the meristem and the quiescent center of the *Arabidopsis* primary root. Plant Physiol *166*, 632-643.

Laurenzio, L.D., Wysocka-Diller, J., Malamy, J.E., Pysh, L., Helariutta, Y., Freshour, G., Hahn, M.G., Feldmann, K.A., and Benfey, P.N. (1996). The SCARECROW Gene Regulates an Asymmetric Cell Division That Is Essential for Generating the Radial Organization of the *Arabidopsis* Root. Cell *86*, 0-433.

1131 Li, J., Zhou, H., Zhang, Y., Li, Z., Yang, Y., and Guo, Y. (2020). The GSK3-like Kinase BIN2 Is a
1132 Molecular Switch between the Salt Stress Response and Growth Recovery in *Arabidopsis* thaliana.
1133 Dev Cell *55*, 367-380 e366.
1134 Li, L., and Clevers, H. (2010). Coexistence of quiescent and active adult stem cells in mammals.
1135 Science *327*, 542-545.
1136 Li, Y.M., and Casida, J.E. (1992). Cantharidin-binding protein: identification as protein phosphatase
1137 2A. Proc Natl Acad Sci U S A *89*, 11867-11870.
1138 Long, Y., Smet, W., Cruz-Ramírez, A., Castelijns, B., de Jonge, W., Mähönen, A.P., Bouchet, B.P.,
1139 Perez, G.S., Akhmanova, A., Scheres, B*., et al.* (2015). *Arabidopsis* BIRD Zinc Finger Proteins
1140 Jointly Stabilize Tissue Boundaries by Confining the Cell Fate Regulator SHORT-ROOT and
1141 Contributing to Fate Specification. The Plant Cell *27*, 1185-1199.
1142 Long, Y., Stahl, Y., Weidtkamp-Peters, S., Postma, M., Zhou, W., Goedhart, J., Sánchez-Pérez, M.-I.,
1143 Gadella, T.W.J., Simon, R., Scheres, B*., et al.* (2017). In vivo FRET–FLIM reveals cell-type-specific
1144 protein interactions in *Arabidopsis* roots. Nature *548*, 97-102.
1145 Lu, R., Canher, B., Bisht, A., Heyman, J., and De Veylder, L. (2021). Three-dimensional quantitative
1146 analysis of the *Arabidopsis* quiescent center. Journal of Experimental Botany.
1147 MacDonald, B.T., Tamai, K., and He, X. (2009). Wnt/β-Catenin Signaling: Components, Mechanisms,
1148 and Diseases. Developmental Cell *17*, 9-26.
1149 Matosevich, R., and Efroni, I. (2021). The quiescent center and root regeneration. J Exp Bot *72*, 6739-
1150 6745.
1151 Meyer, R.D., Srinivasan, S., Singh, A.J., Mahoney, J.E., Gharahassanlou, K.R., and Rahimi, N. (2011).
1152 PEST motif serine and tyrosine phosphorylation controls vascular endothelial growth factor receptor 2
1153 stability and downregulation. Mol Cell Biol *31*, 2010-2025.
1154 Nakajima, K., ., Sena, G., ., Nawy, T., ., and Benfey, P.N. (2001). Intercellular movement of the
1155 putative transcription factor SHR in root patterning. Nature *413*, 307-311.
1156 Patel, P., and Woodgett, J.R. (2017). Glycogen Synthase Kinase 3: A Kinase for All Pathways? Curr
1157 Top Dev Biol *123*, 277-302.
1158 Pi, L., Aichinger, E., Vandergraaff, E., Llavata-Peris, C., Weijers, D., Hennig, L., Groot, E., and Laux,
1159 T. (2015). Organizer-Derived WOX5 Signal Maintains Root Columella Stem Cells through
1160 Chromatin-Mediated Repression of CDF4 Expression. Developmental Cell *33*, 576-588.
1161 Planas-Riverola, A., Gupta, A., Betegon-Putze, I., Bosch, N., Ibanes, M., and Cano-Delgado, A.I.
1162 (2019). Brassinosteroid signaling in plant development and adaptation to stress. Development *146*.
1163 Rahman, A., Takahashi, M., Shibasaki, K., Wu, S., Inaba, T., Tsurumi, S., and Baskin, T.I. (2010).
1164 Gravitropism of *Arabidopsis* thaliana roots requires the polarization of PIN2 toward the root tip in
1165 meristematic cortical cells. The Plant cell *22*, 1762-1776.
1166 Rahni, R., and Birnbaum, K.D. (2019). Week-long imaging of cell divisions in the *Arabidopsis* root
1167 meristem. Plant Methods *15*.
1168 Rechsteiner, M., and Rogers, S.W. (1996). PEST sequences and regulation by proteolysis. Trends in
1169 biochemical sciences *21*, 267-271.
1170 Rodriguez, K., Perales, M., Snipes, S., Yadav, R.K., Diaz-Mendoza, M., and Reddy, G.V. (2016).
1171 DNA-dependent homodimerization, sub-cellular partitioning, and protein destabilization control
1172 WUSCHEL levels and spatial patterning. Proc Natl Acad Sci U S A *113*, E6307-E6315.
1173 Rogers, S., Wells, R., and Rechsteiner, M. (1986). Amino acid sequences common to rapidly degraded
1174 proteins: the PEST hypothesis. Science *234*, 364-368.
1175 Sabatini, S., Heidstra, R., Wildwater, M., and Scheres, B. (2003). SCARECROW is involved in
1176 positioning the stem cell niche in the *Arabidopsis* root meristem. Genes Dev *17*, 354-358.
1177 Sandhu, K.S., and Dash, D. (2006). Conformational flexibility may explain multiple cellular roles of
1178 PEST motifs. Proteins: Structure, Function, and Bioinformatics *63*, 727-732.
1179 Sarkar, A.K., Luijten, M., Miyashima, S., Lenhard, M., Hashimoto, T., Nakajima, K., Scheres, B.,
1180 Heidstra, R., and Laux, T. (2007). Conserved factors regulate signalling in *Arabidopsis* thaliana shoot
1181 and root stem cell organizers. Nature *446*, 811-814.

Savina, M.S., Pasternak, T., Omelyanchuk, N.A., Novikova, D.D., Palme, K., Mironova, V.V., and Lavrekha, V.V. (2020). Cell Dynamics in WOX5-Overexpressing Root Tips: The Impact of Local Auxin Biosynthesis. Front Plant Sci *11*, 560169.

Shi, Y. (2009). Serine/threonine phosphatases: mechanism through structure. Cell *139*, 468-484.

Shimotohno, A., Heidstra, R., Blilou, I., and Scheres, B. (2018). Root stem cell niche organizer specification by molecular convergence of PLETHORA and SCARECROW transcription factor modules. Genes & development *32*, 1085-1100.

Sokol, S.Y. (2011). Maintaining embryonic stem cell pluripotency with Wnt signaling. Development *138*, 4341-4350.

Spinner, L., Gadeyne, A., Belcram, K., Goussot, M., Moison, M., Duroc, Y., Eeckhout, D., De Winne, N., Schaefer, E., Van De Slijke, E.*, et al.* (2013). A protein phosphatase 2A complex spatially controls plant cell division. Nat Commun *4*, 1863.

Stahl, Y., Grabowski, S., Bleckmann, A., Kühnemuth, R., Weidtkamp-Peters, S., Pinto, Karine G., Kirschner, Gwendolyn K., Schmid, Julia B., Wink, René H., Hülsewede, A.*, et al.* (2013). Moderation of *Arabidopsis* Root Stemness by CLAVATA1 and *Arabidopsis* CRINKLY4 Receptor Kinase Complexes. Current Biology *23*, 362-371.

Stahl, Y., Wink, R.H., Ingram, G.C., and Simon, R. (2009). A Signaling Module Controlling the Stem Cell Niche in *Arabidopsis* Root Meristems. Current Biology *19*, 909-914.

Su, Y., Fu, C., Ishikawa, S., Stella, A., Kojima, M., Shitoh, K., Schreiber, E.M., Day, B.W., and Liu, B. (2008). APC Is Essential for Targeting Phosphorylated β-Catenin to the SCFβ-TrCP Ubiquitin Ligase. Molecular Cell *32*, 652-661.

Tan, S., Luschnig, C., and Friml, J. (2021). Pho-view of Auxin: Reversible Protein Phosphorylation in Auxin Biosynthesis, Transport and Signaling. Mol Plant *14*, 151-165.

Tang, W., Yuan, M., Wang, R., Yang, Y., Wang, C., Oses-Prieto, J.A., Kim, T.W., Zhou, H.W., Deng, Z., Gampala, S.S.*, et al.* (2011). PP2A activates brassinosteroid-responsive gene expression and plant growth by dephosphorylating BZR1. Nat Cell Biol *13*, 124-131.

Tian, H., Wabnik, K., Niu, T., Li, H., Yu, Q., Pollmann, S., Vanneste, S., Govaerts, W., Rolcik, J., Geisler, M.*, et al.* (2014). WOX5-IAA17 feedback circuit-mediated cellular auxin response is crucial for the patterning of root stem cell niches in *Arabidopsis*. Mol Plant *7*, 277-289.

Truernit, E., Bauby, H., Dubreucq, B., Grandjean, O., Runions, J., Barthelemy, J., and Palauqui, J.C. (2008). High-resolution whole-mount imaging of three-dimensional tissue organization and gene expression enables the study of Phloem development and structure in *Arabidopsis*. Plant Cell *20*, 1494-1503.

Ubogoeva, E.V., Zemlyanskaya, E.V., Xu, J., and Mironova, V. (2021). Mechanisms of stress response in the root stem cell niche. J Exp Bot *72*, 6746-6754.

Vanstraelen, M., Baloban, M., Da Ines, O., Cultrone, A., Lammens, T., Boudolf, V., Brown, S.C., De Veylder, L., Mergaert, P., and Kondorosi, E. (2009). APC/C^{CCS52A} complexes control meristem maintenance in the *Arabidopsis* root. Proceedings of the National Academy of Sciences *106*, 11806-11811.

Vilarrasablasi, J., Gonzálezgarcía, M.P., Frigola, D., Fàbregas, N., Alexiou, K.G., Lópezbigas, N., Rivas, S., Jauneau, A., Lohmann, J.U., and Benfey, P.N. (2014). Regulation of plant stem cell quiescence by a brassinosteroid signaling module. Developmental Cell *30*, 36-47.

Walter, M., Chaban, C., Schutze, K., Batistic, O., Weckermann, K., Nake, C., Blazevic, D., Grefen, C., Schumacher, K., Oecking, C.*, et al.* (2004). Visualization of protein interactions in living plant cells using bimolecular fluorescence complementation. The Plant journal : for cell and molecular biology *40*, 428-438.

Worby, C.A., and Dixon, J.E. (2019). Reversible phosphorylation: a birthday tribute to Herb Tabor. The Journal of biological chemistry *294*, 1638-1642.

Yadav, R.K., Perales, M., Gruel, J., Girke, T., Jönsson, H., and Reddy, G.V. (2011). WUSCHEL protein movement mediates stem cell homeostasis in the *Arabidopsis* shoot apex. Genes & development *25*, 2025-2030.

1233 Yamamoto, H., Kishida, S., Kishida, M., Ikeda, S., Takada, S., and Kikuchi, A. (1999).
1234 Phosphorylation of Axin, a Wnt Signal Negative Regulator, by Glycogen Synthase Kinase-3β
1235 Regulates Its Stability*. Journal of Biological Chemistry *274*, 10681-10684.
1236 Yan, Z., Zhao, J., Peng, P., Chihara, R.K., and Li, J. (2009). BIN2 functions redundantly with other
1237 *Arabidopsis* GSK3-like kinases to regulate brassinosteroid signaling. Plant Physiol *150*, 710-721.
1238 Ye, H., Li, L., Guo, H., and Yin, Y. (2012). MYBL2 is a substrate of GSK3-like kinase BIN2 and acts
1239 as a corepressor of BES1 in brassinosteroid signaling pathway in *Arabidopsis*. Proc Natl Acad Sci U S
1240 A *109*, 20142-20147.
1241 Youn, J.H., and Kim, T.W. (2015). Functional insights of plant GSK3-like kinases: multi-taskers in
1242 diverse cellular signal transduction pathways. Mol Plant *8*, 552-565.
1243 Zhai, H., Zhang, X., You, Y., Lin, L., Zhou, W., and Li, C. (2020). SEUSS integrates transcriptional
1244 and epigenetic control of root stem cell organizer specification. Embo j, e105047.
1245 Zhang, Y., Jiao, Y., Liu, Z., and Zhu, Y.X. (2015). ROW1 maintains quiescent centre identity by
1246 confining WOX5 expression to specific cells. Nature Communications *6*, 6003.
1247 Zhou, Y., Yan, A., Han, H., Li, T., Geng, Y., Liu, X., and Meyerowitz, E.M. (2018). HAIRY
1248 MERISTEM with WUSCHEL confines CLAVATA3 expression to the outer apical meristem layers.
1249 Science *361*, 502-506.
1250 Zhu, Y., Hu, C., Cui, Y., Zeng, L., Li, S., Zhu, M., Meng, F., Huang, S., Long, L., Yi, J.*, et al.* (2021).
1251 Conserved and differentiated functions of CIK receptor kinases in modulating stem cell signaling in
1252 *Arabidopsis*. Mol Plant *14*, 1119-1134.

1253

1254

1255

1256

1257

1258

1259

1260

1261

1262
1263
1264
1265
1266
1267
1268
1269
1270
1271
1272
1273
1274
1275

Main figures

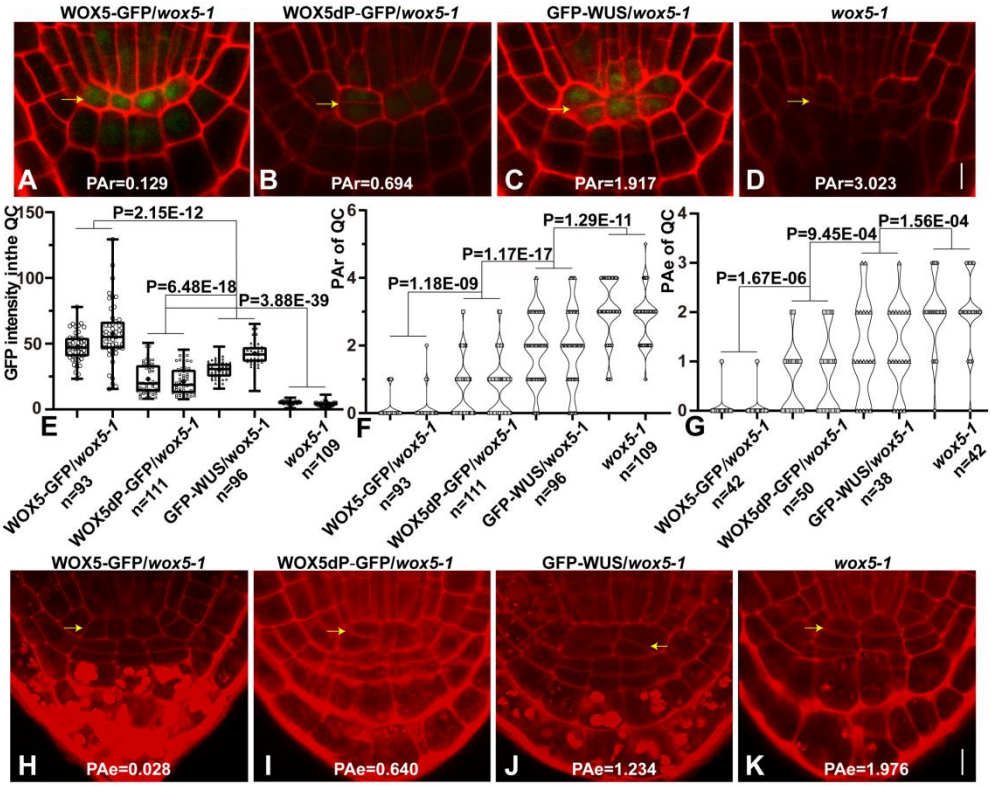

Figure 1: The PEST domain stabilizes WOX5 protein and maintains low proliferative activity of QC cells from the embryonic stage to the post-embryonic stage

(A~D) PI staining images of (A) WOX5-GFP/*wox5-1* rescued lines (PAr = 0.129); (B) WOX5△PEST-GFP/*wox5-1* rescued lines (PAr = 0.694); (C) GFP-WUS/*wox5-1* rescued lines (PAr = 1.917); (D) *wox5-1* (PAr = 3.023). (E) GFP intensity in the QC at 5DAG of 93 strains of WOX5-GFP/*wox5-1* rescued lines (46 strains of W5-3 line plus 47 strains of W5-4 line); of 111 strains of WOX5△PEST-GFP/*wox5-1* rescued lines (55 strains of dP-2 line plus 56 strains of dP-3 line); of 96 strains of GFP-WUS/*wox5-1* rescued lines (49 strains of WU-1 line plus 47 strains of WU-2 line); and of 109 strains of *wox5-1*. (F) PAr of QC at 5DAG of 93 strains of WOX5-GFP/*wox5-1* rescued lines (46 strains of W5-3 line plus 47 strains of W5-4 line); of 111 strains of WOX5△PEST-GFP/*wox5-1* rescued lines (55 strains of dP-2 line plus 56 strains of dP-3 line); of 96 strains of GFP-WUS/*wox5-1* rescued lines (49 strains of WU-1 line plus 47 strains of WU-2 line); and of 109 strains of *wox5-1*. (G) PAe of QC at the mature embryonic stage of 42 strains of WOX5-GFP/*wox5-1* rescued lines (21 strains of W5-3 line plus 21 strains of W5-4 line); of 50 strains of WOX5△PEST-GFP/*wox5-1* rescued lines (25 strains of dP-2 line plus 25 strains of dP-3 line); of 38 strains of GFP-WUS/*wox5-1* rescued lines (19 strains of WU-1 line plus 19 strains of WU-2 line); and of 42 strains of *wox5-1*. (H~K) mPS-PI staining images of (H) WOX5-GFP/*wox5-1* rescued lines (PAe = 0.028); (I) WOX5△PEST-GFP/*wox5-1* rescued lines (PAe = 0.640); (J) GFP-WUS/*wox5-1* rescued lines (PAe = 1.234); (K) *wox5-1* (PAe = 1.976). Student's t test indicates statistical difference. Bar = 10 μm, yellow arrows show the QC cells or the cell plates of QC cells.

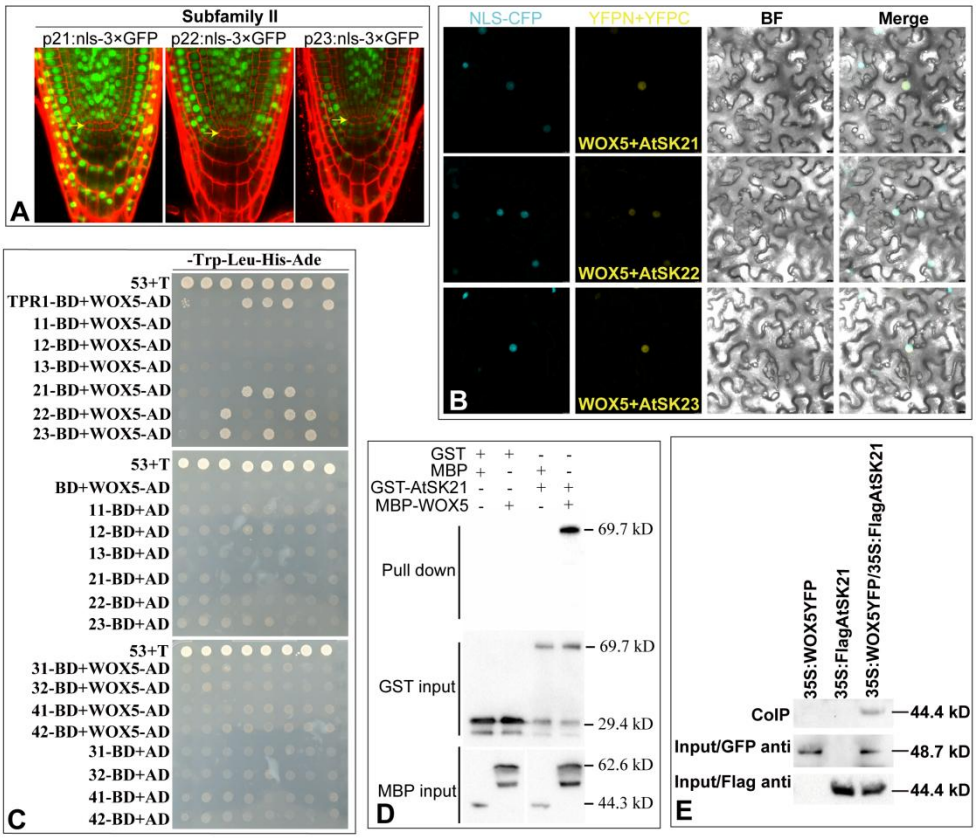

Figure 2: The subfamily II of AtSKs (AtSK21, AtSK22, AtSK23) interact with WOX5 in vitro and in vivo

(A) Transcriptional reporters of the subfamily II of AtSKs (AtSK21, AtSK22 and AtSK23) all expressed in the QC at 5DAG. (B) BiFC assay: NLS-CFP is a nuclear marker, YFPN+YFPC means WOX5-YFPN interacted with AtSK21-YFPC, AtSK22-YFPC and AtSK23-YFPC in nucleus in the nicotiana tabacum, BF is bright filed. (C) Y2H assay: In the Yeast Base Medium without Trp, Leu, His and Ade, the AH109 strain of positive control groups 53+T all grew (8/8), and TPR1-BD+WOX5-AD mostly grew (5/8); only experiment groups AtSK21-BD+WOX5-AD, AtSK22-BD+WOX5-AD and AtSK23-BD+WOX5-AD grew some (3/8), but experiment groups AtSK11-BD+WOX5-AD, AtSK12-BD+WOX5-AD, AtSK13-BD+WOX5-AD, AtSK31-BD+WOX5-AD, AtSK32-BD+WOX5-AD, AtSK41-BD+WOX5-AD, AtSK42-BD+WOX5-AD not grew (0/8); the negative control groups AtSK11-BD+AD, AtSK12-BD+AD, AtSK13-BD+AD, AtSK21-BD+AD, AtSK22-BD+AD, AtSK23-BD+AD, AtSK31-BD+AD, AtSK32-BD+AD, AtSK41-BD+AD and AtSK42-BD+AD all not grew (0/8). (D) Pull down in vitro assay: MBP input means MBP protein (44.3 kD) and MBP-WOX5 protein (62.6 kD) exist in the transfer membrane presenting by MBP mouse anti; GST input means GST protein (29.4 kD) and GST-AtSK21 (69.7 kD) exist in the transfer membrane presenting by GST mouse anti; Pull down means only when MBP-WOX5 protein and GST-AtSK21 protein both exist in reaction solution, the GST-AtSK21 protein (69.7 kD) could be pull down by MBP beads. (E) CoIP assay: 35S:WOX5YFP is 35S : LhGR-pOp : WOX5-YFP/Col-0 line, 35S:FlagAtSK21 is 35S : Flag-AtSK21/Col-0 line, 35S:WOX5YFP/35S:FlagAtSK21 means the double homozygous line of 35S : LhGR-pOp : WOX5-YFP/Col-0 line cross to 35S : Flag-AtSK21/Col-0 line. Input/GFP anti means WOX5YFP protein (48.7 kD) exist in the transfer membrane presenting by GFP mouse anti, Input/Flag anti means FlagAtSK21 protein (44.4 kD) exist in the transfer membrane presenting by Flag mouse anti, CoIP means Flag-AtSK21 protein could be co-immunoprecipitated by GFP beads only in the double homozygous line. Bar = 10 μm, yellow arrows show the QC cells.

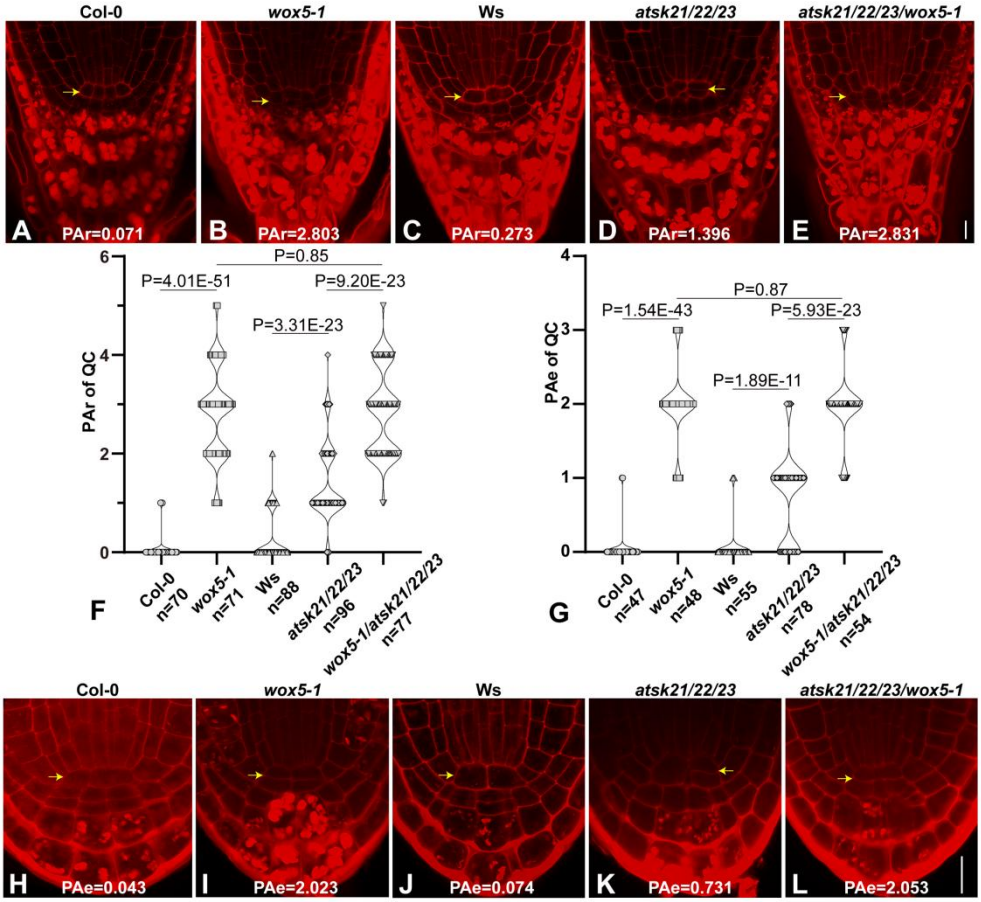

Figure 3: WOX5 is epistatic to the subfamily II of AtSKs in inhibiting proliferative activity of QC cells from the embryonic stage to the post-embryonic stage

(A~E) mPS-PI staining images of (A) Col-0 (PAr = 0.071); (B) *wox5-1* (PAr = 2.803); (C) Wassilewskija (Ws) (PAr = 0.273); (D) *atsk21/22/23* (PAr = 1.396); (E) *atsk21/22/23wox5-1* (PAr = 2.831). (F) PAr of QC at 5DAG of Col-0 (n=70), *wox5-1* (n=71), Ws (n=88), *atsk21/22/23* (n=96), *atsk21/22/23wox5-1* (n=77). (G) PAe of QC at the mature embryonic stage of Col-0 (n=46), *wox5-1* (n=48), Ws (n=55), *atsk21/22/23* (n=78), *atsk21/22/23wox5-1* (n=54). (H~L) mPS-PI staining images of (H) Col-0 (PAe = 0.059); (I) *wox5-1* (PAe = 2.023; (J) Ws (PAe = 0.073); (K) *atsk21/22/23* (PAe = 0.731); (L) *atsk21/22/23wox5-1* (PAe = 2.053). Student's t test indicates statistical difference, bar = 10 μm, yellow arrows show the QC cells or the cell plates of QC cells.

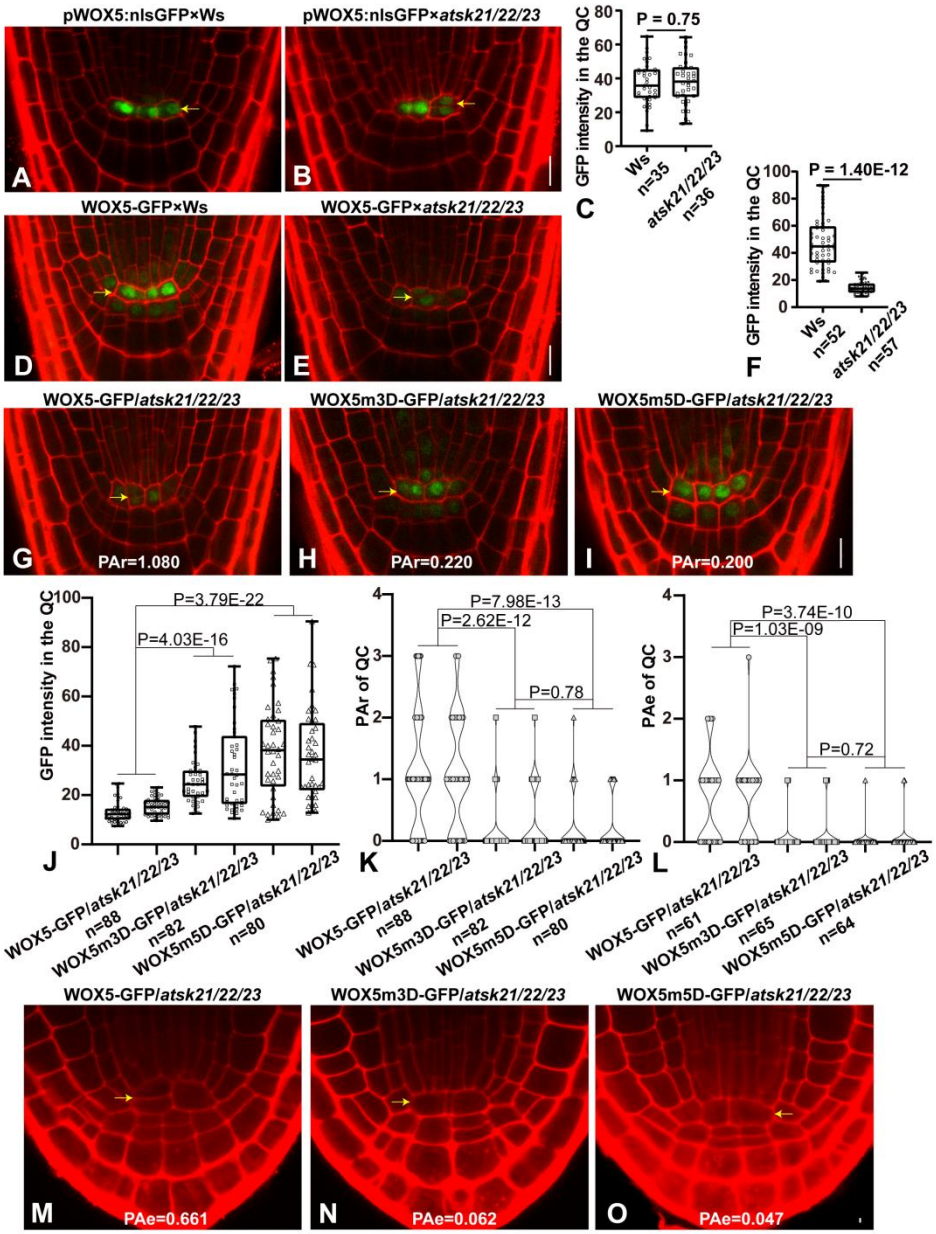

Figure 4: The subfamily II of AtSKs stabilize WOX5 protein by phosphorylating the GMs

(A, B) PI staining images of (A) pWOX5:nlsGFP × Ws and (B) pWOX5:nlsGFP × *atsk21/22/23*. (C) GFP intensity in the QC at 5DAG of pWOX5:nlsGFP × Ws (n=35) and pWOX5:nlsGFP × *atsk21/22/23* (n=36). (D, E) PI staining images of (D) pWOX5:WOX5GFP × Ws and (E) pWOX5:WOX5GFP × *atsk21/22/23*. (F) GFP intensity in the QC at 5DAG of pWOX5:WOX5GFP × Ws (n=52) and pWOX5:WOX5GFP × *atsk21/22/23* (n=57). (G~I) PI staining images of WOX5GFP/*atsk21/22/23* line (PAr = 1.080), WOX5m3DGFP/*atsk21/22/23* line (PAr = 0.220) and WOX5m5DGFP/*atsk21/22/23* line (PAr = 0.200). (J) GFP intensity in the QC of 88 strains of WOX5GFP/*atsk21/22/23* lines (45 strains of W5-1 line plus 43 strains of W5-2 line); of 82 strains of WOX5m3DGFP/*atsk21/22/23* lines (40 strains of 3D-1 line plus 42 strains of 3D-2 line); and of 80 strains of WOX5m5DGFP/*atsk21/22/23* lines (40 strains of 5D-1 line plus 40 strains of 5D-2 line). (K) PAr of QC at 5DAG of 88 strains of WOX5GFP/*atsk21/22/23* lines (45 strains of W5-1 line plus 43 strains of W5-2 line); of 82 strains of WOX5m3DGFP/*atsk21/22/23* lines (40 strains of 3D-1 line plus 42 strains of 3D-2 line); and of 80 strains of WOX5m5DGFP/*atsk21/22/23* lines (40 strains of 5D-1

line plus 40 strains of 5D-2 line). (L) PAe of QC at the mature embryonic stage of 61 strains of WOX5GFP/*atsk21/22/23* lines (30 strains of W5-1 line plus 31 strains of W5-2 line); of 65 strains of WOX5m3DGFP/*atsk21/22/23* lines (32 strains of 3D-1 line plus 33 strains of 3D-2 line); and of 64 strains of WOX5m5DGFP/*atsk21/22/23* lines (32 strains of 5D-1 line plus 32 strains of 5D-2 line). (M~O) mPS-PI staining images of (M) WOX5GFP/*atsk21/22/23* line (PAe = 0.661); (N) WOX5m3DGFP/*atsk21/22/23* line (PAe = 0.062) and (O) WOX5m5DGFP/*atsk21/22/23* line (PAe = 0.047). Student's t test indicates statistical difference, bar = 10 μm, yellow arrows show the QC cells or the cell plates of QC cells.

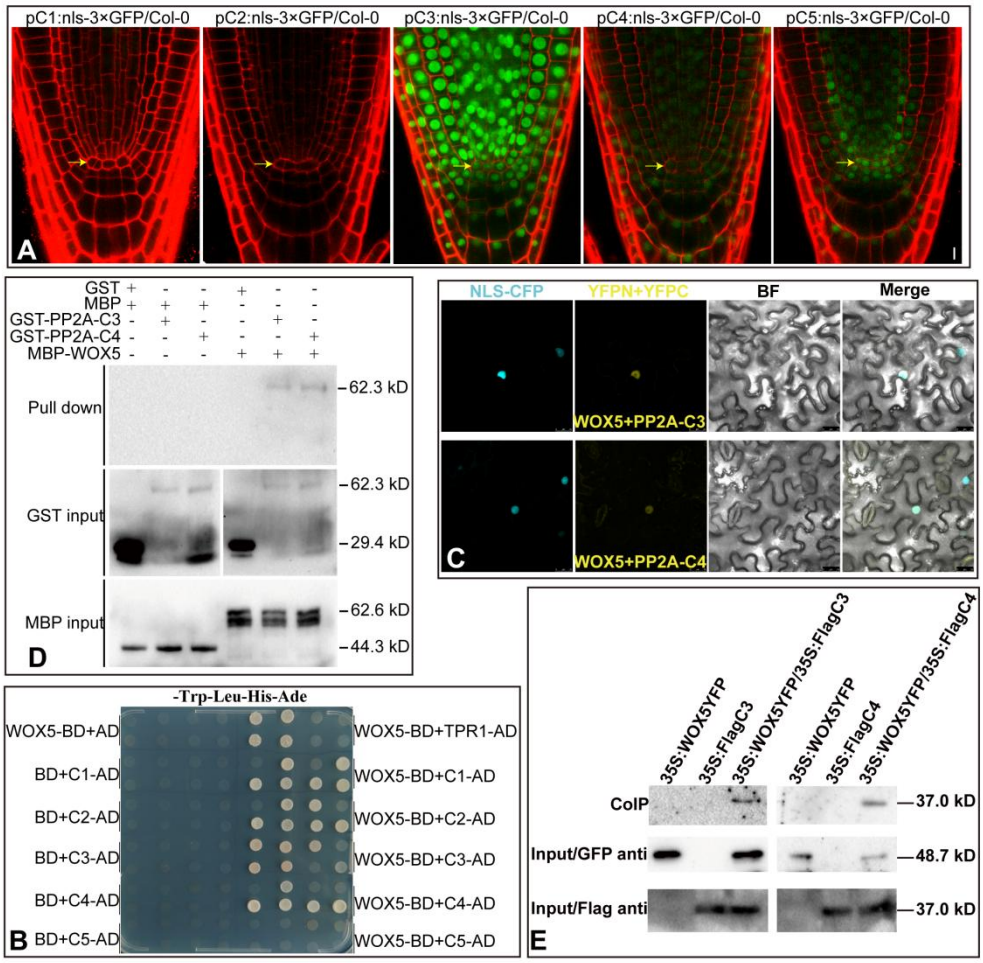

Figure 5: The subfamily II of AtPP2A-Cs (AtPP2A-C3 and AtPP2A-C4) interact with WOX5 in vitro and in vivo

(A) Transcriptional reporters of the subfamily II of AtPP2A-Cs (AtPP2A-C3, and AtPP2A-C4) and AtPP2A-C5 expressed in the QC at 5DAG. (B) Y2H assay: In the Yeast Base Medium without Trp, Leu, His and Ade, the AH109 strain of positive control group TPR1-BD + WOX5-AD halfly grew (4/8); experiment groups AtPP2A-C1-BD + WOX5-AD and AtPP2A-C1-BD + WOX5-AD mostly grew (6/8), experiment groups AtPP2A-C3-BD + WOX5-AD and AtPP2A-C4-BD + WOX5-AD mostly grew (5/8), but experiment groups AtPP2A-C5-BD + WOX5-AD not grew (0/8). (C) BiFC assay: NLS-CFP is a nuclear marker, YFPN+YFPC means WOX5-YFPN interacted with AtPP2A-C3-YFPC and AtPP2A-C4-YFPC in nucleus in the nicotiana tabacum, , BF is bright filed. (D) Pull down in vitro assay: MBP input means MBP protein (44.3 kD) and MBP-WOX5 protein (62.6 kD) exist in the transfer membrane presenting by MBP mouse anti; GST input means GST protein (29.4 kD) and GST-AtSK21 (69.7 kD) exist in the transfer membrane presenting by GST mouse anti; Pull down means only when MBP-WOX5 protein and GST-AtPP2A-C3 or GST-AtPP2A-C4 protein both exist in reaction solution, the GST-AtPP2A-C3 (62.6 kD) or GST-AtPP2A-C4 protein (62.3 kD) could

be pull down by MBP beads. (E) CoIP assay: 35S:WOX5YFP is 35S : LhGR-pOp : WOX5-YFP/Col-0 line, 35S:FlagC3 and 35S:FlagC4 are 35S : FlagAtPP2A-C3/Col-0 line and 35S : FlagAtPP2A-C4/Col-0 line, 35S:WOX5YFP/ 35S:FlagC3 means the double homozygous line of 35S : LhGR-pOp : WOX5-YFP/Col-0 line cross to 35S : FlagC3/Col-0 line, 35S:WOX5YFP/ 35S:FlagC4 means the double homozygous line of 35S : LhGR-pOp : WOX5-YFP/Col-0 line cross to 35S : FlagC4/Col-0 line. Input/GFP anti means WOX5YFP protein (48.7 kD) exist in the transfer membrane presenting by GFP mouse anti, Input/Flag anti means FlagC3 protein (37.0 kD) and FlagC4 protein (36.9 kD) exist in the transfer membrane presenting by Flag mouse anti, CoIP means FlagC3 and FlagC4 protein could be co-immunoprecipitated by GFP beads only in the double homozygous line. Bar = 10 μm, yellow arrows show the QC cells.

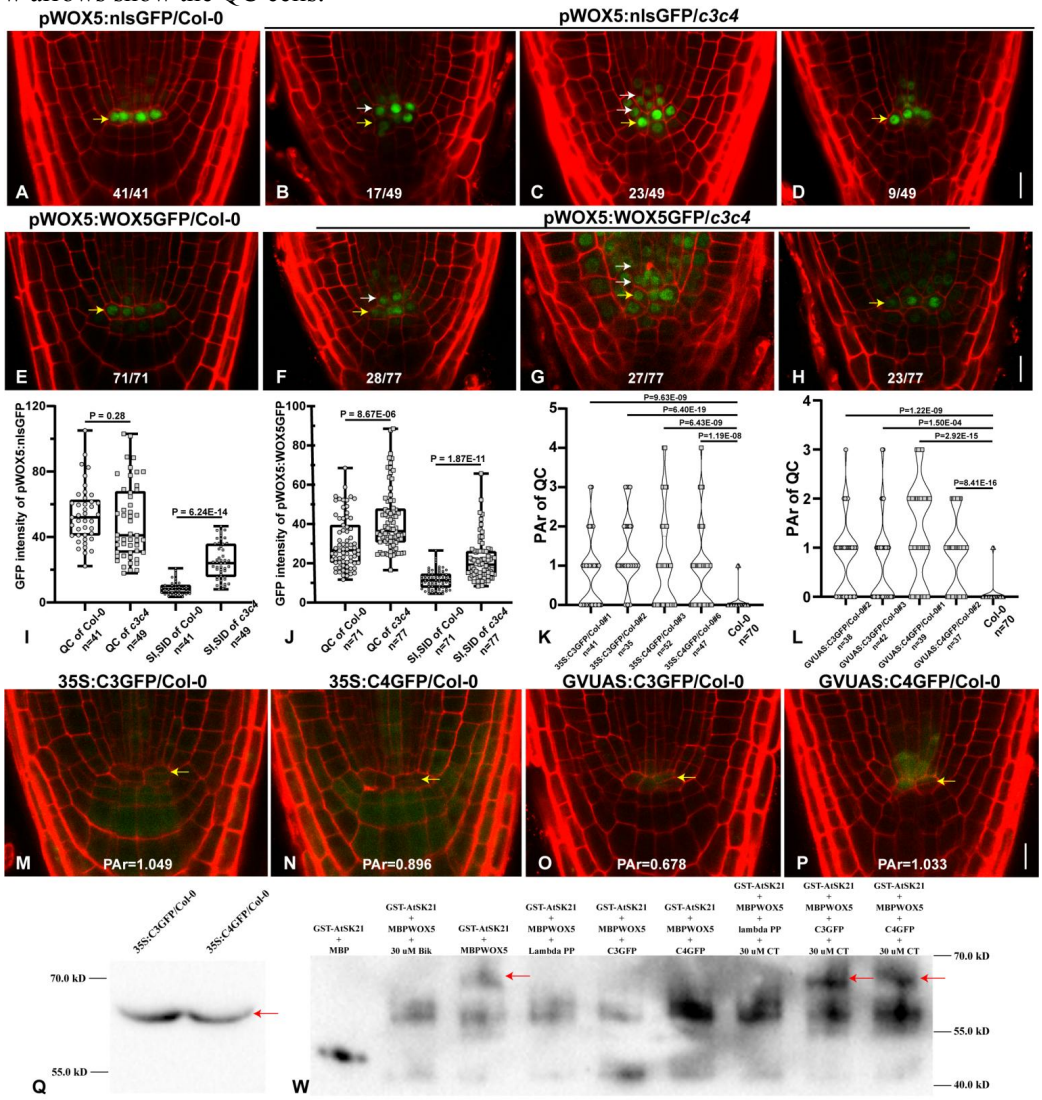

Figure 6: The subfamily II of AtPP2A-Cs enhance the proliferative activity of QC cells by dephosphorylating and destabilizing the WOX5 protein

(A~D) PI staining images of (A) pWOX5:nlsGFP/Col-0 and (B~D) pWOX5:nlsGFP/*c3c4*. (E~H) PI staining images of (E) pWOX5:WOX5GFP/Col-0 line and (F-H) pWOX5:WOX5GFP pWOX5:nlsGFP/*c3c4*. (I) GFP intensity in the QC, SI and SID at 5DAG of pWOX5:nlsGFP/Col-0 (n=41) and pWOX5:nlsGFP/*c3c4* (n=49). (J) GFP intensity in the QC, SI and SID at 5DAG of pWOX5:WOX5GFP/Col-0 (n=71) and pWOX5:WOX5GFP/*c3c4* (n=77). (K) PAr of QC at 5DAG of 35S:C3GFP/Col-0 line #1 (n=41), 35S:C3GFP/Col-0 line #2 (n=35), 35S:C4GFP/Col-0 line #3 (n=52), 35S:C4GFP/Col-0 line #6 (n=47) and Col-0 (n=70). (L) PAr of QC at 5DAG of GVUAS:C3GFP/Col-

0 line #2 (n=38), GVUAS:C3GFP/Col-0 line #3 (n=42), GVUAS:C4GFP/Col-0 line #1 (n=39), GVUAS:C4GFP/Col-0 line #2 (n=37) and Col-0 (n=70). (M~P) PI staining images of (M) 35S:C3GFP/Col-0 line (PAr = 1.049); (N) 35S:C4GFP/Col-0 line (PAr = 0.896); (O) GVUAS:C3GFP/Col-0 line (PAr = 0.678) and (P) GVUAS:C4GFP/Col-0 line (PAr=1.033). (Q) C3GFP (63.3 kD) and C4GFP (63.2 kD) fused protein are immunoprecipitated by GFP beads and presented by GFP mouse anti from the 35S:C3GFP and 35S:C4GFP lines. (W) The Mn2+-Phos-tag™ SDS-PAGE assay, from the left to the right, the first lane showed the negative control (NC) group 1 (GST-AtSK21 + MBP), the second lane showed NC group 2 (GST-AtSK21 + MBP-WOX5 + 30 μM Bik), the third lane showed the experiment group 1 (GST-AtSK21 + MBP-WOX5) with a band (the red arrow) bigger than the MBP-WOX5 band, the fourth lane showed the experiment group 2 [GST-AtSK21 + MBP-WOX5 + lambda Protein Phosphase (PP)], the fivth lane showed the experiment group 3 (GST-AtSK21 + MBP-WOX5 + C3GFP holoenzyme), the sixth lane showed the experiment group 4 (GST-AtSK21 + MBP-WOX5 + C4GFP holoenzyme), the seventh lane showed the experiment group 5 (GST-AtSK21 + MBP-WOX5 + lambda PP + 30 μM CT), the eighth lane showed the experiment group 6 (GST-AtSK21 + MBP-WOX5 + C3GFP holoenzyme + 30 μM CT) with a band (the red arrow) bigger than the MBP-WOX5 band, and the ninth lane showed the experiment group 7 (GST-AtSK21 + MBP-WOX5 + C4GFP holoenzyme + 30 μM CT) with a band (the red arrow) bigger than the MBP-WOX5 band. Yellow arrows show the QC or the cell plates of QC cells, white arrows show the SI and SID cells; Student's t test indicates statistical difference, bar = 10 μm.

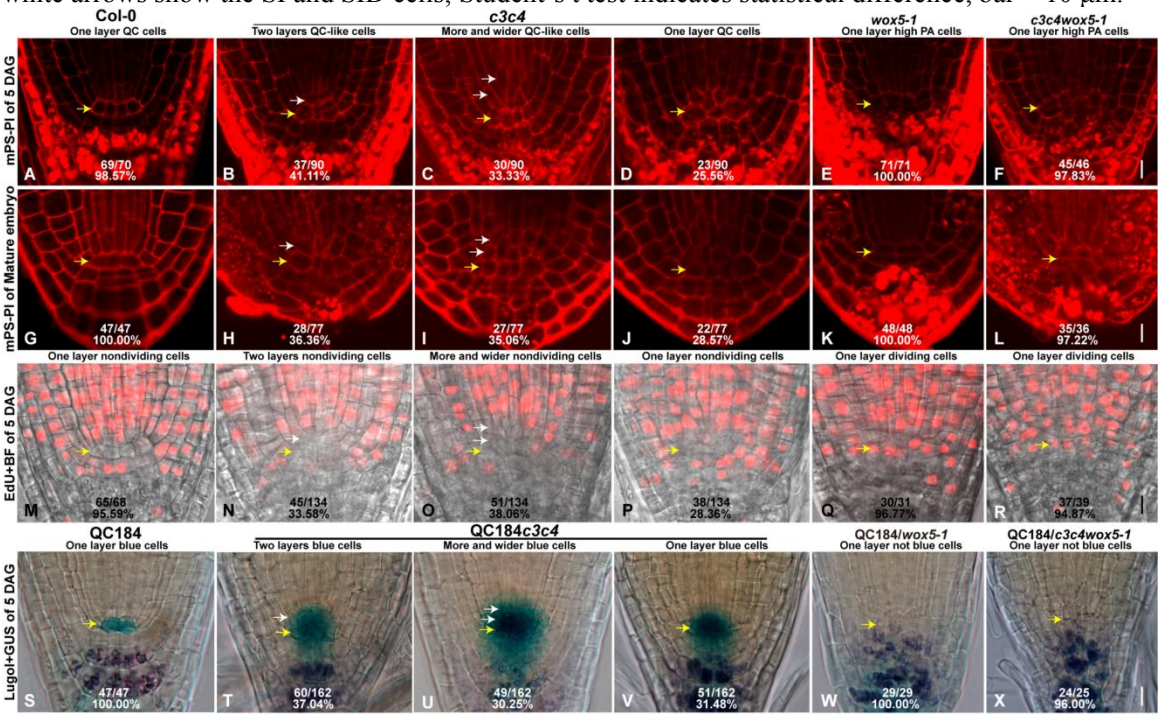

Figure 7: WOX5 is necessary for producing more quiescent cells when loss of function the subfamily II of AtPP2A-Cs.

(A~F) mPS-PI staining images of 5DAG of (A) Col-0 (98.57% are one layer QC cells); (B~D) *c3c4* (41.11% are two layers QC-like cells, 33.33% are more and wider QC-like cells, 25.56% are one layer QC cells); (E) *wox5-1* (100.00% are one layer high PA cells); (F) *c3c4wox5-1* (97.83% are one layer high PA cells), yellow arrows show the QC cells, white arrows show the QC-like cells. (G~L) mPS-PI staining images of mature embryo of (G) Col-0 (100.00% are one layer QC cells); (H~J) *c3c4* (36.36% are two layers QC-like cells, 35.07% are more and wider QC-like cells, 28.57% are one layer QC cells); (K) *wox5-1* (95.59% are one layer high PA cells); (L) *c3c4wox5-1* (97.22% are one layer high PA cells), yellow arrows show the QC cells, white arrows show the QC-like cells. (M~R) EdU staining and bright filed images of 5DAG of (M) Col-0 (95.59% are one layer nondividing cells); (N~P) *c3c4* (33.58% are two layers nondividing cells, 38.06% are more and wider nondividing cells,

28.36% are one layer nondividing cells); (Q) *wox5-1* (96.77% are one layer dividing cells); (R) *c3c4wox5-1* (94.87% are one layer dividing cells), yellow arrows show the dividing or nondividing cells, white arrows show the QC-like cells. (S~X) GUS staining images of 5DAG of (S) QC184 (100.00% are one layer blue cells); (T~V) QC184*c3c4* (37.04% are two layers blue cells, 30.25% are more and wider blue cells, 31.48% are one layer blue cells); (W) QC184/*wox5-1* (100.00% are one layer not blue cells); (X) QC184/*c3c4wox5-1* (96.00% are one layer not blue cells), yellow arrows show the not blue or blue cells, white arrows show the QC-like cells. Bar = 10 μm.

Supplemental figures

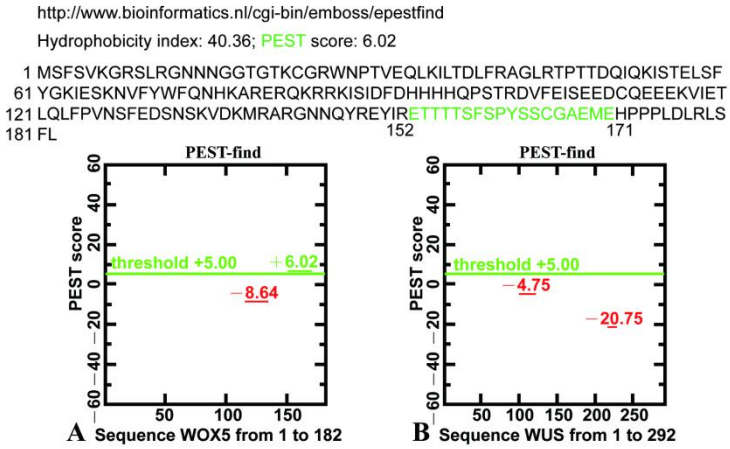

Figure S1: The comparison of PEST domain find of WOX5 and WUS protein sequence

We typed the protein sequence of WOX5 and WUS into the website https://www.bioinformatics.nl/cgi-bin/emboss/epestfind separately, then click the "Run epestfind", the results show a potential PEST domain with 18 amino acids between position 152 and 171 of WOX5 protein sequence, with hydrophobicity index of 40.36 and PEST score was +6.02 (greater than threshold value +5.00 means a possible PEST domain with real interest), no potential PEST domain in the WUS protein sequence.
(A) The output of PEST-find of WOX5 protein sequence.
(B) The output of PEST-find of WUS protein sequence.

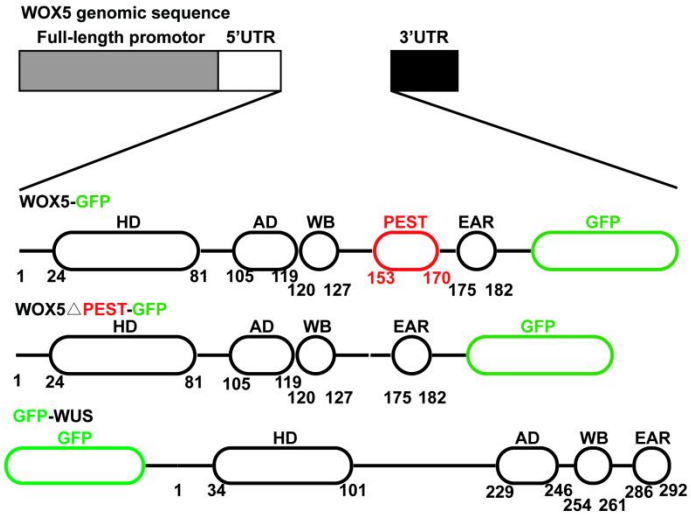

Figure S2: The sketch of plasmids construction of pWOX5:WOX5-GFP, pWOX5:WOX5△PEST-GFP and pWOX5:GFP-WUS

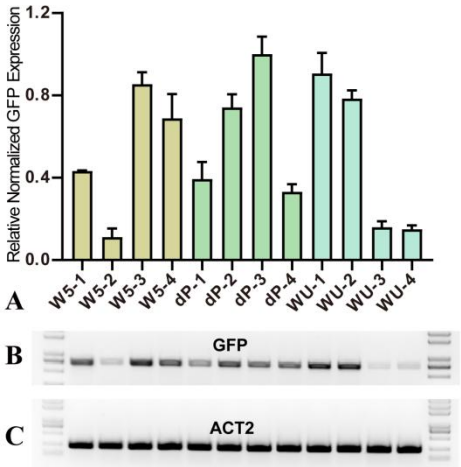

Figure S3: qPCR and sqRT-PCR of the different rescued lines identified 6 lines (W5-3, W5-4, dP-2, dP-3, WU-1, WU-2 separately) with almost equal GFP expression

(A) Relative normalized GFP expression compared with the ACT2 internal reference expression in the qPCR assay. (B and C) GFP bands (B) and ACT2 bands (C) of sqRT-PCR separately. Here W5 means WOX5GFP/*wox5-1* rescued lines, dP means WOX5△PEST-GFP/*wox5-1* rescued lines, WU means GFP-WUS/*wox5-1* rescued lines.

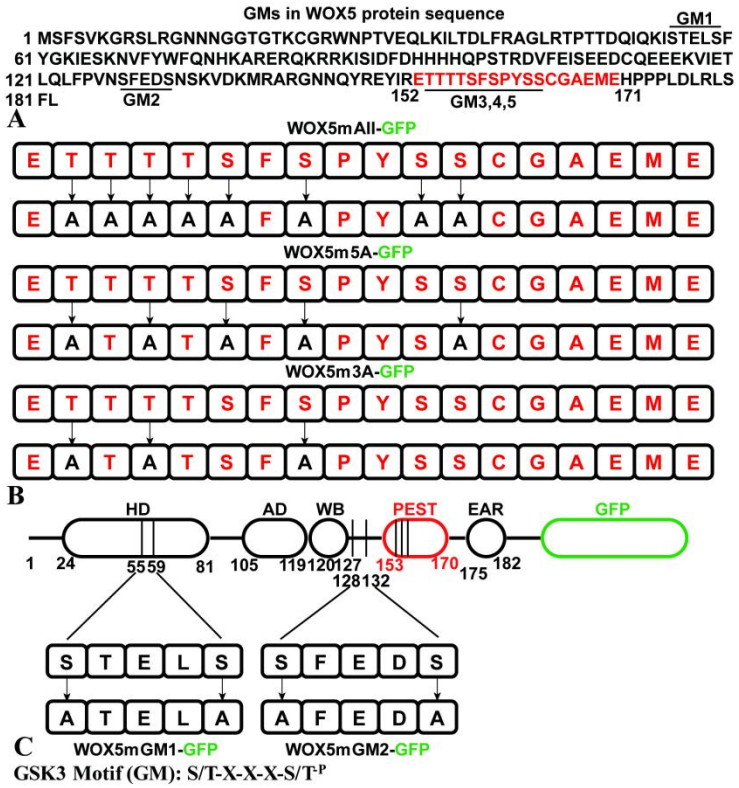

Figure S4: The GSK3 motifs (GMs) and its mutated types of the WOX5 protein

(A) Positions of 5 GMs in the WOX5 protein sequence. (B) The 3 types (mutated all T and S in the PEST, mAll; mutated the GSK3 phosphorylation sites and the primed phosphorylation sites, m5A; only mutated the GSK3 phosphorylation sites, m3A) of mutated GMs (GM3,4,5) in the PEST domain of the WOX5-GFP fusion protein. (C) The mutated GM1 and GM2 of WOX5-GFP fusion protein.

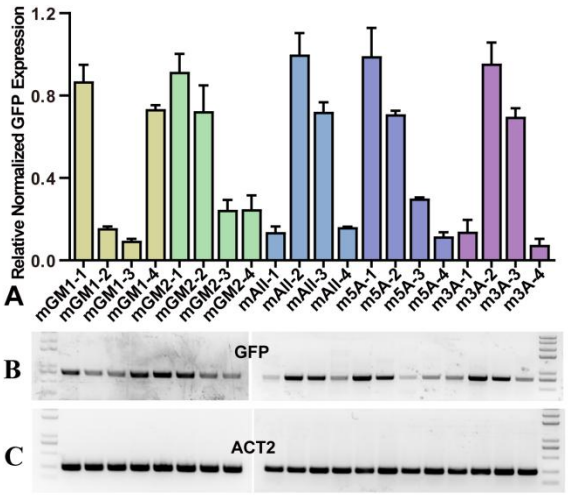

Figure S5: qPCR and sqRT-PCR of the different rescued lines identified 10 lines (mGM1-1, mGM1-4; mGM2-1, mGM2-2; mAll-2, mAll-3; m5A-1, m5A-2; m3A-2, m3A-3 separately) with almost equal GFP expression

(A) Relative normalized GFP expression compared with the ACT2 internal reference expression in the qPCR assay. (B and C) GFP bands and ACT2 bands of sqPCR separately. Here mGM1 means WOX5mGM1-GFP/*wox5-1* rescued lines, mGM2 means WOX5mGM2-GFP/*wox5-1* rescued lines, mAll means WOX5mAll-GFP/*wox5-1* rescued lines m5A means WOX5m5A-GFP/*wox5-1* rescued lines, m3A means WOX5m3A-GFP/*wox5-1* rescued lines.

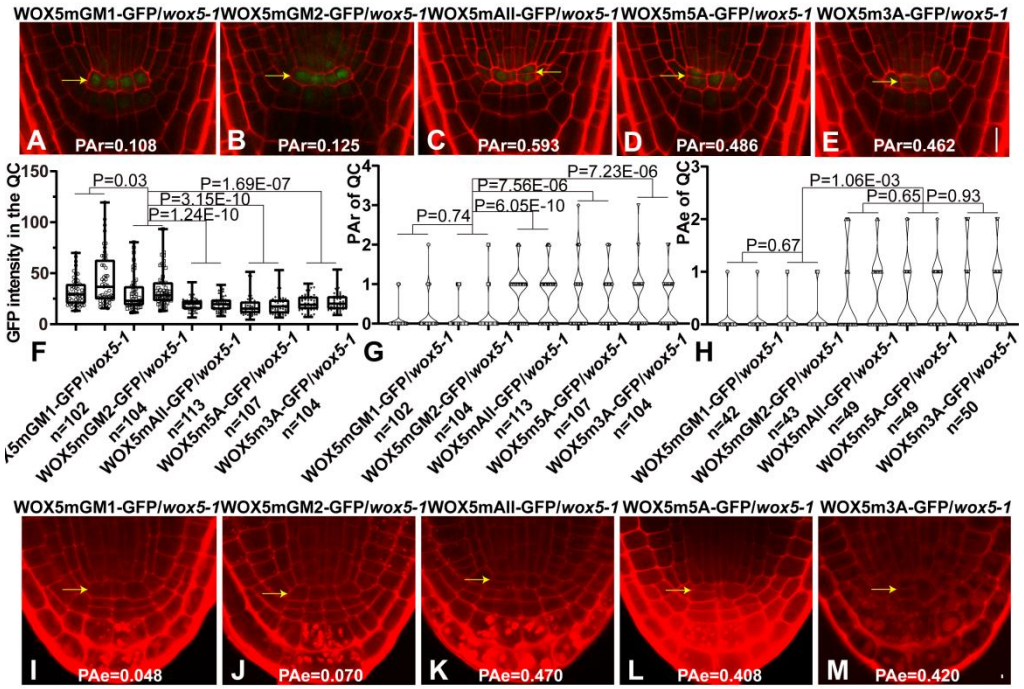

Figure S6: The GMs in the PEST domain stabilizes WOX5 protein and maintains low proliferative activity of QC cells from the embryonic stage to the post-embryonic stage

(A~E) PI staining and LCSM images of (A) WOX5mGM1-GFP/*wox5-1* rescued lines with PAr equal to 0.108; (B) WOX5mGM2-GFP/*wox5-1* rescued lines with PAr equal to 0.125; (C) WOX5mAll-GFP/*wox5-1* rescued lines with PAr equal to 0.593; (D) WOX5m5A-GFP/*wox5-1* lines with PAr equal to 0.486 (E) WOX5m3A-GFP/*wox5-1* lines with PAr equal to 0.462. (F) GFP intensity in the QC at 5DAG of 102 strains of WOX5mGM1-GFP/*wox5-1* rescued lines (51 strains of mGM1-1 line plus 51 strains of mGM1-4 line) is almost similar to the 104 strains of WOX5mGM2-GFP/*wox5-1*

1497 rescued lines (53 strains of mGM2-1 line plus 51 strains of mGM2-2 line) with the P value = 0.03, the
1498 later lines are significantly higher than the 113 strains of WOX5mAll-GFP/*wox5-1* rescued lines (56
1499 strains of mAll-2 line plus 57 strains of mAll-3 line) with the P value = 1.24E-10, the 107 strains of
1500 WOX5m5A-GFP/*wox5-1* rescued lines (55 strains of m5A-1 line plus 52 strains of m5A-2 line) with
1501 the P value = 3.15E-10 and the 104 strains of WOX5m3A-GFP/*wox5-1* lines (51 strains of m3A-2 line
1502 plus 53 strains of m3A-3 line) with the P value = 1.69E-07. (G) PAr of QC at 5DAG of 102 strains of
1503 WOX5mGM1-GFP/*wox5-1* rescued lines (51 strains of mGM1-1 line plus 51 strains of mGM1-4 line)
1504 is almost similar to the 104 strains of WOX5mGM2-GFP/*wox5-1* rescued lines (53 strains of mGM2-
1505 1 line plus 51 strains of mGM2-2 line) with the P value = 0.74, the later lines are significantly lower
1506 than the 113 strains of WOX5mAll-GFP/*wox5-1* rescued lines (56 strains of mAll-2 line plus 57
1507 strains of mAll-3 line) with the P value = 6.05E-10, the 107 strains of WOX5m5A-GFP/*wox5-1*
1508 rescued lines (55 strains of m5A-1 line plus 52 strains of m5A-2 line) with the P value = 7.56E-06 and
1509 the 104 strains of WOX5m3A-GFP/*wox5-1* lines (51 strains of m3A-2 line plus 53 strains of m3A-3
1510 line) with the P value = 7.23E-06. (H) PAe of QC at the mature embryonic stage of 42 strains of
1511 WOX5mGM1-GFP/*wox5-1* rescued lines (21 strains of mGM1-1 line plus 21 strains of mGM1-4 line)
1512 is almost similar to the 43 strains of WOX5mGM2-GFP/*wox5-1* rescued lines (21 strains of mGM2-1
1513 line plus 22 strains of mGM2-2 line) with the P value = 0.67, the later lines are significantly lower
1514 than the 49 strains of WOX5mAll-GFP/*wox5-1* rescued lines (24 strains of mAll-2 line plus 25 strains
1515 of mAll-3 line) with the P value = 7.45E-04, the 49 strains of WOX5m5A-GFP/*wox5-1* rescued lines
1516 (24 strains of m5A-1 line plus 25 strains of m5A-2 line) with the P value = 1.06E-03 and the 50 strains
1517 of WOX5m3A-GFP/*wox5-1* lines (25 strains of m3A-2 line plus 25 strains of m3A-3 line) with the P
1518 value = 1.81E-03. (I~M) mPS-PI staining and LCSM images of (I) WOX5mGM1-GFP/*wox5-1*
1519 rescued lines with PAe equal to 0.048; (J) WOX5mGM2-GFP/*wox5-1* rescued lines with PAe equal to
1520 0.070; (K) WOX5mAll-GFP/*wox5-1* rescued lines with PAe equal to 0.470; (L) WOX5m5A-
1521 GFP/*wox5-1* rescued lines with PAe equal to 0.408; (M) WOX5m3A-GFP/*wox5-1* rescued lines with
1522 PAe equal to 0.42. Student's t test indicates statistical difference, bar = 10 μm, yellow arrows show
1523 the QC cells or the cell plates of the QC cells.

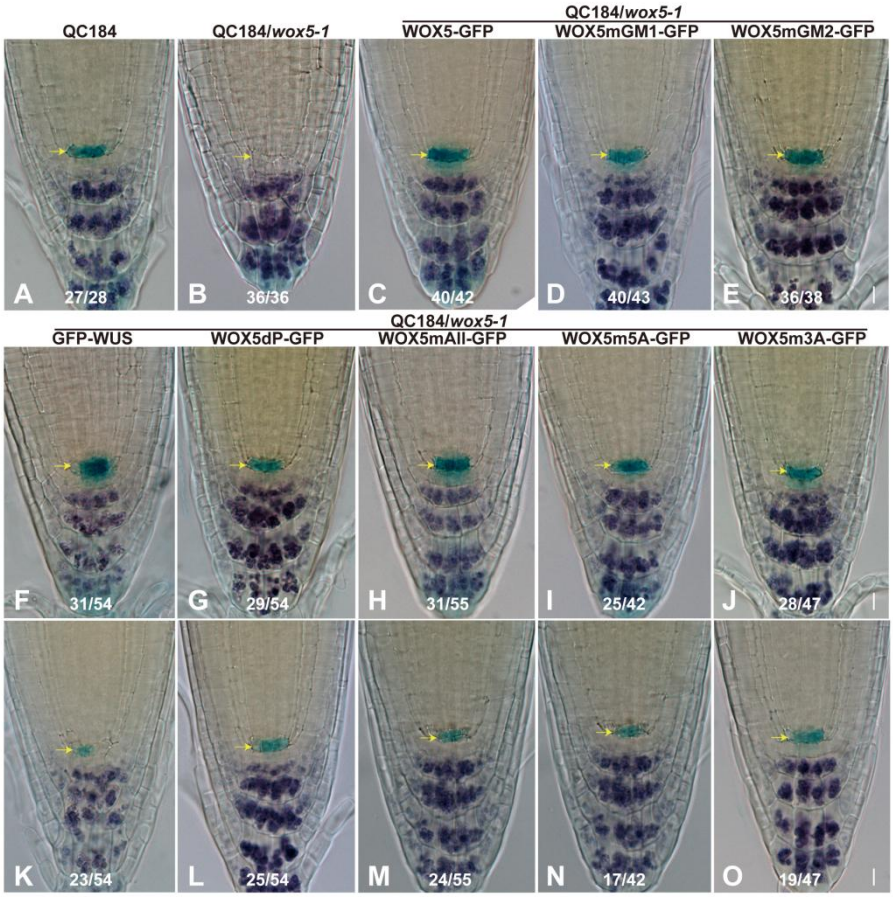

Figure S7: GUS staining on all types of rescued lines of QC184/*wox5-1*.

(A) QC184. (B) QC184/*wox5-1*. (C) pWOX5:WOX5-GFP rescued line of QC184/*wox5-1*. (D) pWOX5:WOX5mGM1-GFP rescued line of QC184/*wox5-1*. (E) pWOX5:WOX5mGM2-GFP rescued line of QC184/*wox5-1*. (F, K) pWOX5:GFP-WUS rescued line of QC184/*wox5-1*. (G, L) pWOX5:WOX5△PEST-GFP rescued line of QC184/*wox5-1*. (H, M) pWOX5:WOX5mAll-GFP rescued line of QC184/*wox5-1*. (I, N) pWOX5:WOX5m5A-GFP rescued line of QC184/*wox5-1*. (J, O) pWOX5:WOX5m3A-GFP rescued line of QC184/*wox5-1*. Bar = 10 μm, yellow arrows show the QC.

Figure S8: All AtSKs expressed in the root tips of *Arabidopsis*

(A) Subfamily I, II, III, IV of All ten AtSKs. (B) Semi-quantitative PCR showed the ten AtSKs expressed in the root tips of *Arabidopsis*.

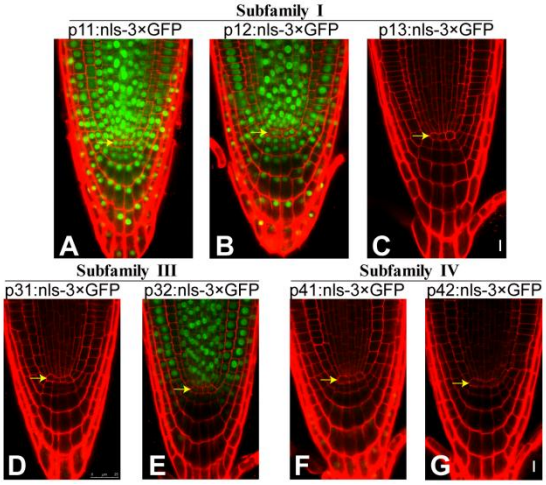

Figure S9: Expression pattern of subfamily I, III, IV of AtSKs in the RAM of *Arabidopsis*
(A) AtSK11 expressed in the QC. (B) AtSK12 expressed in the QC. (C) AtSK13 not expressed in the RAM. (D) AtSK31 not expressed in the RAM. (E) AtSK32 expressed in the QC. (F) AtSK41 not expressed in the RAM. (G) AtSK42 not expressed in the QC. Bar = 10 μm, yellow arrows show the QC.

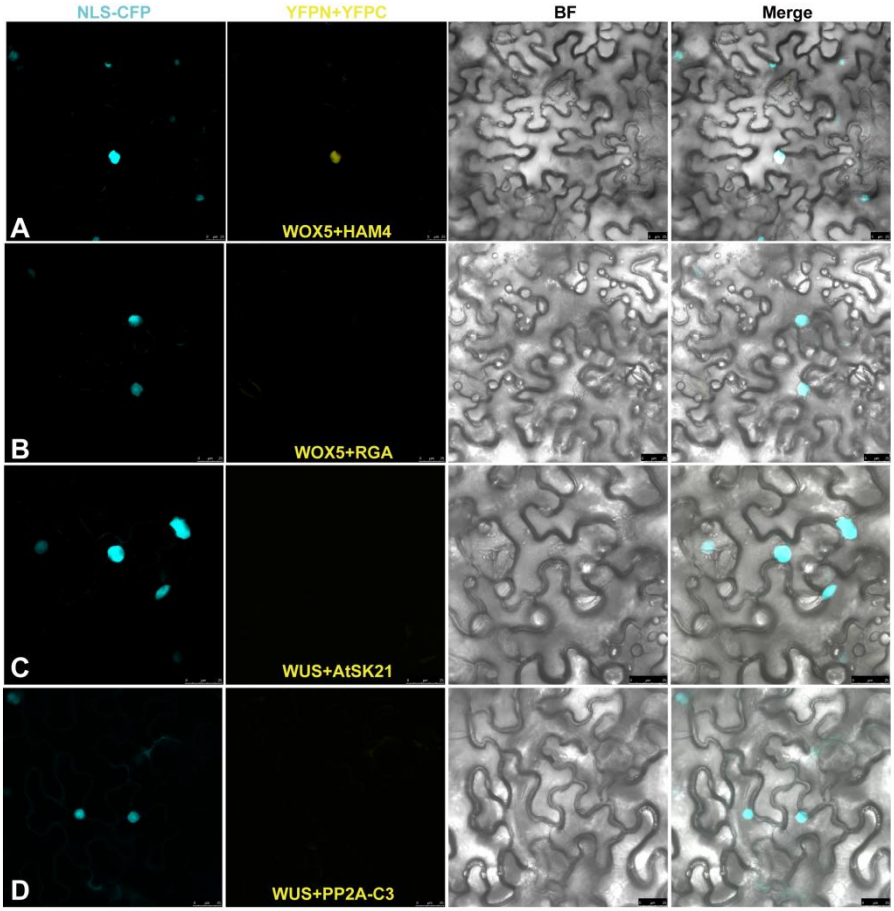

Figure S10: BiFC assay in *Thenicotiana tabacum*
(A) Positive control: WOX5-YFPN interacts with HAM4-YFPC. (B) Negative control: WOX5-YFPN not interacts with RGA-YFPC. (C) Negative control: WUS-YFPN not interacts with AtSK21-YFPC. (D) Negative control: WUS-YFPN not interacts with AtPP2A-C3-YFPC.

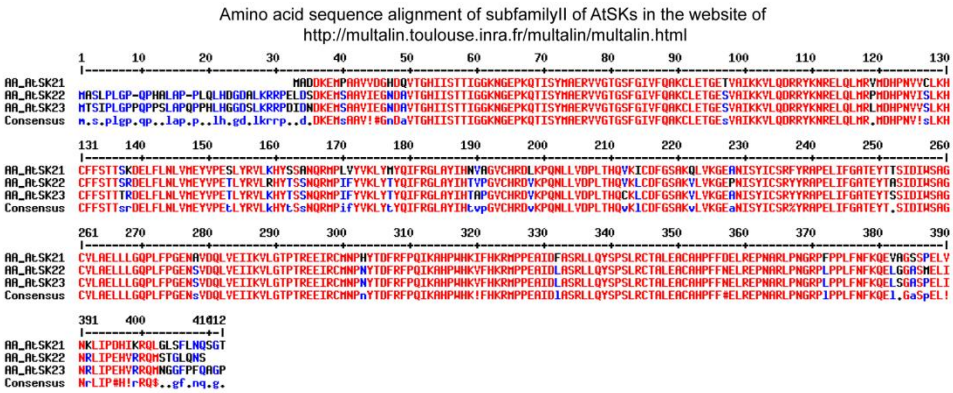

Figure S11: The amino acid sequence alignment of subfamily II of AtSKs

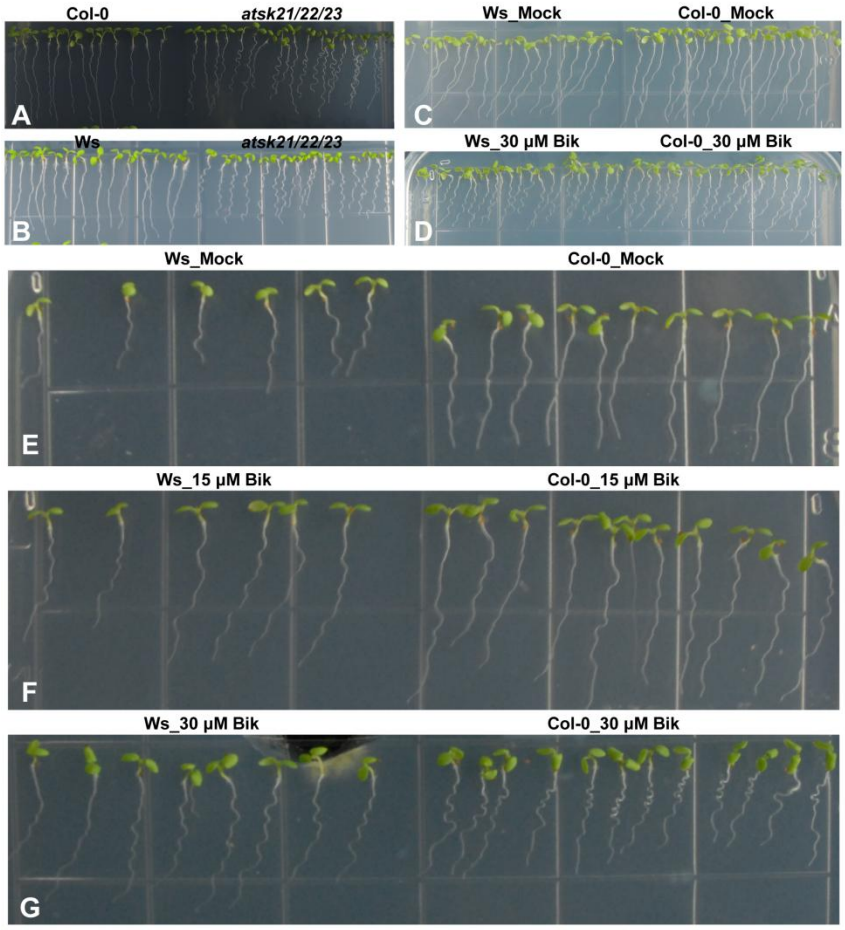

Figure S12: The phenotypes of roots

(A) Col-0 and *atsk21/22/23*. (B) Ws and *atsk21/22/23*. (C, D) Ws and Col-0 on the medium with the Mock and 30 μM Bik. (E~G) Ws and Col-0 on the medium with the Mock, 15 μM Bik and 30 μM Bik.

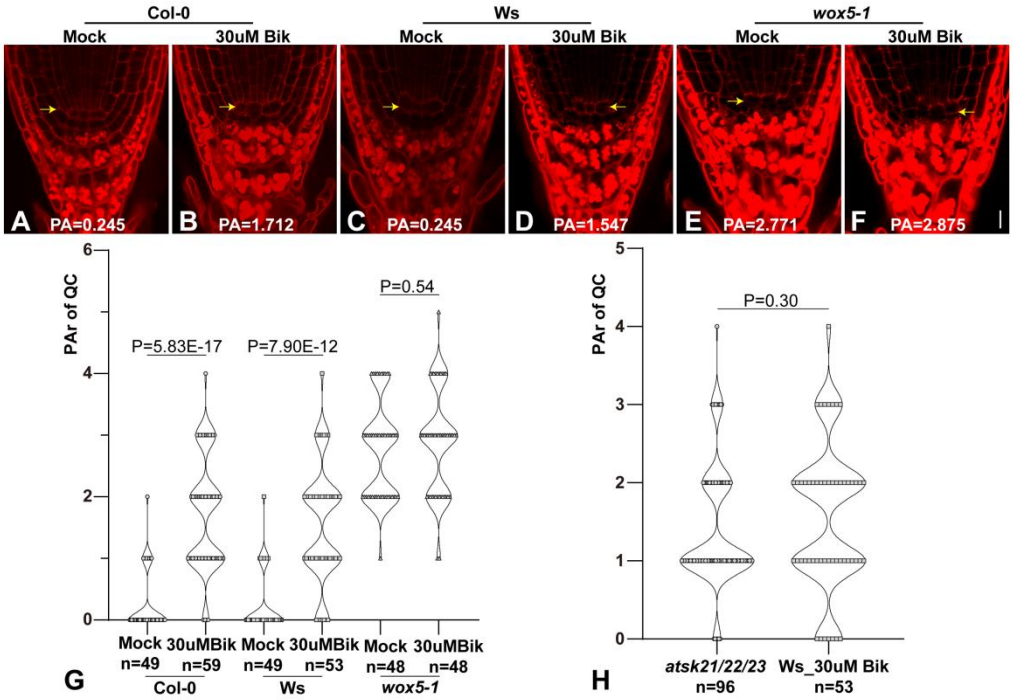

Figure S13: The QC proliferative activity increased by chemical inhibiting the subfamily of AtSKs in 30 μM Bik

(A, B) Col-0 on the medium with the Mock and 30 μM Bik. (C, D) Ws on the medium with the Mock and 30 μM Bik. (E, F) *wox5-1* on the medium with the Mock and 30 μM Bik. (G) PAr of QC at 5DAG of Col-0, Ws, *wox5-1* in Mock and in 30 μM Bik. (H) PAr comparison between *atsk21/22/23* and Ws with 30 μM Bik.Student's t test indicates statistical difference, bar = 10 μm, yellow arrows show the QC.

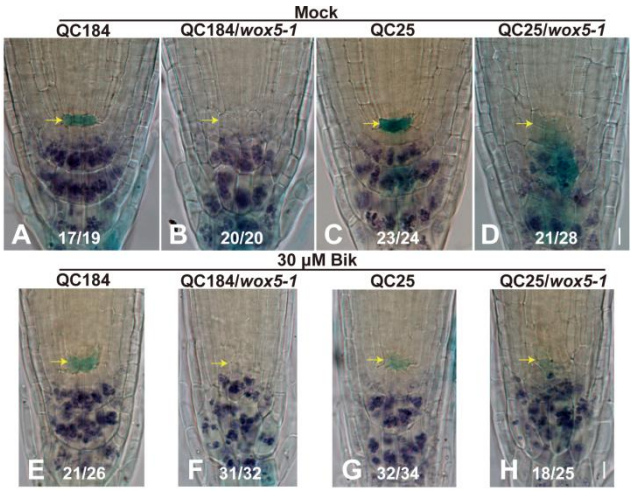

Figure S14: The GUS activity of QC184 and QC25 reduced by chemical inhibiting the subfamily of AtSKs in 30 μM Bik

(A~D) The GUS activity of QC184, QC184/*wox5-1* and QC25, QC25/*wox5-1* in the Mock. (E~H) The GUS activity of QC184, QC184/*wox5-1* and QC25, QC25/*wox5-1* in the 30 μM Bik. Yellow arrows show the QC.

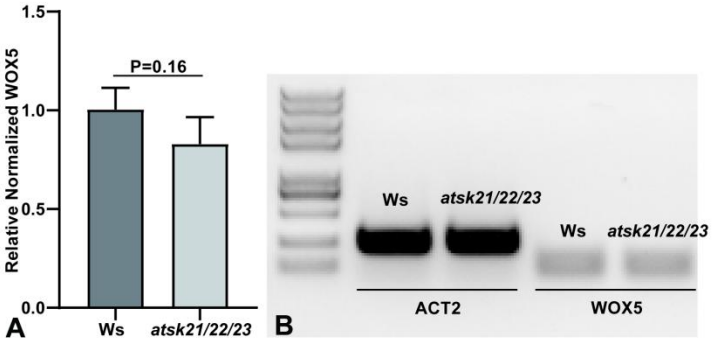

Figure S15: Quantitative-PCR and semi-quantitative PCR of Ws and *atsk21/22/23*

(A) No difference (P>0.05) between Ws and *atsk21/22/23* of relative expression value of WOX5 in the qPCR assay. (B) The ACT2 bands and the WOX5 bands between Ws and *atsk21/22/23* are almost no difference in the sqRT-PCR assay.

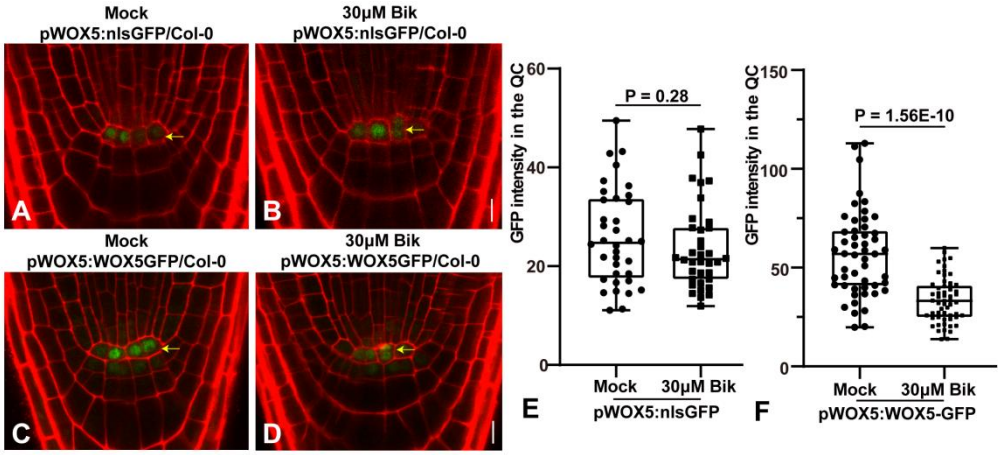

Figure S16: Treatment of pWOX5:nlsGFP/Col-0 and pWOX5:WOX5GFP/Col-0 lines with 30 μM Bik

(A, B) Treatment of pWOX5:nlsGFP/Col-0 line with (A) the mock and (B) 30 μM Bik. (C, D) Treatment of pWOX5:WOX5GFP/Col-0 line with (C) the mock and (D) 30 μM Bik. (E) GFP intensity in the QC of pWOX5:nlsGFP/Col-0 of the Mock and 30 μM Bik. (F) GFP intensity in the QC of pWOX5:WOX5-GFP/Col-0 of the Mock and 30 μM Bik. Student's t test indicates statistical difference, bar = 10 μm, yellow arrows show the QC.

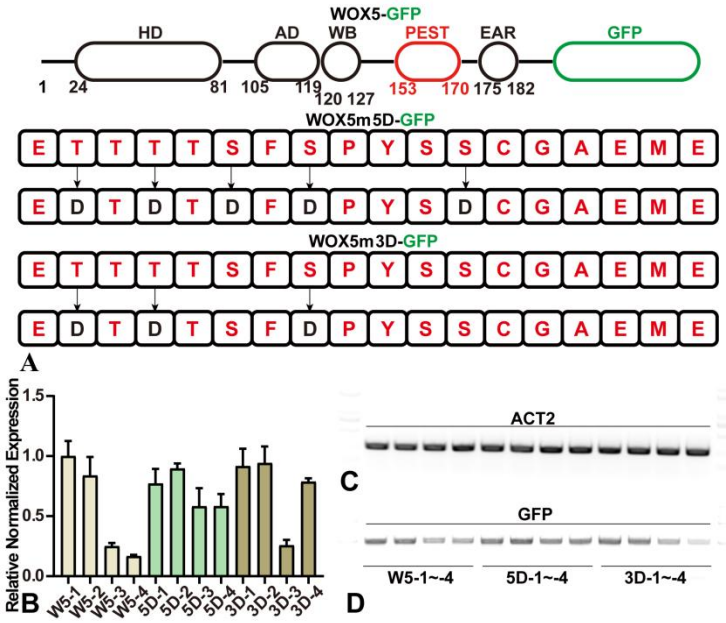

Figure S17: qPCR and sqRT-PCR of the different rescued lines identified 6 lines (W5-1, W5-2; 5D-1, 5D-2; 3D-1, 3D-2 separately) with almost equal GFP expression

(A) The WOX5-GFP fusion protein and phosphate-mimicked (m5D, m3D) WOX5-GFP fusion protein. (B) Relative normalized GFP expression compared with the ACT2 internal reference expression in the qPCR assay. (C, D) ACT2 bands and GFP bands of sqRT-PCR separately.

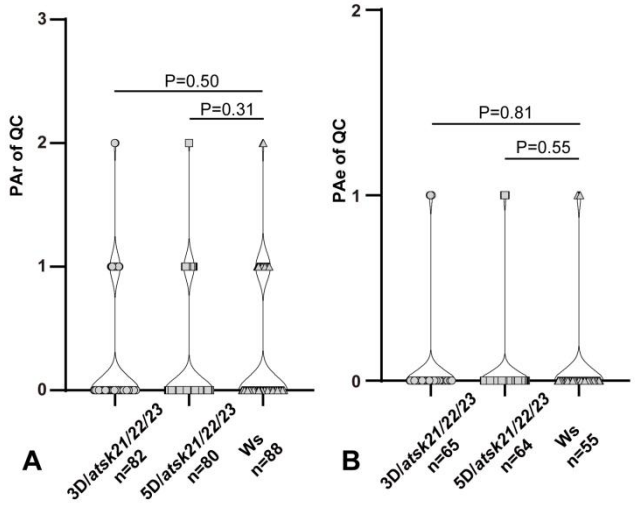

Figure S18: Phosphate-mimicked WOX5 protein can rescue the PAr and PAe of *atsk21/22/23* to be similar to the wild type (Ws)

(A) The PAr of WOX5m3D-GFP/*atsk21/22/23* line (P = 0.50) and WOX5m5D-GFP/*atsk21/22/23* line (P = 0.31) almost be equal to Ws. (B) The PAe of WOX5m3D-GFP/*atsk21/22/23* line (P = 0.81) and WOX5m5D-GFP/*atsk21/22/23* line (P = 0.55) almost be equal to Ws. Student's t test indicates statistical difference.

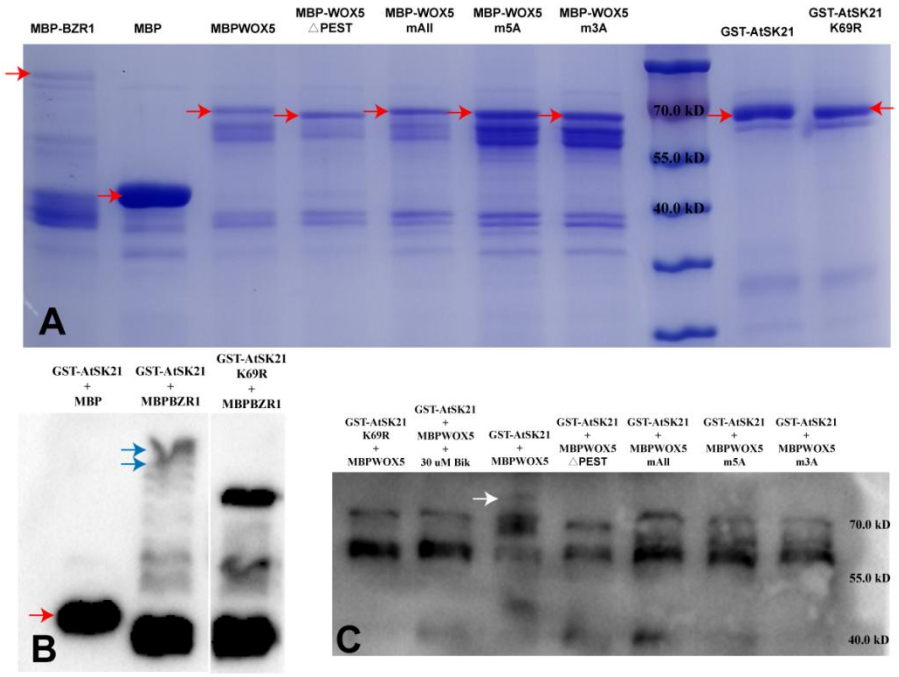

Figure S19: Kinase assay in vitro

(A) Coomassie brilliant blue (CBB) staining of purified MBP-tagged substrate proteins and GST-tagged kinase proteins, red arrows show all purified target proteins. (B) The negative controls (GST-AtSK21 + MBP; GST-AtSK21K69R + MBP-BZR1) and positive control (GST-AtSK21 + MBP-BZR1) of kinase assay in Mn2+-Phos-tag™ SDS-PAGE, red arrow show the band of MBP protein, blue arrows show the bands of phosphorylated MBP-BZR1 protein. (C) The experiment groups (GST-AtSK21K69R + MBP-WOX5; GST-AtSK21 + MBP-WOX5 + 30μM Bik; GST-AtSK21 + MBP-WOX5; GST-AtSK21 + MBP-WOX5△PEST; GST-AtSK21 + MBP-WOX5mAll; GST-AtSK21 + MBP-WOX5m5A; GST-AtSK21 + MBP-WOX5m3A) of kinase assay in Mn2+-Phos-tag™ SDS-PAGE, white arrow show the band of phosphorylated MBP-WOX5 protein.

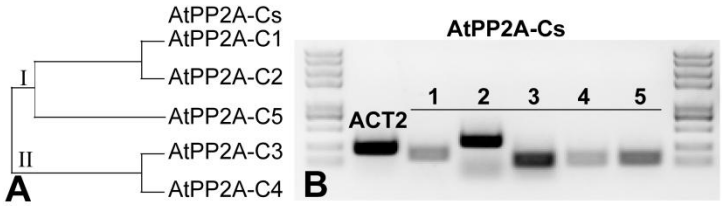

Figure S20: All AtPP2A-Cs expressed in the root tips of *Arabidopsis*

(A) Subfamily I and II of All five AtPP2A-Cs. (B) sqRT-PCR showed the five AtPP2A-Cs expressed in the root tips of *Arabidopsis*.

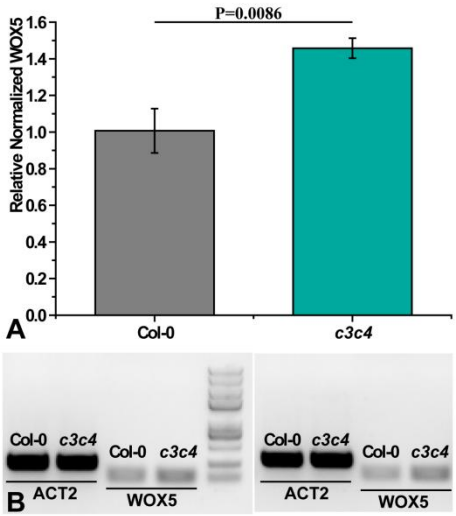

Figure S21: qPCR and sqRT-PCR of WOX5 in Col-0 and *c3c4*

(A): The relative expression value of WOX5 of Col-0 is markedly lower than *c3c4* in the qPCR assay. (B): The ACT2 bands between Col-0 and *c3c4* are almost no difference, but the WOX5 bands of Col-0 is markedly weaker than *c3c4* in the sqRT-PCR assay. Student's t test indicates statistical difference.

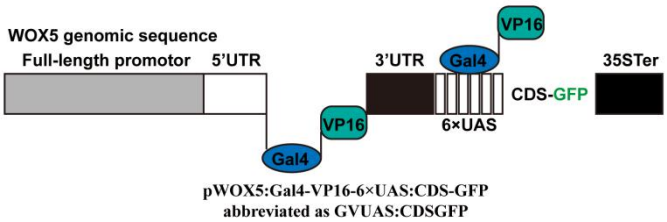

Figure S22: The sketch of GVUAS:CDS-GFP

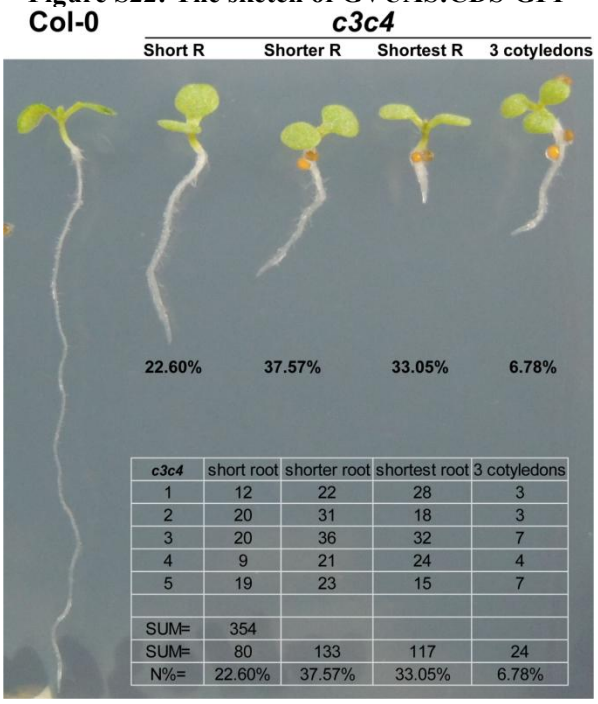

c3c4	short root	shorter root	shortest root	3 cotyledons
1	12	22	28	3
2	20	31	18	3
3	20	36	32	7
4	9	21	24	4
5	19	23	15	7
SUM=	354			
SUM=	80	133	117	24
N%=	22.60%	37.57%	33.05%	6.78%

Figure S23: The phenotypes of *c3c4* seedling at 5 DAG including 4 types. First, short root account for 22.60%; second, shorter root 37.57%; third, shortest root 33.05%; fourth, 3 cotyledons 6.78%.

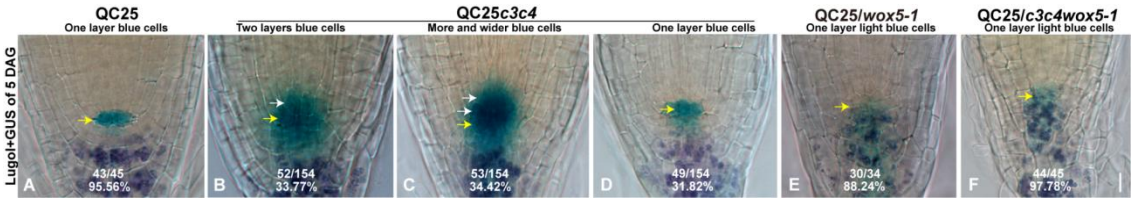

Figure S24: WOX5 is necessary for producing increasing GUS activity of QC25 when loss of function the subfamily II of AtPP2A-Cs

(A~F) GUS staining images of 5DAG of (A) QC25 (95.56% are one layer blue cells); (B~D) QC25*c3c4* (33.77% are two layers blue cells, 34.42% are more and wider blue cells, 31.82% are one layer blue cells); (E) QC25/*wox5-1* (88.24% are one layer light blue cells); (F) QC25/*c3c4wox5-1* (97.78% are one layer light blue cells). Bar = 10 μm, yellow arrows show the blue cells or light blue cells, white arrows show the QC-like cells.

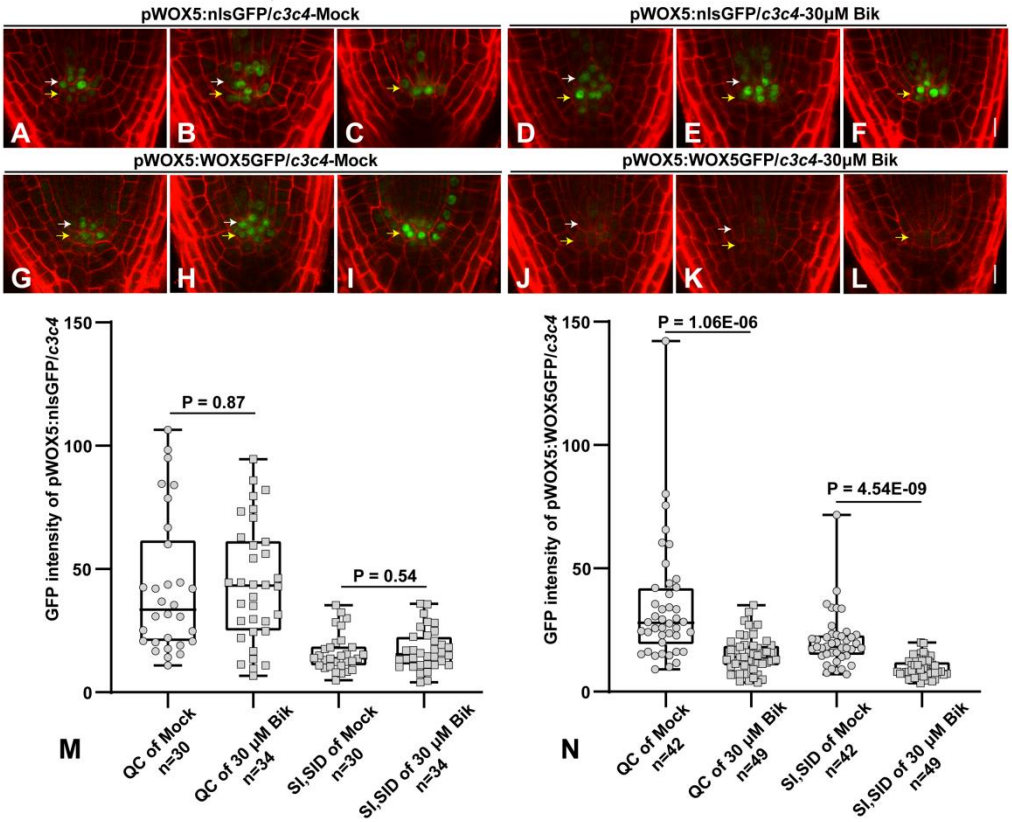

Figure S25: Chemical inhibiting the activity of subfamily II of AtSKs destabilized the increased WOX5 protein in *c3c4*

(A~F) PI staining images of pWOX5:nlsGFP/*c3c4* in the Mock (A~C) and in the 30 μM Bik (D~F). (G~L) PI staining images of pWOX5:WOX5GFP/*c3c4* in the Mock (G~I) and in the 30 μM Bik (J~L). (M,N) GFP intensity in QC, SI and SID of pWOX5:nlsGFP/*c3c4* (N) and pWOX5:WOX5GFP/*c3c4* (O) in the Mock and 30 μM Bik. Student's t test indicates statistical difference, bar = 10 μm, yellow arrows show the QC cells, white arrows show the QC-like cells.

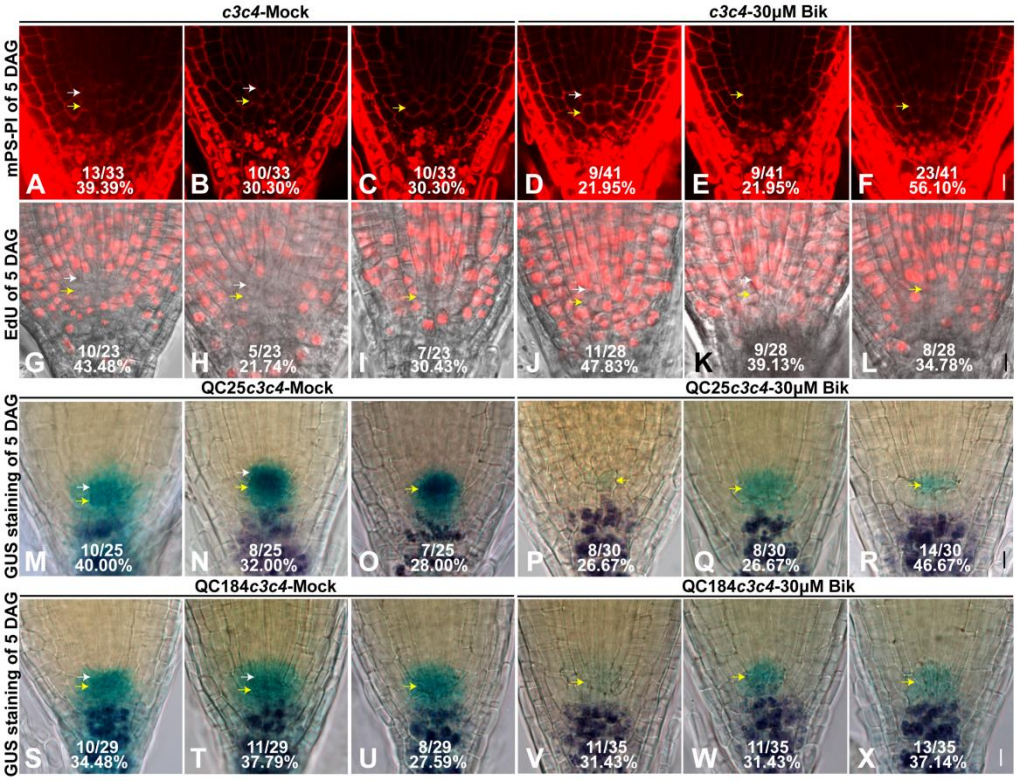

Figure S26: Chemical inhibiting the activity of subfamily II of AtSKs enhanced the proliferative activity of the increased quiescent cells in *c3c4*

(A~F) mPS-PI images of *c3c4* in the Mock (A~C) and in the 30 μM Bik (D~F), yellow arrows show the QC cells, white arrows show the QC-like cells. (G~L) EdU staining images of *c3c4* in the Mock (G~I) and in the 30 μM Bik (J~L), yellow arrows show the nondividing cells or dividing QC cells, white arrows show the QC-like cells or dividing QC-like cells. (M~R) GUS staining images of QC184*c3c4* in the Mock (M~O) and in the 30 μM Bik (P~R), yellow arrows show the blue cells or light blue cells, white arrows show the QC-like cells. (S~X) GUS staining images of QC25*c3c4* in the Mock (S~U) and in the 30 μM Bik (V~X), yellow arrows show the blue cells or light blue cells, white arrows show the QC-like cells. Bar = 10 μm.

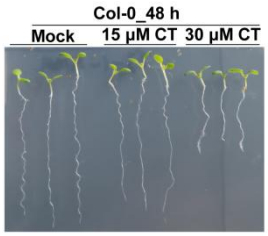

Figure S27: Processing seedling of Col-0 for 48 hours with different concentration of Cantharidin (CT): Mock (DMSO), 15 μM CT and 30 μM CT

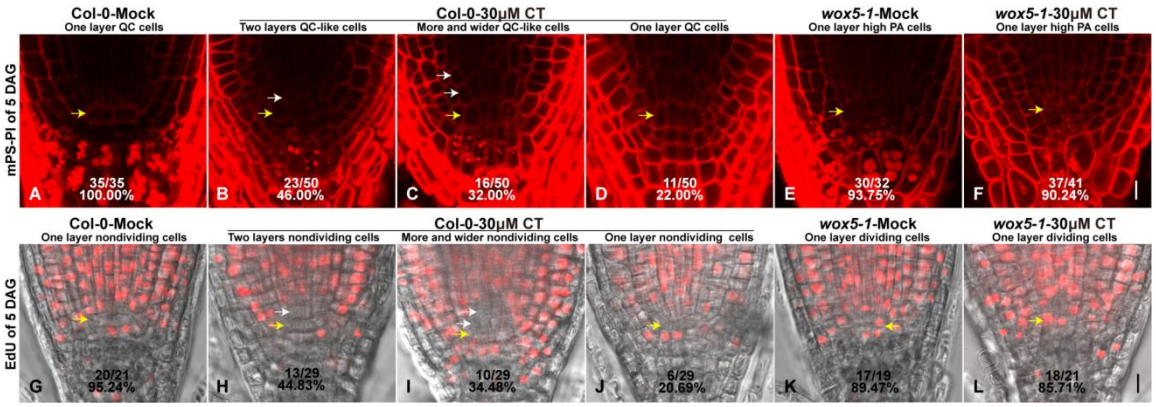

Figure S28: WOX5 is necessary for the production of more quiescent cells when inhibiting the subfamily II of AtPP2A-Cs by 30 μM CT

(A~D) mPS-PI images of Col-0 in the Mock (A) and in the 30 μM CT (B~D), yellow arrows show the QC cells, white arrows show the QC-like cells. (E, F) mPS-PI images of *wox5-1* in the Mock (E) and in the 30 μM CT (F), yellow arrows show the cell plates of QC cells. (G~J) EdU staining of Col-0 in the Mock (G) and in the 30 μM CT (H~J), yellow arrows show the nondividing cells, white arrows show the QC-like cells. (K, L) EdU staining of *wox5-1* in the Mock (K) and in the 30 μM CT (L), yellow arrows show the dividing cells. Bar = 10 μm.

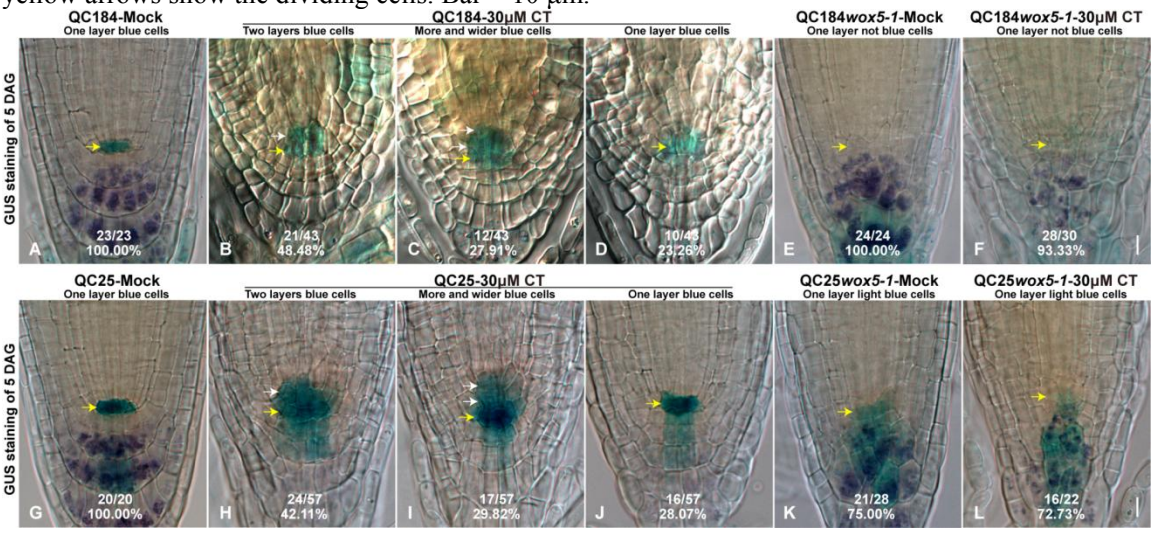

Figure S29: WOX5 is necessary for increasing GUS activity of QC184 and QC25 when inhibiting the subfamily II of AtPP2A-Cs by 30 μM CT

(A~D) GUS staining of QC184 in the Mock (A) and in the 30 μM CT (B~D), yellow arrows show the blue cells, white arrows show the QC-like cells. (E, F) GUS staining of QC184*wox5-1* in the Mock (E) and in the 30 μM CT (F), yellow arrows show the not blue cells. (G~J) GUS staining of QC25 in the Mock (G) and in the 30 μM CT (H~J), yellow arrows show the blue cells, white arrows show the QC-like cells. (K, L) GUS staining of QC25*wox5-1* in the Mock (K) and in the 30 μM CT (L), yellow arrows show the light blue cells. Bar = 10 μm.

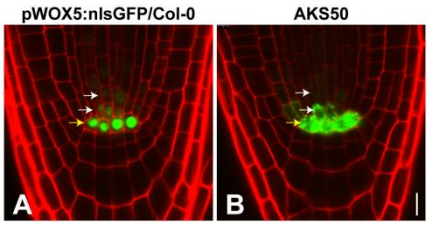

Figure S30: Different transcriptional reporters of pWOX5:nlsGFP/Col-0 and GVUAS:erGFP/Col-0 (AKS50)

(A) PI staining images of pWOX5:nlsGFP/Col-0 line with PMT40 of 488 nm laser. (B) PI staining images of GVUAS:erGFP/Col-0 (AKS50) line with PMT5 of 488 nm laser. Yellow arrows show the QC cells, white arrows show the SI and SID cells, bar = 10 μm.

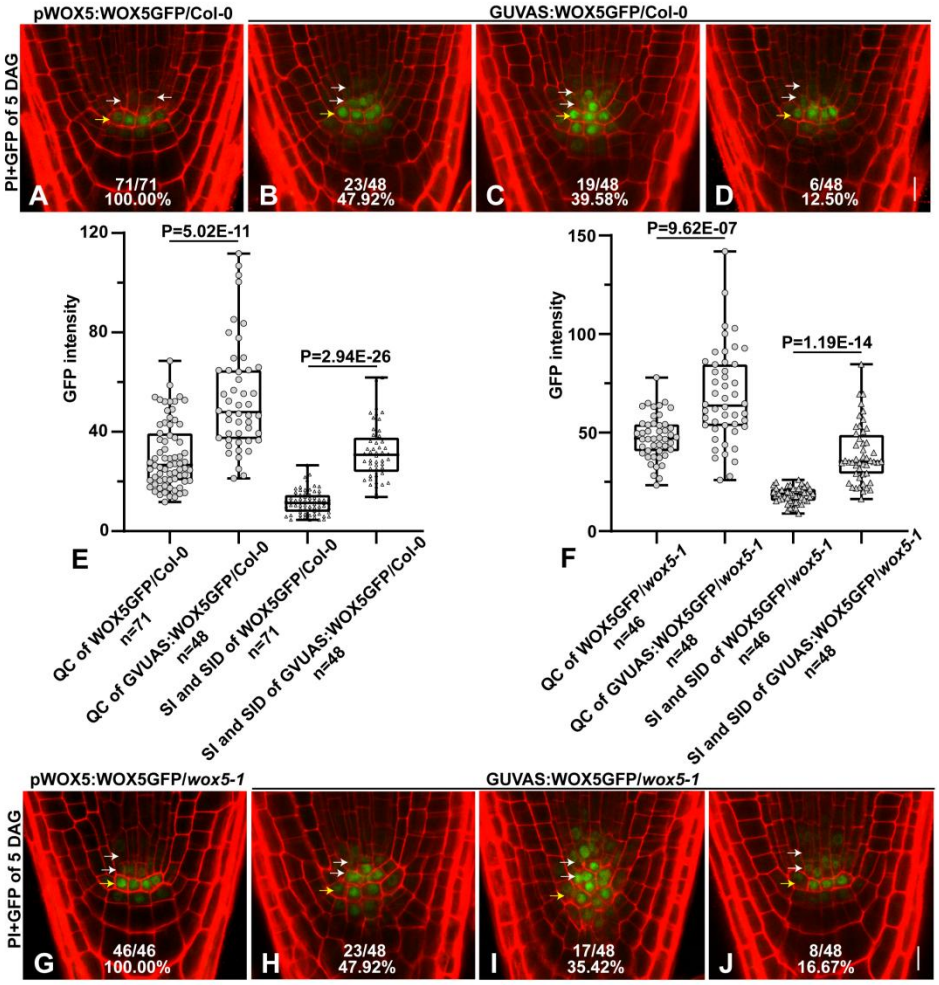

Figure S31: In situ overexpressed WOX5 protein in Col-0 and *wox5-1* successfully

(A~D) PI staining images of (A) pWOX5:WOX5GFP/Col-0 and (B~D) GUVAS:WOX5GFP/Col-0. (E, F) GFP intensity of (E) pWOX5:WOX5GFP/Col-0 and GUVAS:WOX5GFP/Col-0, (F) pWOX5:WOX5GFP/*wox5-1* and GUVAS:WOX5GFP/*wox5-1*. (G~J) PI staining images of (G) pWOX5:WOX5GFP/*wox5-1* and (H~J) GUVAS:WOX5GFP/*wox5-1*. Yellow arrows show the QC cells, white arrows show the SI and SID cells or QC-like cells; Student's t test indicates statistical difference, bar = 10 μm.

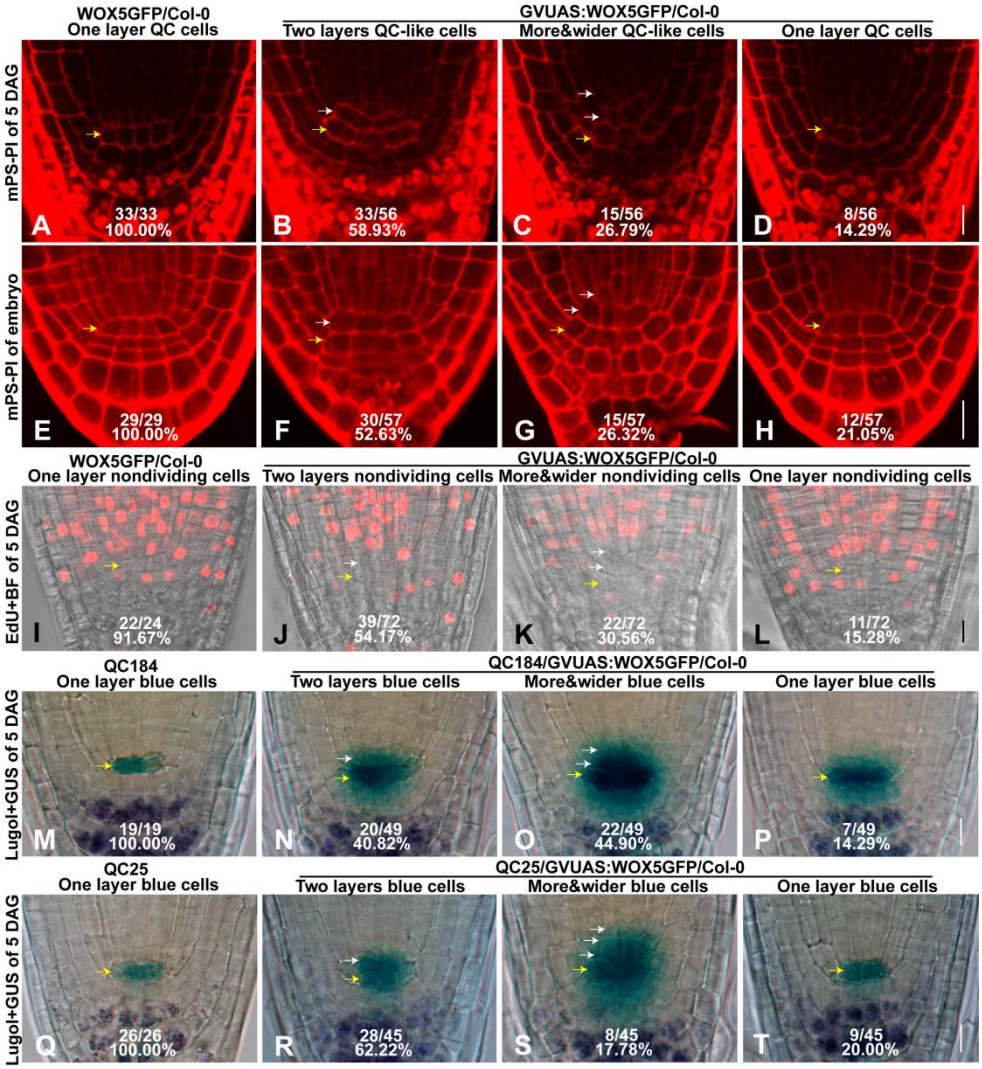

Figure S32: In situ overexpressed WOX5 protein in Col-0 recapitulated the phenotypes of more quiescent cells of loss of the subfamily II of AtPP2A-Cs

(A~D) mPS-PI images of 5DAG of (A) WOX5GFP/Col-0 (100.00% are one layer QC cells), (B~D) GVUAS:WOX5GFP/Col-0 (58.93% are two layers QC-like cells, 26.79% are more and wider QC-like cells, 14.29% are one layer QC cells), yellow arrows show the QC cells, white arrows show the QC-like cells. (E~H) mPS-PI images of mature embryos of (E) WOX5GFP/Col-0 (100.00% are one layer QC cells), (F~H) GVUAS:WOX5GFP/Col-0 (52.63% are two layers QC-like cells, 26.32% are more and wider QC-like cells, 21.06% are one layer QC cells), yellow arrows show the QC cells, white arrows show the QC-like cells. (I~L) EdU staining of 5DAG of (I) WOX5GFP/Col-0 (91.67% are one layer nondividing cells), (J~L) GVUAS:WOX5GFP/Col-0 (54.17% are two layers nondividing cells, 30.58% are more and wider nondividing cells, 15.28% are one layer nondividing cells), yellow arrows show the nondividing cells, white arrows show the QC-like cells. (M~P) GUS staining of 5DAG of (M) QC184 (100.00% are one layer blue cells), (N~P) QC184/GVUAS:WOX5GFP/Col-0 (40.82% are two layers blue cells, 44.90% are more and wider blue cells, 14.29% are one layer blue cells), yellow arrows show the blue cells, white arrows show the QC-like cells. (Q~T) GUS staining of 5DAG of (M) QC25 (100.00% are one layer blue cells), (R~T) QC25/GVUAS:WOX5GFP/Col-0 (62.22% are two layers blue cells, 17.78% are more and wider blue cells, 20.00% are one layer blue cells), yellow arrows show the blue cells, white arrows show the QC-like cells. Bar = 10 μm.

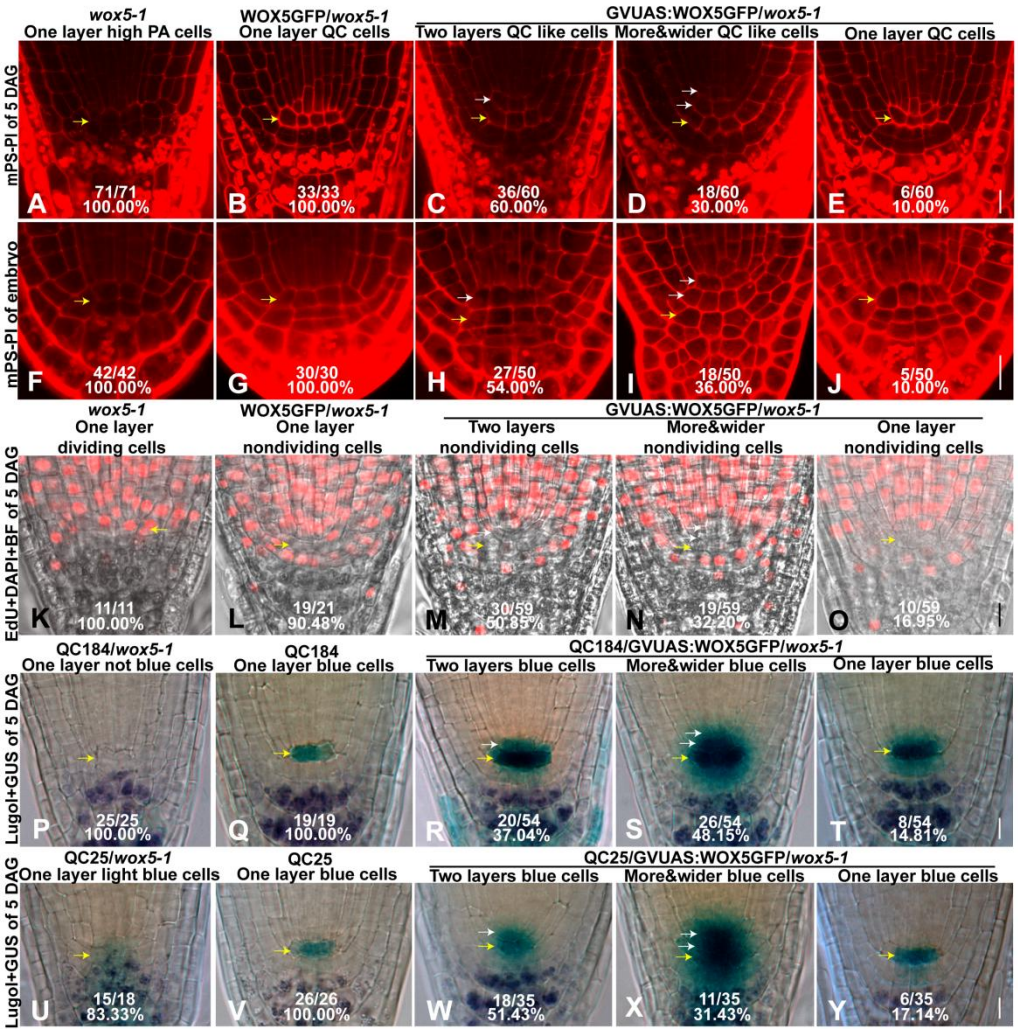

Figure S33: In situ overexpressed WOX5 protein in *wox5-1* also recapitulated the phenotypes of more quiescent cells of loss of the subfamily II of AtPP2A-Cs

(A~E) mPS-PI images of 5DAG of (A) *wox5-1* (100.00% are one layer high PA cells), (B) WOX5GFP/*wox5-1* (100.00% are one layer QC cells), (C~E) GVUAS:WOX5GFP/*wox5-1* (60.00% are two layers QC-like cells, 30.00% are more and wider QC-like cells, 10.00% are one layer QC cells), yellow arrows show the QC cells, white arrows show the QC-like cells. (F~J) mPS-PI images of mature embryos of (F) *wox5-1* (100.00% are one layer high PA cells), (G) WOX5GFP/*wox5-1* (100.00% are one layer QC cells), (H~J) GVUAS:WOX5GFP/*wox5-1* (54.00% are two layers QC-like cells, 36.00% are more and wider QC-like cells, 10.00% are one layer QC cells), yellow arrows show the QC cells, white arrows show the QC-like cells. (K~O) EdU staining of 5DAG of (K) *wox5-1* (100.00% are one layer dividing cells), (L) WOX5GFP/*wox5-1* (90.84% are one layer nondividing cells), (M~O) GVUAS#WOX5GFP/*wox5-1* (50.85% are two layers nondividing cells, 32.20% are more and wider nondividing cells, 16.95% are one layer nondividing cells), yellow arrows show the dividing and nondividing cells, white arrows show the QC-like cells. (P~T) GUS staining of 5DAG of (P) QC184/*wox5-1* (100.00% are one layer not blue cells), (Q) QC184 (100.00% are one layer blue cells), (R~T) QC184/GVUAS#WOX5GFP/*wox5-1* (37.04% are two layers blue cells, 48.15% are more and wider blue cells, 14.81% are one layer blue cells), yellow arrows show the not blue or blue cells, white arrows show the QC-like cells. (U~Y) GUS staining of 5DAG of (U) QC25/*wox5-1* (83.33% are one layer light blue cells), (V) QC25 (100.00% are one layer blue cells), (W~Y) QC25/GVUAS#WOX5GFP/*wox5-1* (51.43% are two layers blue cells, 31.43% are more and wider

blue cells, 17.14% are one layer blue cells), yellow arrows show the light blue or blue cells, white arrows show the QC-like cells. Bar = 10 μm.

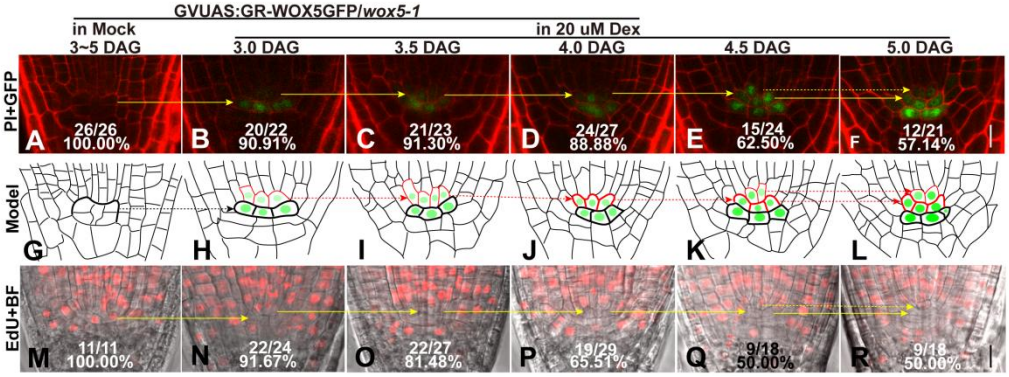

Figure S34: Dynamic accumulation of WOX5 protein in QC and SI and SID through 20 μM Dexamethasone (Dex) induction

(A) PI staining images at 3~5 DAG of GVUAS:GRWOX5GFP/*wox5-1* on the medium with DMSO (the Mock), Yellow arrows show the dynamic accumulation of WOX5 protein in QC, SI and SID cells; (B~F) PI staining images at 3.0, 3.5, 4.0, 4.5, 5.0 DAG of GVUAS:GRWOX5GFP/*wox5-1* on the medium with 20 μM Dex, Yellow arrows show the dynamic accumulation of WOX5 protein in QC, SI and SID cells. (G) The model at 3~5 DAG of GVUAS:GRWOX5GFP/*wox5-1* on the medium with DMSO (the Mock); black bold lines show the cell wall of QC cells stained by PI, red bold lines show the cell wall of QC-like cells stained by PI. (H~L) The model at 3.0, 3.5, 4.0, 4.5, 5.0 DAG of GVUAS:GRWOX5GFP/*wox5-1* on the medium with 20 μM Dex, black bold lines show the cell wall of QC cells stained by PI, red bold lines show the cell wall of QC-like cells stained by PI. (M) EdU staining at 3~5 DAG of GVUAS:GRWOX5GFP/*wox5-1* on the medium with DMSO (the Mock), Yellow arrows show the dividing cells and the nondividing cells. (N~R) EdU staining at 3.0, 3.5, 4.0, 4.5, 5.0 DAG of GVUAS:GRWOX5GFP/*wox5-1* on the medium with 20 μM Dex, Yellow arrows show the dividing cells and the nondividing cells. Bar = 10 μm.

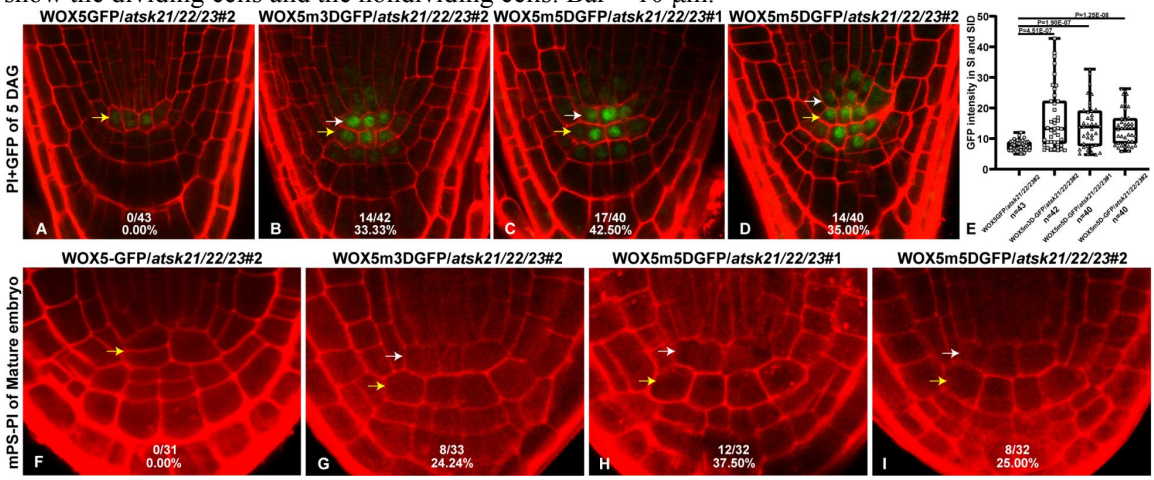

Figure S35: Phosphate-mimicked rescued lines (WOX5m3D-GFP/*atsk21/22/23* and WOX5m5D-GFP/*atsk21/22/23*) recapitulated the phenotype of two layers QC-like cells in *c3c4* from the embryonic stage to the postembryonic stage

(A~D) PI staining images show two layers QC-like cells at 5 DAG of (A) WOX5-GFP/*atsk21/22/23* line #2 (0.00% appeared two layers QC-like cells) (B) WOX5m3DGFP/*atsk21/22/23* line #2 (33.33% appeared two layers QC-like cells) (C) WOX5m5DGFP/*atsk21/22/23* line #1 (42.50% appeared two layers QC-like cells) and (D) WOX5m5DGFP/*atsk21/22/23* line #2 (35.00% appeared more and wider QC-like cells). (E) GFP intensity in SI and SID of WOX5-GFP/*atsk21/22/23* line #2 (n = 43), WOX5m3DGFP/*atsk21/22/23* line #2 (n = 42), WOX5m5DGFP/*atsk21/22/23* line #1 (n = 40) and line #2 (n = 40). (F~I) mPS-PI images show two layers QC-like cells at the mature embryonic stage of

(F) WOX5-GFP/*atsk21/22/23* line #2 (0.00%), (G) WOX5m3DGFP/*atsk21/22/23* line #2 (24.24%) and (H, I) WOX5m5DGFP/*atsk21/22/23* line #1 (37.50%) and line #2 (25.00%).Yellow arrows show the QC, white arrows show the QC-like cells; Student's t test indicates statistical difference, bar = 10 µm.

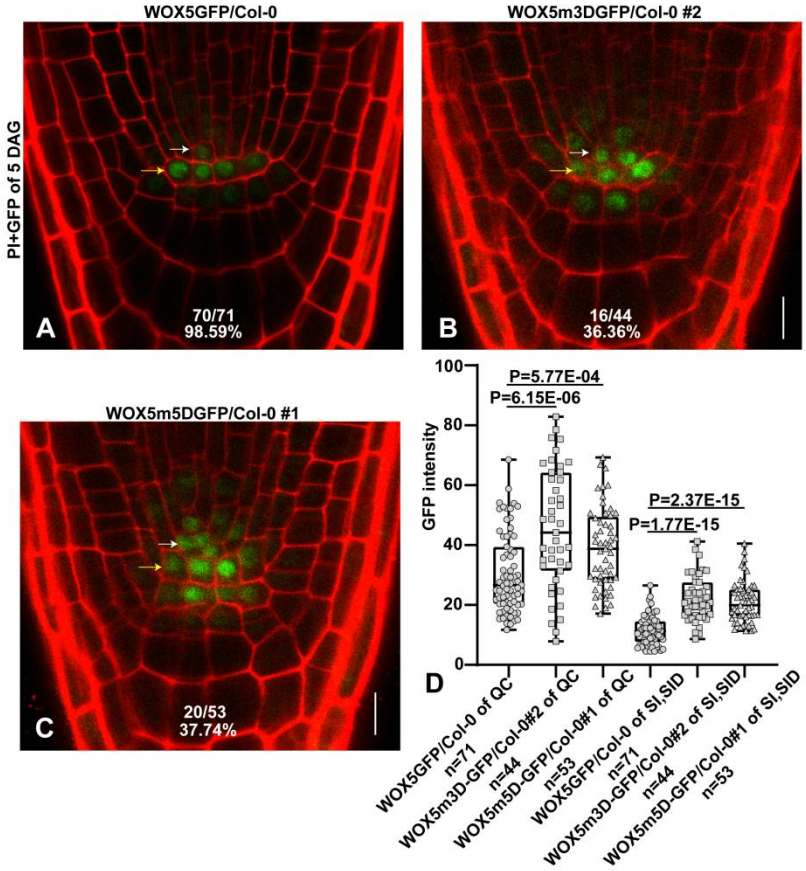

Figure S36: Phosphate-mimicked lines (WOX5m3D-GFP/Col-0 #2 and WOX5m5D-GFP/Col-0 #1) increased WOX5 protein in QC and in SI and SID

(A) PI staining images at 5 DAG of WOX5GFP/Col-0 (98.59% show one layer QC cells). (B) PI staining images at 5 DAG of WOX5m3DGFP/Col-0 line #2 (36.36% show more QC-like cells). (C) PI staining images at 5 DAG of WOX5m5DGFP/Col-0 line #1 (37.74% show more QC-like cells). (D) GFP intensity in QC of WOX5GFP/Col-0, WOX5m3DGFP/Col-0 line #2 and WOX5m5DGFP/Col-0 line #1, in SI and SID of WOX5GFP/Col-0, WOX5m3DGFP/Col-0 line #2 and WOX5m5DGFP/Col-0 line #1.Yellow arrows show the QC, white arrows show the SI or QC-like cells. Student's t test indicates statistical difference, bar = 10 µm.

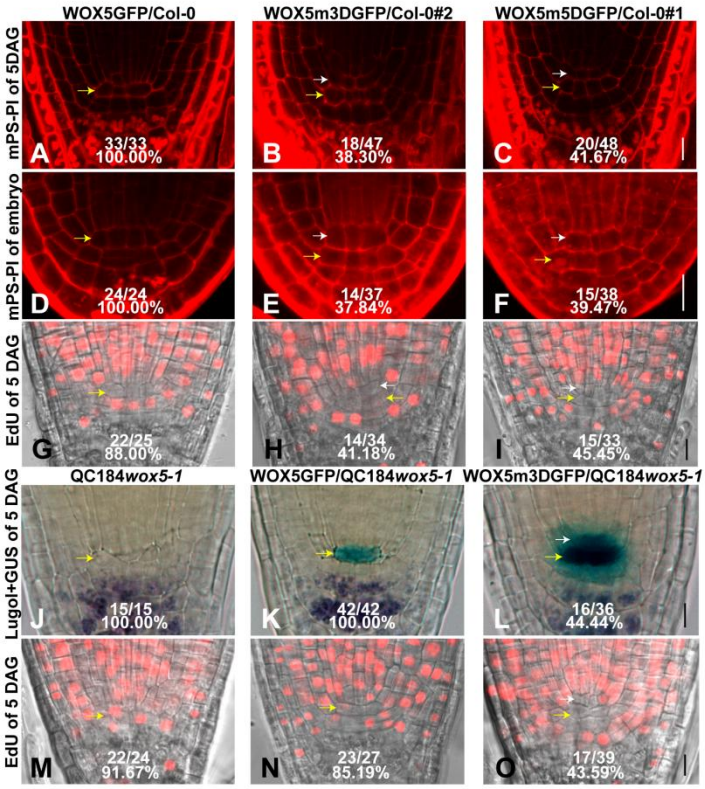

Figure S37: Phosphate-mimicked lines (WOX5m3D-GFP/Col-0, WOX5m5D-GFP/Col-0 and WOX5m3D-GFP/QC184/*wox5-1*) recapitulated the phenotype of more quiescent cells in *c3c4*

(A~C) mPS-PI images of 5DAG of (A) WOX5GFP/Col-0 (100.00% show one layer QC cells), (B) WOX5m3DGFP/Col-0 line #2 (38.30% show two layers QC-like cells), (C) WOX5m5DGFP/Col-0 line #1 (41.67% show two layers QC-like cells), yellow arrows show the QC cells, white arrows show the QC-like cells. (D~F) mPS-PI images of mature embryos of (D) WOX5GFP/Col-0 (100.00% show one layer QC cells), (E) WOX5m3DGFP/Col-0 line #2 (37.84% show two layers QC-like cells), (F) WOX5m5DGFP/Col-0 line #1 (39.47% show two layers QC-like cells), yellow arrows show the QC cells, white arrows show the QC-like cells. (G~I) EdU staining of 5DAG of (G) WOX5GFP/Col-0 (88.00% show one layer nondividing cells), (H) WOX5m3DGFP/Col-0 line #2 (41.18% show two layers nondividing cells), (I) WOX5m5DGFP/Col-0 line #1 (45.45% show two layers nondividing cells), yellow arrows show the nondividing cells, white arrows show the QC-like cells. (J~L) GUS staining of 5DAG of (J) QC184*wox5-1* (100.00% show one layer not blue cells), (K) WOX5GFP/ QC184*wox5-1* (100.00% show one layer blue cells), (L) WOX5m3DGFP/QC184*wox5-1* (44.44% show two layers blue cells), yellow arrows show the QC or blue cells, white arrows show the QC-like cells. (M~O) EdU staining of 5DAG of (M) QC184*wox5-1* (91.67% show one layer dividing cells), (N) WOX5GFP/ QC184*wox5-1* (85.19% show one layer nondividing cells), (L) WOX5m3DGFP/QC184*wox5-1* (43.59% show two layers nondividing cells), yellow arrows show the nondinviding cells, white arrows show the QC-like cells. Bar = 10 μm.

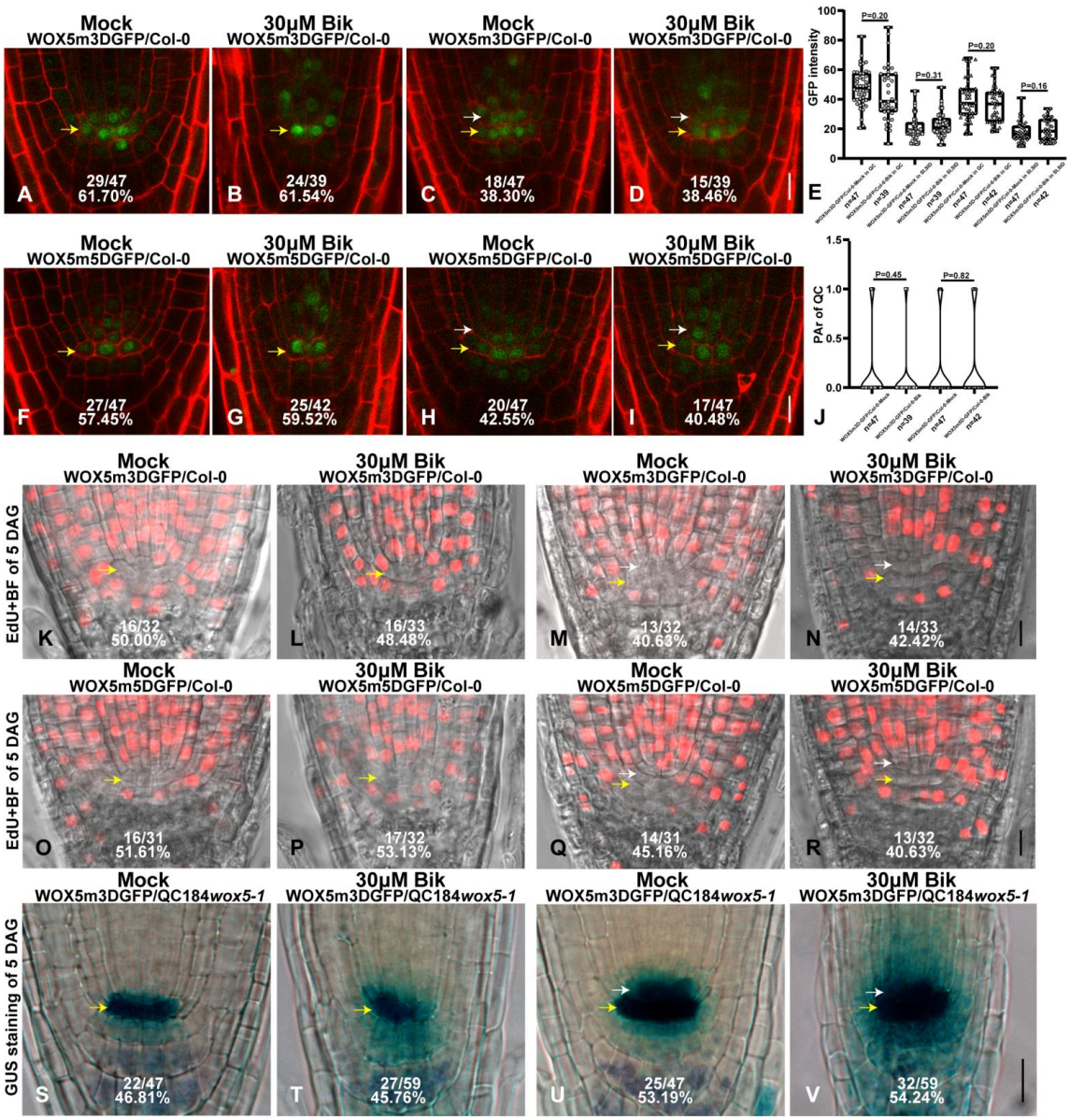

Figure S38: Recapitulated the phenotype of more quiescent cells in *c3c4* by phosphate-mimicked WOX5 protein can not be antagonized by 30 μM Bik

(A, B) PI staining images of 5DAG of WOX5m3DGFP/Col-0 (A) in Mock (61.70% show one layer QC cells) and (B) in 30 μM Bik (61.54% show one layer QC cells). (C, D) PI staining images of 5DAG of WOX5m3DGFP/Col-0 (C) in Mock (38.30% show two layers QC-like cells) and (D) in 30 μM Bik (38.46% show two layers QC-like cells). (E) GFP intensity in QC, SI and SID of WOX5m3DGFP/Col-0 and WOX5m5DGFP/Col-0 in Mock and in 30 μM Bik. (F, G) PI staining images of 5DAG of WOX5m5DGFP/Col-0 (H) in Mock (57.45% show one layer QC cells) and (I) in 30 μM Bik (59.52% show one layer QC cells). (H, I) PI staining images of 5DAG of WOX5m5DGFP/Col-0 (J) in Mock (42.55% show two layers QC-like cells) and (K) in 30 μM Bik (40.48% show two layers QC-like cells). (J) PAr of QC at 5 DAG of WOX5m3DGFP/Col-0 and WOX5m5DGFP/Col-0 in Mock and in 30 μM Bik. (K, L) EdU staining images of 5DAG of WOX5m3DGFP/Col-0 (K) in Mock (50.00% show one layer nondividing cells) and (L) in 30 μM Bik (48.48% show one layer nondividing cells). (M, N) EdU staining images of 5DAG of WOX5m3DGFP/Col-0 (H) in Mock (40.63% show two layers nondividing cells) and (I) in 30 μM Bik (42.42% show two layers nondividing cells). (O, P) EdU staining images of 5DAG of

1849 WOX5m5DGFP/Col-0 (O) in Mock (51.61% show one layer nondividing cells) and (P) in 30 μM Bik
1850 (53.13% show one layer nondividing cells). (Q, R) EdU staining images of 5DAG of
1851 WOX5m5DGFP/Col-0 (Q) in Mock (45.16% show two layers no ndividing cells) and (R) in 30 μM
1852 Bik (40.63% show two layers nondividing cells). (S, T) GUS staining of 5DAG of
1853 WOX5m3DGFP/QC184*wox5-1* (S) in Mock (46.81% show one layer blue cells) and (T) in 30 μM
1854 Bik (45.76% show one layer blue cells). (U, V) GUS staining of 5DAG of
1855 WOX5m5DGFP/QC184*wox5-1* (U) in Mock (53.19% show two layers blue cells) and (V) in 30 μM
1856 Bik (54.24% show two layers blue cells). Yellow arrows show the QC/nondividing/blue cells, white
1857 arrows show the QC-like cells. Student's t test indicates statistical difference, bar = 10 μm.